

ADA 040997

JADC 77157-30



NOR 76-190



# WAVE DRAG REDUCTION FOR AIRCRAFT FUSELAGE - WING CONFIGURATIONS

VOLUME I: Analysis and Results

C.W. Chu, J. Der, Jr., H. Ziegler

Northrop Corporation Aircraft Division

FINAL REPORT      OCTOBER 1977



Contract N62269-75-C-0537

APPROVED FOR PUBLIC RELEASE;  
DISTRIBUTION UNLIMITED

NAVAL AIR DEVELOPMENT CENTER  
Warminster, Pennsylvania 18974

DDC  
RECEIVED  
JUN 28 1977  
REGISTRY  
D

AD No. \_\_\_\_\_  
DDC FILE COPY

UNCLASSIFIED

SECURITY CLASSIFICATION OF THIS PAGE (When Data Entered)

REPORT DOCUMENTATION PAGE		READ INSTRUCTIONS BEFORE COMPLETING FORM
1. REPORT NUMBER NADC 77157-30	2. GOVT ACCESSION NO.	3. RECIPIENT'S CATALOG NUMBER
4. TITLE (and Subtitle) WAVE DRAG REDUCTION FOR AIRCRAFT FUSELAGE-WING CONFIGURATIONS Volume I. Analyses and Results		5. TYPE OF REPORT & PERIOD COVERED Final 30 June 1975-30 Oct. 1976
7. AUTHOR(s) C. W. Chu, J. Der, Jr., H. Ziegler		6. PERFORMING ORG. REPORT NUMBER NOR 76-190
9. PERFORMING ORGANIZATION NAME AND ADDRESS Northrop Corporation Aircraft Division Hawthorne, CA 90250		8. CONTRACT OR GRANT NUMBER(s) N62269-75-C-0537
11. CONTROLLING OFFICE NAME AND ADDRESS Naval Air Systems Command Washington, D.C.		10. PROGRAM ELEMENT, PROJECT, TASK AREA & WORK UNIT NUMBERS
14. MONITORING AGENCY NAME & ADDRESS (if different from Controlling Office) Naval Air Development Center Warminster, Pennsylvania 18974		12. REPORT DATE October 1976
		13. NUMBER OF PAGES 142
		15. SECURITY CLASS. (of this report) Unclassified
		15a. DECLASSIFICATION DOWNGRADING SCHEDULE
16. DISTRIBUTION STATEMENT (of this Report) Approval for Public Release, Distribution Unlimited		
17. DISTRIBUTION STATEMENT (of the abstract entered in Block 20, if different from Report)		
18. SUPPLEMENTARY NOTES		
19. KEY WORDS (Continue on reverse side if necessary and identify by block number) Wave Drag, Three-Dimensional Flow, Supersonic Flow, Characteristics Methods, Aircraft Fuselage, Wing-Body Configuration, Optimization, Latin Squares, Numerical Method		
20. ABSTRACT (Continue on reverse side if necessary and identify by block number) An optimization procedure has been developed to minimize the wave drag of an aircraft fuselage-wing configuration subject to constraints imposed by design requirements. The theory, methods, computer programs and results are presented in this report in two volumes. Volume I describes analyses, results and the optimization procedure. The procedure makes use of the Latin Square sampling technique and the Three-Dimensional Method of Characteristics. The former is used to efficiently sample the family of configurations, and the latter is used to accurately calculate the		

UNCLASSIFIED

SECURITY CLASSIFICATION OF THIS PAGE (When Data Entered)

UNCLASSIFIED

SECURITY CLASSIFICATION OF THIS PAGE(When Data Entered)

20.

wave drags of the sampled configurations. The calculated wave drag coefficients are then used to derive a functional dependence of the wave drag on the geometric variables that define the family of configurations. The minimum wave drag configuration can be obtained by minimizing the wave drag function subject to a given set of constraints. The wave drag reduction procedure is demonstrated using an F-4 type configuration as the baseline. The results are presented and discussed.

Volume II is the user's manual for the computer programs. The input/output information is described in detail. Listings of the programs are given, and samples of built-in program diagnostic messages are explained. Also included are the logical structures of the programs and the descriptions of the subroutines, which in combination with the program listings can be used for possible future modification, improvement, or extension of these computer programs.

UNCLASSIFIED

SECURITY CLASSIFICATION OF THIS PAGE(When Data Entered)

FOREWORD

This work was performed by the Aerodynamics Research Organization of the Aircraft Division of the Northrop Corporation in Hawthorne, California for the Naval Air Development Center in Warminster, Pennsylvania (Contract No. N62269-75-C-0537) under the auspices of the Naval Air Systems Command. The contract monitor was Mr. Carmen Mazza of NADC, whose cooperation and assistance are gratefully acknowledged. The authors are indebted to Messrs. William Becker, David Bailey and K. T. Yen of NADC for their valuable assistance during the course of this work. Special thanks go to Messrs. Ray Siewert and Louis Schmidt of NASC for their encouragement and interest in the present work.

ACCESSION for	
DTIC	With Serials <input checked="" type="checkbox"/>
DDC	With Serials <input type="checkbox"/>
UNANNOUNCED	<input type="checkbox"/>
JUSTIFICATION	
BY.....	
DISTRIBUTION/AVAILABILITY STATE	
Dist.	AVAIL. and/or SPECIAL
A	

DDC  
RECEIVED  
JUN 28 1977  
D

TABLE OF CONTENTS

<u>Section</u>	<u>Page</u>
1. INTRODUCTION . . . . .	1
2. FORMULATION AND METHODS . . . . .	4
a. Formulation. . . . .	4
b. Latin Square Sampling Technique . . . . .	5
c. Three-Dimensional Method of Characteristics. . . . .	6
3. DESCRIPTION AND VARIATION OF FUSELAGE-WING CONFIGURATION . . . . .	7
a. Body Description . . . . .	7
b. Fuselage and Canopy . . . . .	8
c. Wing and Blending . . . . .	10
d. Geometric Variables and Variations . . . . .	13
4. FLOW FIELD CALCULATION AND WAVE DRAG REDUCTION . . . . .	16
a. Calculation of Flow Fields . . . . .	16
b. Wave Drag Equation . . . . .	18
c. Variation of Wave Drag with Geometric Variables. . . . .	19
d. Optimization and Minimum Wave Drag Body. . . . .	21
e. Summary of Wave Drag Reduction Procedure . . . . .	23
5. CONCLUSIONS . . . . .	25
REFERENCES . . . . .	27
APPENDIX A - WAVE DRAG REDUCTION FOR FORWARD FUSELAGES. . . . .	A1
APPENDIX B - THE LATIN SQUARE METHOD . . . . .	B1
APPENDIX C - BODY DESCRIPTION METHOD. . . . .	C1
APPENDIX D - NUMERICAL SEARCH FOR MINIMUM PROCEDURE . . . . .	D1
APPENDIX E - DEMONSTRATION OF LATIN SQUARE PROCEDURE . . . . .	E1

ILLUSTRATIONS

<u>Figure</u>	<u>Page</u>
1. Schematic of Fuselage and Wing Cross Sections Description . . . . .	30
2. Geometric Variables for Fuselage Variation and Wing-Body Blending . . . . .	31
3. Sample Distributions of Blending Radius $r$ . . . . .	32
4. Pressure Distributions Along Centerlines and Wing Leading Edge of F-4 Type Baseline . . . . .	33
5. Cross Section of F-4 Type Baseline at Fuselage Station 430. . . . .	34
6. Front Views of F-4 Type Baseline Cross Sections. . . . .	35
7. Front Views of Configuration 6 Cross Sections. . . . .	36
8. Cross Section and Pressure Distribution at F. S. 350 of Blended Wing Configuration 6 . . . . .	37
9. Variation of Wave Drag Coefficient $C_{DW}$ vs $a$ ( $r_1 = 1.5, r_2 = 1.5$ ) . . . . .	38
10. Variation of Wave Drag Coefficient $C_{DW}$ vs $a$ ( $r_2 = 1.5, h = 0$ ) . . . . .	39
11. Variation of Wave Drag Coefficient $C_{DW}$ vs $a$ ( $r_1 = 1.5, h = 0$ ) . . . . .	40
12. Variation of Wave Drag Coefficient $C_{DW}$ vs $h$ ( $r_1 = 1.5, r_2 = 1.5$ ) . . . . .	41
13. Variation of Wave Drag Coefficient $C_{DW}$ vs $h$ ( $a = 1.0, r_2 = 1.5$ ) . . . . .	42
14. Variation of Wave Drag Coefficient $C_{DW}$ vs $h$ ( $a = 1.0, r_1 = 1.5$ ) . . . . .	43
15. Variation of Wave Drag Coefficient $C_{DW}$ vs $r_1$ ( $r_2 = 1.5, h = 0$ ) . . . . .	44
16. Variation of Wave Drag Coefficient $C_{DW}$ vs $r_1$ ( $a = 1.0, r_2 = 1.5$ ) . . . . .	45
17. Variation of Wave Drag Coefficient $C_{DW}$ vs $r_1$ ( $a = 1.0, h = 0$ ) . . . . .	46
18. Variation of Wave Drag Coefficient $C_{DW}$ vs $r_2$ ( $r_1 = 1.5, h = 0$ ) . . . . .	47
19. Variation of Wave Drag Coefficient $C_{DW}$ vs $r_2$ ( $a = 1.0, r_1 = 1.5$ ) . . . . .	48
20. Variation of Wave Drag Coefficient $C_{DW}$ vs $r_2$ ( $a = 1.0, h = 0$ ) . . . . .	49
21. Front View of a Minimum Wave Drag Body . . . . .	50
22. Minimum Wave Drag Configurations for Various Volumes (% of Baseline Volume) . . . . .	51

TABLES

<u>Table</u>	<u>Page</u>
1. Latin Square Arrangement . . . . .	28
2. Variables, Ranges, and Baseline Values . . . . .	28
3. Wave Drag Coefficients $C_{DW}$ . . . . .	29
4. Coefficients of Wave Drag Equation . . . . .	29

## LIST OF SYMBOLS

$a$	Horizontal displacement of the maximum breadth line
$a_0, a_1, a_{ij}$	Coefficients of wave drag Equation (1)
$b_0, b_1, b_{ij}$	Coefficients of wave drag Equation (28)
$b$	Shape factor for the lower fuselage cross section
$C_{DW}$	Wave drag coefficient
$C_p$	Pressure Coefficient
$f$	Width of the fuselage bottom flat
$h$	Height of the lower deck
$l$	Length of the fuselage nose
$P_j, Q_j, R_j, S_j, T_j$	Coefficients for the $j$ th generating line
$r_1, r_2$	Blending radius
$Vol$	Volume of the fuselage
$Vol_{BL}$	Volume of the baseline fuselage
$X, Y, Z$	Rectangular coordinates
$x_i$	$i$ th geometric variable
$X_j(Y)$	Projection of the $j$ th line on the X-Y plane
$z_i$	$i$ th reduced variable
$Z_j(Y)$	Projection of the $j$ th line on the Y-Z plane

1. INTRODUCTION

Wave drag reduction is one of the important goals of designing a high performance aircraft capable of operating in the supersonic regime. Since there are many design requirements which conflict with one another as far as wave drag reduction is concerned, an optimization procedure is needed to determine the minimum wave drag configuration subject to the constraints imposed by these requirements. Until recently, the procedure relied heavily on experience gained through extensive wind tunnel testing of various geometries. Such a design procedure, which usually could not be carried out systematically, was expensive and time consuming. However, the advances of recent years in numerical methods and computer technology have made feasible systematic optimization procedures using exact numerical methods. Consequently, a wave drag reduction procedure using the method of characteristics has been developed which is presented in this report.

The present wave drag reduction procedure makes use of two basic methods: the Latin Square sampling technique and the Three-Dimensional Method of Characteristics. The former is used to select sample configurations so efficiently that a small number of samples can well represent the entire family of configurations. The latter is used to calculate accurately the wave drags of the sampled configurations. Briefly stated, the present approach consists of calculating the wave drag of a baseline configuration and some variations specified by the Latin Square sampling technique, determining a functional dependence of the wave drag on these variation parameters, and minimizing this wave drag function to obtain the configuration with minimum wave drag. The procedure is general with respect to the number of geometric parameters (or variables); the higher the number, the larger the required Latin-Square size. The computer programs developed under this study cover the most often used 3 x 3 and 5 x 5 Latin Squares.

## Best Available Copy

The complete wave drag reduction program has been carried out in two phases. In the first phase, a procedure was developed for minimizing the wave drag of a forward fuselage and canopy configuration as reported in Reference 1. In the second phase, the procedure has been expanded to account for the influence of the wing and wing-body blending on the overall wave drag. In this final report, the research performed under the wave drag reduction contract is presented. The phase I work, which was reported in Reference 1, is included as Appendix A for ready reference, whereas the main text of the report presents the phase II work and touches upon some of the phase I work. A 3 x 3 Latin Square was used in phase II and a 5 x 5 Latin Square in phase I. The surface fitting method using Latin Squares as presented in Reference 2 was improved during the phase I study; the improvement which is presented in Appendix A, is essential for the success of the optimization procedure (here applied to wave drag reduction). The procedure using the improved Latin Square surface fitting method has been proven in both phases through application to the F-4 configuration. For further validation of the procedure, it was applied to the von Karman ogive. For given configuration length and base, the present optimization procedure correctly predicted the von Karman ogive as the minimum wave drag body.

In this report, the basic approach is given first, which consists of the formulation of the problem and a brief account of the two basic methods. It is followed by a discussion of the method of describing the body and the selection of geometric variables and their ranges for defining a family of configurations. Then the flow field calculation and the wave drag equation are presented. Sample results of the calculated flow fields are given, and calculated wave drag coefficients are tabulated. These coefficients were used to derive the wave drag equation which expresses the wave drag as a function of the geometric variables. Once the wave drag equation is obtained, the dependence of the wave drag on the geometric variables is established.

## Best Available Copy

A set of figures are given to illustrate some of the characteristics of the wave drag equation. This is followed by a presentation of the optimization procedure and the prediction of the minimum wave drag body. Finally, conclusions are drawn and some recommendations given. The Latin Square technique including the method of construction is presented in Appendix B. A discussion of the general body description method is given in Appendix C. The Numerical Search Procedure for the minimum wave drag configuration is presented in Appendix D. The validation of the optimization procedure using the von Karman ogive is presented in Appendix E.

2. FORMULATION AND METHODS

The wave drag of a configuration is a function of a number of factors. For given flight conditions the wave drag depends on how the configuration is shaped. Since the shape of an aircraft, at least in the initial design phase, is mainly determined by considerations other than the wave drag, it is practical to consider the problem of reducing the wave drag of a given baseline configuration by obtaining a variation configuration that satisfies all the design constraints yet has the least wave drag. Such a baseline configuration could be a new configuration at a certain stage of development or it could be an existing airplane that is to be modified or improved.

In this section, the formulation of the wave drag reduction problem is outlined, and the two basic methods to be used in this study are introduced.

a. Formulation

The baseline configuration can be described by a set of geometric variables. A family of configurations including the baseline can be generated by assigning different values to some or all of the geometric variables. If the wave drag can be expressed as a function of these variables, a particular set of values of these variables that gives the least wave drag can be found by minimizing the function. This set of values then produces the minimum wave drag configuration.

The key to this problem is how to obtain such a functional expression for the wave drag. For the present study, four geometric variables are considered in defining the family of configurations. If each variable assumes three values, the evaluation of the partial derivatives with respect to these four variables for a Taylor-series type expression would require 81 wave drag calculations. It will be shown that through Latin Square sampling the present procedure proves useful using only

10 wave drag calculations. In the present approach, the wave drag coefficient  $C_{DW}$  is first assumed to be of the form

$$C_{DW} = a_0 + \sum_{i=1}^4 (a_i x_i + a_{ij} x_i^2) + a_{23} x_2 x_3 \quad (1)$$

where  $x_i$  ( $i = 1, 4$ ) are the geometric variables and  $a_i$  and  $a_{ij}$  are to be determined. The Latin Square sampling technique<sup>2</sup> is used to sample 9 sets of values of  $x_i$  out of the total population of 81 sets. The wave drag coefficients for the F-4 type baseline and the configurations defined by each of the 9 sets are then calculated by the Three-Dimensional Method of Characteristics.<sup>3, 4</sup> When the 10 calculated wave drag coefficients  $C_{DW}$  and the corresponding values of the geometric variables  $x_i$  are substituted into Equation 1, 10 linear equations for the 10 unknowns  $a_i$  and  $a_{ij}$  are obtained. These equations are then solved for the  $a_i$  and  $a_{ij}$ , which are substituted back into Equation 1 to produce the functional expression for the wave drag in terms of the geometric variables. By minimizing  $C_{DW}$  in Equation 1 subject to a given set of constraints, e. g., a given volume of the aircraft, the minimum wave drag configuration corresponding to the given set of constraints is determined. In the present study, a numerical search procedure is used to find the minimum wave drag configuration (Appendix D).

#### b. Latin Square Sampling Technique

The Latin Square method, which has mostly been used in agriculture and biological research, is a very efficient sampling technique and is much better than random sampling.\* For this study a particular type of Latin Square (the orthogonal squares) suitable for a variety of technical problems<sup>2</sup> is adopted. With this type of Latin Square arrangement, a 3 x 3 square is the correct size for four geometric variables  $x_i$ , each taking three values. It is convenient to introduce the reduced

\*See Appendix B.

variables  $z_i$ , which are related to the geometric variable  $x_i$  through

$$x_i = \frac{x_{i \max} + x_{i \min}}{2} + \frac{z_i (x_{i \max} - x_{i \min})}{2} \quad (2)$$

where subscripts max and min denote the maximum and minimum values, respectively. Corresponding to the three values of the geometric variables  $x_i$ , the reduced variables  $z_i$  always assume the three levels of 0,  $\pm 1$ . The 3x3 Latin Square arrangement in terms of the levels of the reduced variables and the cell number is shown in Table 1.\* It is seen that in this way, the Latin Square arrangement remains the same whatever the values of the geometric variables.

#### c. Three-Dimensional Method of Characteristics

In this study the Three-Dimensional Method of Characteristics<sup>3,4</sup> is used to calculate the wave drag coefficients for the fuselage-wing configurations sampled by the Latin Square technique. This method has been previously applied to calculate the flow fields over a wide variety of configurations including spherically-capped three-dimensional bodies and wings<sup>5</sup>, aircraft fuselages and wings at general angles of attack,<sup>6</sup> and slab delta wings and space shuttle wing-body configurations.<sup>7-9</sup> Whenever experimental data were available for comparison, good agreement between theory and experiments was observed. The capability of treating the canopy, however, was developed during phase I of this study.

In a related research program, the Three-Dimensional Method of Characteristics was further extended and improved to treat realistic aircraft wing-body configurations including wing-body blending. With some modification and adaptation, this improved method was applied to calculate the flow fields and wave drags of the variation configurations.

---

\*A discussion of the Latin Square construction is given in Appendix B.

### 3. DESCRIPTION AND VARIATION OF FUSELAGE-WING CONFIGURATION

Three-dimensional body description requires a great deal of effort which at times becomes extremely tedious. Basically, two types of description can be made, analytical and numerical. The latter can describe complicated geometry accurately, but is cumbersome for preparing input data. The former is much simpler to input and can define a family of configurations based on a few geometric variables. Hence, analytical description is chosen for the present study.

#### a. Body Description

Every configuration has a number of generating lines, such as the upper profile, the lower profile, the maximum breadth line, or the wing leading edge. In the present body description procedure, each generating line is divided into a number of segments to permit each segment to be described by a conic-section curve. At each cross section of the configuration, simple analytic curves, e. g., the ellipse or cubic, connect any two adjacent generating lines to form the contour of the cross section. The configuration is thus described analytically by simple low-order curves. For a smooth body a unique normal to the surface exists everywhere, and this condition usually requires slope continuity at the junctures between two contour curves or two segments of a generating line.

The fuselage is located in a right-handed coordinate system where the Y-axis is aligned with the fuselage axis; the X-axis is spanwise and the Z-axis is up. All generating lines are represented by a general curve fit of conic sections in several segments. The conic-section curve takes the form

$$\begin{pmatrix} Z \\ X \end{pmatrix} = P Y + Q \pm \left( R Y^2 + S Y + T \right)^{1/2} \quad (3)$$

A straight line is a special case with  $R = S = T = 0$ . Each curve can

be divided into as many segments as necessary to provide adequate body description. Each segment must be continuous with the previous segment and with very few exceptions the slope must be continuous at the junctures to satisfy the requirement of a unique normal to the surface.

A typical cross section of the wing-body configuration is shown schematically in Figure 1. The contour of the cross section begins with a straight line representing the canopy flat. The canopy contour from points C to  $\phi$  is circular but can be elliptic in general. The upper fuselage is represented by an elliptic curve from points U to M. A straight side flat from points M to  $F_f$  joins the upper fuselage to the lower fuselage, which is also represented by an elliptic curve from  $F_f$  to L. A straight line from point L to the centerline describes the bottom flat. For the description of the wing, straight lines EG and FH represent the upper and lower surfaces of the wing, respectively. Partial ellipses GI and HI complete the wing description near the leading edge I. The wing-body blending is effected by circular arcs 34 and 56 with radii  $r_U$  and  $r_L$ , respectively. A further discussion of the body description method illustrated by the description of the fuselage and canopy of Phase I is presented in Appendix B.

b. Fuselage and Canopy

The equation of the canopy is given by

$$\left[ \frac{Z - Z_\phi(Y)}{Z_\phi(Y) - Z_c(Y)} \right]^2 + \left[ \frac{X - X_\phi(Y)}{X_c(Y) - X_\phi(Y)} \right]^2 - 1 = 0 \quad (4)$$

If it is a circular arc, then  $(Z_\phi - Z_c)^2 = (X_c - X_\phi)^2$ . The equation for the upper fuselage is

$$\left[ \frac{Z - Z_M(Y)}{Z_U(Y) - Z_M(Y)} \right]^2 + \left[ \frac{X - X_U(Y)}{X_M(Y) - X_U(Y)} \right]^2 - 1 = 0 \quad (5)$$

The intersection between the canopy and fuselage is faired by a cubic from points 1 to 2 (Figure 1). The projections  $Z_1(Y)$  and  $Z_2(Y)$  of lines 1 and 2 on the Y-Z plane are given by Equation 3 where the coefficients P, Q, R, S, T are input quantities. The projections  $X_1(Y)$  and  $X_2(Y)$  on the X-Y plane are obtained by solving Equations 4 and 5, respectively.

$$X_1(Y) = X_C + (X_\phi - X_C) \left[ 1 - \left( \frac{Z_1 - Z_\phi}{Z_C - Z_\phi} \right)^2 \right]^{1/2} \quad (6)$$

$$X_2(Y) = X_U + (X_M - X_U) \left[ 1 - \left( \frac{Z_2 - Z_M}{Z_U - Z_M} \right)^2 \right]^{1/2} \quad (7)$$

The fairing curve matches the slopes of the ellipses at both end points 1 and 2. The slopes are obtained by differentiation of Equation 4 and 5

$$X'_1(Y) = \left( \frac{\partial X}{\partial Z} \right)_1 = - \left( \frac{Z_1 - Z_\phi}{X_1 - X_C} \right) \left( \frac{X_C - X_\phi}{Z_C - Z_\phi} \right)^2 \quad (8)$$

$$X'_2(Y) = \left( \frac{\partial X}{\partial Z} \right)_2 = - \left( \frac{Z_2 - Z_M}{X_2 - X_U} \right) \left( \frac{X_U - X_M}{Z_U - Z_M} \right)^2 \quad (9)$$

The cubic equation that satisfies Equations 6 and 8 can be written

$$X = X_1 + X'_1 (Z - Z_1) + c \left( \frac{Z - Z_1}{Z_2 - Z_1} \right)^2 + d \left( \frac{Z - Z_1}{Z_2 - Z_1} \right)^3 \quad (10)$$

The coefficients c and d are obtained by applying Equations 7 and 9

$$c = 3 (X_2 - X_1) - (X'_2 + 2X'_1) (Z_2 - Z_1) \quad (11)$$

$$d = -2(X_2 - X_1) + (X'_2 + X'_1) (Z_2 - Z_1) \quad (12)$$

Equation 10 with c and d given by Equations 11 and 12 is then the cubic equation for

the fairing curve from points 1 to 2. The quantities  $X_1$ ,  $X_2$ ,  $X_1'$  and  $X_2'$  are given by Equations 6 and 7 while  $X_U$ ,  $X_M$ ,  $X_C$ ,  $X_\phi$ ,  $Z_U$ ,  $Z_M$ ,  $Z_C$ ,  $Z_\phi$ ,  $Z_1$ , and  $Z_2$  are obtained from Equation 3 where coefficients P, Q, R, S and T are input quantities.

The lower fuselage is described by an equation similar to Equation 5

$$\left[ \frac{Z - Z_{F_f}(Y)}{Z_L(Y) - Z_{F_f}(Y)} \right]^2 + \left[ \frac{X - X_L(Y)}{X_{E_f}(Y) - X_L(Y)} \right]^2 - 1 = 0 \quad (13)$$

All flats are given by simple straight-line equations.

c. Wing and Blending

The upper and lower surfaces of the wing are given by straight-line equations for E G and F H. Near the leading edge I, the partial ellipses G I and H I are derived as follows. The equation may be written in the form

$$\frac{(X - X_I + a)^2}{a^2} + \frac{(Z - Z_I)^2}{b^2} = 1 \quad (14)$$

where a and b are the axes to be determined. Differentiation of Equation 14 gives

$$\frac{X - X_I + a}{a^2} + \frac{Z - Z_I}{b^2} \frac{dZ}{dX} = 0 \quad (15)$$

at point G,  $X = X_G$ ,  $Z = Z_G$ , and  $\frac{dZ}{dX} = \left( \frac{dZ}{dX} \right)_G$ , which is the slope of line E G. Substituting these values into Equation 14 and 15 leads to

$$\frac{(X_G - X_I + a)^2}{a^2} + \frac{(Z_G - Z_I)^2}{b^2} = 1 \quad (14a)$$

$$\frac{X_G - X_I + a}{a^2} + \frac{X_G - Z_I}{b^2} \left( \frac{dZ}{dX} \right)_G = 0 \quad (15a)$$

Elimination of  $b^2$  from Equations 14a and 14b yields

$$a = \frac{(X_G - X_I)^2 \left( \frac{dZ}{dX} \right)_G - (X_G - X_I)(Z_G - Z_I)}{Z_G - Z_I - 2(X_G - X_I) \left( \frac{dZ}{dX} \right)_G} \quad (16)$$

Elimination of  $a^2$  from Equations 14a and 14b leads to

$$b^2 = (Z_G - Z_I)^2 - (Z_G - Z_I)(X_G - X_I + a) \left( \frac{dZ}{dX} \right)_G \quad (17)$$

where  $a$  is given by Equation 16. Equation 14 with  $a$  and  $b$  given by Equations 16 and 17 describes the partial ellipse G I. By changing the subscript G to H, the equation for the partial ellipse H I is obtained.

The projections of lines passing through E, F, G, H and I on the Z-Y plane and X-Y plane are input quantities for defining the wing. In order for the partial ellipses to exist, points G and H must be located within a certain range, which depends on the relative positions of these five points. When the wing span is very small, it is difficult to input both projections of lines through G and H such that these points are located within acceptable ranges. In such cases, the X coordinates of G and H are calculated inside the program to satisfy the range requirement.

The upper and lower blendings between the fuselage and the wing are described by circular arcs with radii  $r_U$  and  $r_L$ , respectively. When the blending radii  $r_U$  and  $r_L$  are specified by geometric variables (see Section 3d.), points 3 and 5 of Figure 1 can be obtained numerically through an iteration procedure. However, in order to obtain analytical normals to the blending surface, an analytic expression must be derived. Hence, the following procedure was used and is illustrated by the upper blending. The numerically obtained line passing through point 3 is considered a generating line. The projection  $Z_3$  (Y) on the Y - Z plane is expressed in the form of Equation 3, where

the coefficients are input quantities. At a given fuselage station,  $X_3(Y)$  are obtained by solving Equation 5.

$$X_3(Y) = (X_M - X_U) \left[ 1 - \left( \frac{Z_3 - Z_M}{Z_U - Z_M} \right)^2 \right]^{1/2} + X_U \quad (18)$$

The slope of the tangent at point 3 can also be obtained from Equation 5 as

$$M_3 = - \left( \frac{Z_U - Z_M}{X_M - X_U} \right)^2 \left( \frac{X_3 - X_U}{Z_3 - Z_M} \right) \quad (19)$$

Thus, the equation of the tangent  $\overline{3P}$  (see Figure 1) at point 3 is given by

$$Z = M_3 (X - X_3) + Z_3 \quad (20)$$

The equation of line EG can be written as

$$Z = M_4 (X - X_E) + Z_E \quad (21)$$

$$\text{where } M_4 = \frac{Z_G - Z_E}{X_G - X_E} \quad (22)$$

Intersection P of these two lines is obtained from Equations 20 and 21

$$\begin{cases} X_p = \frac{Z_E - Z_3 + M_3 X_3 - M_4 X_E}{M_3 - M_4} \\ Z_p = \frac{M_3 Z_E - M_4 Z_3 + M_3 M_4 (X_3 - X_E)}{M_3 - M_4} \end{cases} \quad (23)$$

The equation of the line bisecting the angle  $\angle 3PG$  is given by:

$$Z = M_5 (X - X_p) + Z_p \quad (24)$$

$$\text{where } M_5 = \tan \left( \frac{\pi + \tan^{-1} M_3 + \tan^{-1} M_4}{2} \right) \quad (24a)$$

and  $M_3$  is given by Equation 19 and  $M_4$  by Equation 22. The intersection between the bisecting line and the normal at point 3

$$X - X_3 + M_3(Z - Z_3) = 0 \quad (25)$$

is the center 0 of the arc; hence from Equations 24 and 25

$$\left\{ \begin{array}{l} X_0 = \frac{X_3 + M_3 Z_3 + M_3(M_5 X_p - Z_p)}{1 + M_3 M_5} \\ Z_0 = \frac{Z_p - M_5 X_p + M_5(X_3 - M_3 Z_3)}{1 + M_3 M_5} \end{array} \right. \quad (26)$$

where  $X_p$  and  $Z_p$  are given by Equation 23,  $M_3$  by Equation 19 and  $M_5$  by Equation 24a. The equation of the circular arc for the upper blending is thus

$$(X - X_0)^2 + (Z - Z_0)^2 = (X_0 - X_3)^2 + (Z_0 - Z_3)^2 = R_U^2 \quad (27)$$

where  $X_0$  and  $Z_0$  are given by Equation 26. Notice that the radius  $R_U$  is slightly different from  $r_U$  because of slight errors introduced by the iteration procedure in obtaining point 3 and by the fitting of the generating line passing through that point.

#### d. Geometric Variables and Variations

Four geometric variables were selected to generate a family of fuselage-wing configurations including the F-4 baseline. As illustrated in Figure 2, these variables are the horizontal displacement  $a$  of the maximum horizontal breadth line, the lower deck height  $h$  (which increases as the lower profile is raised), and the blending radii  $r_1$  and  $r_2$  at F. S. 280 and F. S. 360, respectively. All configurations generated by these variables have the same canopy as the F-4 and must satisfy the over-the-side view line limitation. The correspondence between

the geometric variables and the reduced variables defined in Equation 2, the ranges of variation of these geometric variables, and the baseline values of these variables are tabulated in Table 2.

The geometric variables specify the blending radii at two fuselage stations only. In order to fully describe the blending between the fuselage and wing, a procedure is needed to provide the blending radius systematically at any given fuselage station in the blending region. The blending radius distribution as a function of the fuselage station must satisfy the following conditions:

1. At fuselage stations 220 or 430, the radius is equal to the minimum radius of the baseline.
2. At F.S. 280 and F.S. 360, they are equal to  $r_1$  and  $r_2$ , respectively.
3. Between F.S. 280 and F.S. 360, the radius must not overshoot; i. e., it must not exceed the greater of  $r_1$  and  $r_2$ .
4. When  $r_1$  and  $r_2$  are equal to the minimum radius, the baseline must be recovered; i. e., the radius must be constant throughout.
5. When either  $r_1$  or  $r_2$  is equal to the minimum radius, the blending radius must not undershoot anywhere.

Figure 3 illustrates some of the possible radius distributions and serves as a reference for the following discussion of the procedure. The radius distribution is given by three cubic interpolation formulas for the three intervals. The slope of the distribution curve is zero at F.S. 220, 280 and 360 for  $r = 1.5$  and at F.S. 280 and 360 for  $r = 61.5$ . At F.S. 280 the slope at  $r = 46.5$  is assumed to be equal to that of the straight line  $S_1$ . At any other  $r$  the slope is obtained from a spline fit of the slope versus  $r$  in such a way that the spline curve passing through these three points with assumed zero curvature at both end points. The slopes at F.S. 360 are obtained in an analogous way. Thus, for a given pair of  $r_1$  and  $r_2$ , the radius distribution curve is determined by three cubic interpolation formulas: the first cubic passes through

$r = 1.5$  at F.S. 220 with a zero slope and  $r = r_1$  at F.S. 280 with a slope given by the spline fit; the second cubic passes through  $r = r_1$  at F.S. 280 with the same slope as the first cubic and through  $r = r_2$  at F.S. 360 with a slope given by the second spline fit; the third cubic passes through  $r = r_2$  at F.S. 360 with the same slope as the second cubic and through  $r = 1.5$  at F.S. 430 with an assumed zero curvature. The radius distribution curve as composed of these cubics are then described by conic-section curves for input into the computer programs.

While the lower blending radius could be varied, its range would be very much limited in the case of the F-4. Therefore, a fixed lower blending is used to assure a smooth body for the 3DMoC calculations. This blending is specified by assigning a fixed distance between points 5 and F (see Figure 1).

#### 4. FLOW FIELD CALCULATION AND WAVE DRAG REDUCTION

Once the geometric variables and their ranges of variation have been selected, the fuselage-wing configurations corresponding to the nine cells of the 3 x 3 Latin Square can be described. The Three-Dimensional Method of Characteristics together with a blunt body program for providing the initial data surface can then be used to calculate the flow fields around and hence wave drag coefficients of these variation configurations. The wave drag coefficients, in turn, can be used to determine the coefficients of the wave drag equations (1), from which the dependence of the wave drag on various geometric variables and the minimum wave drag body can be obtained.

##### a. Calculation of Flow Fields

The Three-Dimensional Method of Characteristics program together with a blunt body and axisymmetric characteristic program was used to calculate the flow fields around the baseline F-4 type fuselage-canopy-wing configuration and the variation configurations corresponding to the cells of the Latin Square. The wave drag coefficients were computed as part of the results to be printed out. Since the fuselage nose is slightly blunted, the blunt body and axisymmetric characteristic program was used to provide a completely supersonic initial data surface for the Three-Dimensional Method of Characteristics program to proceed. The flow-field calculations were made at Mach 2.5 and zero angle of attack. Since the wing leading edge section is described by an ellipse with a large major-to-minor axes ratio (Equation 14) the leading edge is theoretically blunt. In order to provide completely supersonic flow for the characteristics method to calculate, the leading edge must be subsonic. At Mach 2.5, a subsonic leading edge has a sweep angle greater than  $66.42^\circ$ . Hence a configuration with a leading edge sweep of  $68^\circ$  was chosen, which is greater than F-4's leading edge sweep of about  $51^\circ$ . Fortunately, the main geometric change that is expected to yield appreciable drag reduction is the wing-body

blending which does not extend to the region near the leading edge. Therefore, modified wings with considerable increases in the wing sweep can be used for the present wave drag reduction study without appreciably affecting the results.

As an example of the flow fields calculated by using the Three-Dimensional Method of Characteristics, the flow over the F-4 type baseline at Mach 2.5 and zero angle of attack is presented here. Figure 4 shows the top view of the configuration, the upper and lower centerline pressure distributions and the pressure along the wing leading edge. Along the upper centerline of the configuration, the pressure rises sharply as the flow hits the canopy-fuselage juncture. This signifies the existence of an embedded shock wave created by the canopy. As the flow spreads over the canopy flat section, the pressure drops although the canopy profile is almost straight. A further drop of pressure is experienced as the canopy profile curves back after the flat section. It recovers to near free-stream pressure as the wing leading edge pressure rises. Along the lower centerline the  $C_p$  first drops to a negative value due to further expansion. It recovers somewhat and eventually comes close to zero, consistent with the condition of zero angle of attack. The wing begins with a high sweep, which decreases to a constant value of  $68^\circ$  near F.S. 190. Correspondingly, the slightly higher than free-stream pressure is observed at the beginning of the wing. Because of the wing-body interaction, almost immediately the wing leading edge pressure drops and does not recover until after F.S. 200 when the wing sweep drops to  $68^\circ$  and the larger wing span lessens the interaction. A cross section of the baseline configuration at F.S. 430 is shown in Figure 5; the wing has become very thin and it is thicker near the leading edge than near the root. The front view of the baseline configuration is shown in Figure 6.

Of all the variation configurations, configuration 6 has the maximum wing-body blending. The front view of this configuration is shown in Figure 7. A cross-sectional view at F.S. 350 is shown in Figure 8 together with surface pressure

distribution. At this fuselage station, the blending is nearly maximum, as compared with the baseline cross section shown by a dashed line. At F. S. 350 the blending radius is still increasing; however, the rate of increase has dropped to a very small value. That means expansion has set in upstream of F. S. 350, resulting in a negative  $C_p$  in the blending region as shown.

b. Wave Drag Equation

As shown in Equation (1), for a given Mach number and angle of attack, the wave drag coefficient  $C_{DW}$  is assumed to be a quadric function of the four chosen geometric variables  $x_1, \dots, x_4$  with the coefficients  $a_i$  and  $a_{ij}$  to be determined. The reduced variables  $z_i$ , which take the levels of 0, and  $\pm 1$  according to the Latin Square arrangement shown in Table 1, assign corresponding values to the geometric variables  $x_i$ . For instance, according to the first cell,  $z_1$  and  $z_4$  are assigned level -1, which corresponds to the minimum values of the geometric variables  $x_1$  and  $x_4$  while  $z_2$  is assigned level 1, which corresponds to the maximum value of  $x_2$ , and  $z_3$  is assigned level 0 corresponding to the mean value of the geometric variable  $x_3$ . Thus the first cell specifies a set of values for the geometric variables which in turn defines a configuration whose wave drag coefficient can then be calculated by the method of characteristics program. In this way, each cell leads to one equation for the determination of the coefficients of the wave drag equation.

The wave drag coefficients of the baseline and the 9 variation configurations are tabulated in Table 3. These will be used to determine the wave drag equation in terms of the reduced variables in the form

$$C_{DW} = b_0 + \sum_{i=1}^4 (b_i z_i + b_{ii} z_i^2) + b_{23} z_2 z_3 \quad (28)$$

It should be noted that in the original Latin Square surface fitting method presented in Reference 2, two of the geometric variables have only linear terms resulting in only 8 coefficients  $b_i$  and  $b_{ij}$  for 10 equations and these equations are solved by a least square procedure. However, while the requirement of 2 linear variables can be relaxed (see Appendix A) in the case of 5 x 5 Latin Squares, this requirement does not seem to apply to the case of 3 x 3 Latin Squares. In fact, in the present case, these 10 equations were used to solve for the set of 10 unknowns  $b_i$  and  $b_{ij}$  that included  $z_1^2$  and  $z_4^2$  in addition to the original 8 coefficients. The resulting coefficients of the wave drag equation are tabulated in Table 4.

c. Variation of Wave Drag with Geometric Variables

It is instructive as well as useful to represent the wave drag equation graphically. However, since the wave drag depends on four geometric variables, it is only possible to show the variation of the wave drag coefficient with respect to two of the variables while keeping the other two variables constant, for instance, at the baseline values. Such graphs give some "feel" of the wave drag equation and may offer some insight about the wave drag reduction problem. Figures 9 to 20 depict the nature of the wave drag equation of ten terms with coefficients given in Table 4. These graphs were plotted on a Tektronix equipment. Each graph has five curves that correspond to five values of the geometric variable shown at the top of the graph; these values equally divide the range which is shown in Table 2.

Figures 9 to 11 show the variation of the wave drag coefficient with respect to the width  $a$ , which is normalized with respect to the baseline width. As might be expected, the wave drag coefficient increases with the width of the configuration. The curves are fairly straight, indicating that the wave drag is nearly proportional to the width of the configuration, other conditions being equal. In general, 1% increase of the width increases the wave drag by 0.35%. The dependence of the

wave drag coefficient on the other variables can be seen to be far from linear since the distances between the curves are quite different from one another. The dependence of the wave drag coefficient on the lower deck height  $h$  is shown in Figures 12 to 14. Since the lower profile rises with increasing values of  $h$ , the wave drag coefficient decreases with  $h$ . It is interesting to note that the wave drag attains a minimum at about  $h = 1.2$ , which represents a slight rise of the lower profile from  $h = 0$ . All the curves are nearly flat near  $h = 0$ , suggesting that a slight change of the position of the lower profile has little effect on the wave drag. Note that the curves in any of the figures from Figures 9 to 14 are parallel to one another, because the 10-term wave drag equation contains no cross terms of these variables except  $r_1 r_2$ , which represents the interaction between the two blending radii  $r_1$  and  $r_2$ . When more configurations are included during the progress of the optimization procedure, other cross terms could be included, as explained in Appendix A. However, the interaction between these other variables are expected to be small. This observation was arrived heuristically but has been verified by the ability of Equation 28 to accurately predict the minimum wave drag body as will be shown. The next three figures 15 to 17 show the variation of the wave drag coefficient with  $r_1$ , the blending radius at F.S. 290, for different values of one of the other three variables while the remaining two take the baseline values. Similarly, the variation of the wave drag coefficient with  $r_2$ , the other blending radius at F.S. 360, are shown in Figures 18 to 20. Although all these figures show a general increase of the wave drag coefficient with the blending radius, there is a definite trend for the curves to attain a minimum within the ranges. Most minima occur at the lower side of the radius scale: sometimes it may even reach 15 inches as shown in Figure 20. The occurrence of these minima is significant because this shows that the volume of a wing-body configuration can be increased by using wing-body blending without increasing the wave drag and that when the blending is done properly, the volume can be increased with an accompany-

ing reduction in the wave drag. Some interaction between  $r_1$  and  $r_2$  is evident in Figures 17 and 20, as indicated by the cross over of two or more curves.

d. Optimization and Minimum Wave Drag Body

The wave drag equation can now be investigated to reduce the wave drag. In the process of determining the minimum wave drag configuration, certain geometric constraints, such as minimum fuselage width or a given lower deck height, must be satisfied. For each set of geometric constraints, there exists a minimum wave drag configuration. In this section, the optimization procedure and some minimum wave drag configurations are presented and discussed. During phase I study, a technique was developed (see Appendix A) that greatly improves the original Latin Square surface fitting method of Reference 2, especially for 5 x 5 or larger Latin Squares. The improved optimization procedure using the improved Latin Square surface fitting method is verified in Appendix E.

The simplest and surest way to find the minimum wave drag configuration subject to a given set of geometric constraints is to use Equation 13 to calculate the wave drag coefficients for all allowable sets of levels of the variables and pick the set that gives the least wave drag. The optimization procedure consists of the following steps.\*

1. Make a numerical search through the ranges of all geometric variables, using the wave drag equation to calculate the wave drag coefficients for those sets of levels that satisfy the constraints.
2. Identify the set of levels of the variables that yields the least wave drag.
3. Prepare body description input data for the minimum wave drag configuration.
4. Use the Three-Dimensional Method of Characteristics program to verify

\*The Numerical Search Procedure for 5x5 Latin Squares is presented in Appendix C: it holds true for 3x3 Latin Squares when the space dimension is lowered from 6 to 4.

the prediction of the wave drag equation.

5. If the difference between the predicted and calculated wave drag coefficients exceeds a certain criterion, the calculated wave drag coefficient provides an additional equation for the least square fit, and the optimization procedure is repeated.

For the wave drag reduction problem of the fuselage-wing configuration, as we are concerned with in phase II, two types of constraints are considered. The first corresponds to setting one or more of the variables to a desired value. The second corresponds to assigning a fixed volume to the configuration, for instance, a certain percentage of the baseline volume. When two of the variables are set to the baseline values, any of the figures from Figures 12 to 20 provides one or more minimum wave drag bodies. In this respect these figures can be quite useful. When no constraints other than the range limitations are imposed, the wave drag equation predicts a minimum wave drag body that corresponds to 90% of the baseline width, a raise of the lower profile by 1.2 inches and a blending radius of 3.52 inches at F.S. 280 and 7.65 inches at F.S. 360 (Figure 21). With this configuration, a reduction of wave drag by 4.54% is predicted. The body description input data for this minimum wave drag configuration was then prepared for the verification run by the Three-Dimensional method of Characteristics program. The results showed a 4.35% reduction of wave drag. The difference between the predicted and calculated wave drag reductions is within the accuracy of the procedure; therefore, the validity of the 10-term wave drag equation is established. Figure 22 shows the minimum wave drag configurations for various volume constraints. The percent of wave drag increase was plotted against increasing volumes expressed as percent of the baseline volume. The values of the geometric variables that define the minimum wave drag configurations are also plotted. It is seen that a certain amount of wing-body blending is present for all minimum wave drag configurations. For

a given volume, the forward fuselage becomes more slender to yield lower wave drag, and the lost volume is compensated for by the volume gained through wing-body blending.

e. Summary of Wave Drag Reduction Procedure

The present procedure can be used to improve an existing aircraft or to aid in the design of a new one. In the case of improvement, the existing aircraft naturally serves as the baseline. In the case of new design, the preliminary configuration, which is usually obtained through considerations other than the wave drag, can serve as the baseline for wave drag reduction.

The next step is to select either the 5 x 5 Latin Square for the forward fuselage or the 3 x 3 Latin Square for the blended wing configuration and to describe the baseline and variation configurations using the body description method presented in Appendix C. The sections on the description and variation of configuration in Appendix A or the main text should be consulted in producing the body description. This step is time-consuming but must be done carefully to assure success in wave drag calculations by the method of characteristics.

Input cards are then prepared according to the instructions given in part 1 and 2 of the user's manual (volume II of this report) and fed to the Initial Value Surface Program and the Three-Dimensional Method of Characteristics Program for wave drag calculations. Care needs to be taken in the preparation of these cards, for if the calculation fails to proceed further the first item to check is the correctness of the input cards.

After the wave drag coefficients have been calculated by the Three-Dimensional Method of Characteristics Program, the Surface Fit and Minimum Search Program can be used to define the least wave drag configuration for a given set of constraints as explained in part 3 of the user's manual. The program can be used as one of

the steps of a design procedure by providing the minimum wave drag body corresponding to constraints imposed by other considerations. Or the program can be applied to generate a set of charts for predicting minimum wave drag bodies subject to specified constraints. It should be noted that these charts are valid in some ranges of geometric variables near the baseline. The entire procedure needs to be redone for a different baseline configuration.

## 6. CONCLUSIONS

With regard to the wave drag reduction program, the following remarks and conclusions can be made.

- a. The present optimization procedure developed in the phase I study is useful and versatile. It can be used for other optimization purposes.
- b. Together with the Three-Dimensional Method of Characteristics, the procedure can be used to obtain the minimum wave drag configuration for designing new airplanes or modifying existing ones.
- c. The optimization procedure has been verified through applications to the F-4 forward fuselage using a 5 x 5 Latin Square and to an F-4 type fuselage-wing configuration using a 3 x 3 Latin Square. The procedure has also proven itself by correctly predicting the von Karman ogive as the minimum wave drag body for a given configuration length and base.
- d. Within the ranges of variation of the chosen geometric variables, the following rule-of-thumb percentage reductions of the wave drag are obtained. In the case of the F-4 fuselage, for every inch the nose is lengthened, the wave drag is reduced by slightly over one percent, and for every percent the fuselage volume is decreased, the wave drag is reduced by about three quarters of a percent. In the case of the F-4 type fuselage-wing configuration, the wave drag is reduced by about half a percent for each percent the blended-wing configuration is narrowed.
- e. The present application to wave drag reduction is limited only in the capability of the wave drag computational techniques. First, a completely supersonic flow field is required for the characteristics method to be applicable. For a given configuration, this requirement sets a lower limit on the free-stream Mach number. Secondly, the computer program at the present stage of development requires that all corners and edges be faired with smooth curves to yield a

unique surface normal everywhere on the configuration.

- f. At free-stream Mach numbers below the lower limit stated in e., subsonic regions would occur at the fuselage-canopy juncture of the configuration under consideration. Further studies on calculations of local subsonic regions are needed to provide methods for supplementing to-day's wave drag computational techniques at lower free-stream Mach numbers.

## REFERENCES

1. Chu, C. W., Der, J. Jr., and Ziegler, H., "Wave Drag Reduction for Aircraft Fuselages," Interim Report NOR 75-70, August 1975, Northrop Corporation, Hawthorne, California.
2. Redlich, O., and Watson, F. R., "On Programs for Tests Involving Several Variables," Aeronautical Engineering Review, Vol. 12, No. 6, June 1953, pp. 51-59.
3. Chu, C. W., "Compatibility Relations and a Generalized Finite-Difference Approximation for Three-Dimensional Steady Supersonic Flow," AIAA Journal Vol. 5, No. 3, March 1967, pp. 493-501.
4. Chu, C. W. and Powers, S. A., "The Calculation of Three-Dimensional Supersonic Flows Around Spherically-Capped Smooth Bodies and Wings," AFFDL-TR-72-91, Vol. I, Theory and Applications, September 1972.
5. Chu, C. W., "Calculation of Three-Dimensional Supersonic Flow Fields about Aircraft Fuselages and Wings at General Angles of Attack," NOR 72-182, March 1973, Northrop Corporation, Hawthorne, California.
6. Chu, C. W., and Powers, S. A., "Determination of Space Shuttle Flow Field by the Three-Dimensional Method of Characteristics," TMX 2506, Feb. 1972, pp. 47-63, NASA.
7. Chu, C. W., "A New Algorithm for Three-Dimensional Method of Characteristics," AIAA Journal, Vol. 10, No. 11, November 1972, pp. 1548-1550.
8. Chu, C. W., "Calculation of Supersonic Flow Fields about Slab Delta Wings and Space Shuttle Wing-Body Configurations," NOR 73-007, April 1973, Northrop Corporation, Hawthorne, California.
9. Chu, C. W., "Supersonic Flow About Slab Delta Wings and Wing-Body Configurations," Journal of Spacecraft and Rockets, Vol. 10, No. 11, November 1973, pp. 741-742.

TABLE 1. Latin Square Arrangement

CELL Code:

$z_1$	$z_4$
$z_2$	$z_3$

① -1 -1 1 0	② 0 -1 -1 1	③ 1 -1 0 -1
④ -1 0 -1 -1	⑤ 0 0 0 0	⑥ 1 0 1 1
⑦ -1 1 0 1	⑧ 0 1 1 -1	⑨ 1 1 -1 0

TABLE 2. Variables, Ranges, and Baseline Values

Reduced Variables	Geometric Variables	Ranges of $x_i$		Baseline Values	
		$x_i$ min	$x_i$ max	$z_i$	$x_i$
$z_1$	$x_1$				
$z_1$	a	0.9	1.15	-0.2	1.0
$z_2$	$r_1$	1.5	36.50	-1.0	1.5
$z_3$	$r_2$	1.5	61.50	-1.0	1.5
$z_4$	h	3.0	-6.0	-0.333	0.0

TABLE 3. Wave Drag Coefficients  $C_{DW}$   
 (Base on Wing Area of 530 Sq. Ft.)

0.0104602	0.0116525	0.0107868
0.0094555	0.0104013	0.0128320
0.0116629	0.0114297	0.0114309

Baseline Value  $C_{DW} = 0.00979359$

TABLE 4. Coefficients of Wave Drag Equation

$$b_0 = 0.0104013$$

Values of  $b_i \times 10^4$

i	1	2	3	4
$b_i \times 10^4$	5.7851670	3.638333	7.459000	2.706667

Values of  $b_{ij} \times 10^4$

i \ j	1	2	3	4
1	0.6171822			
2		2.598000	-1.181682	
3			5.391000	
4				2.227318

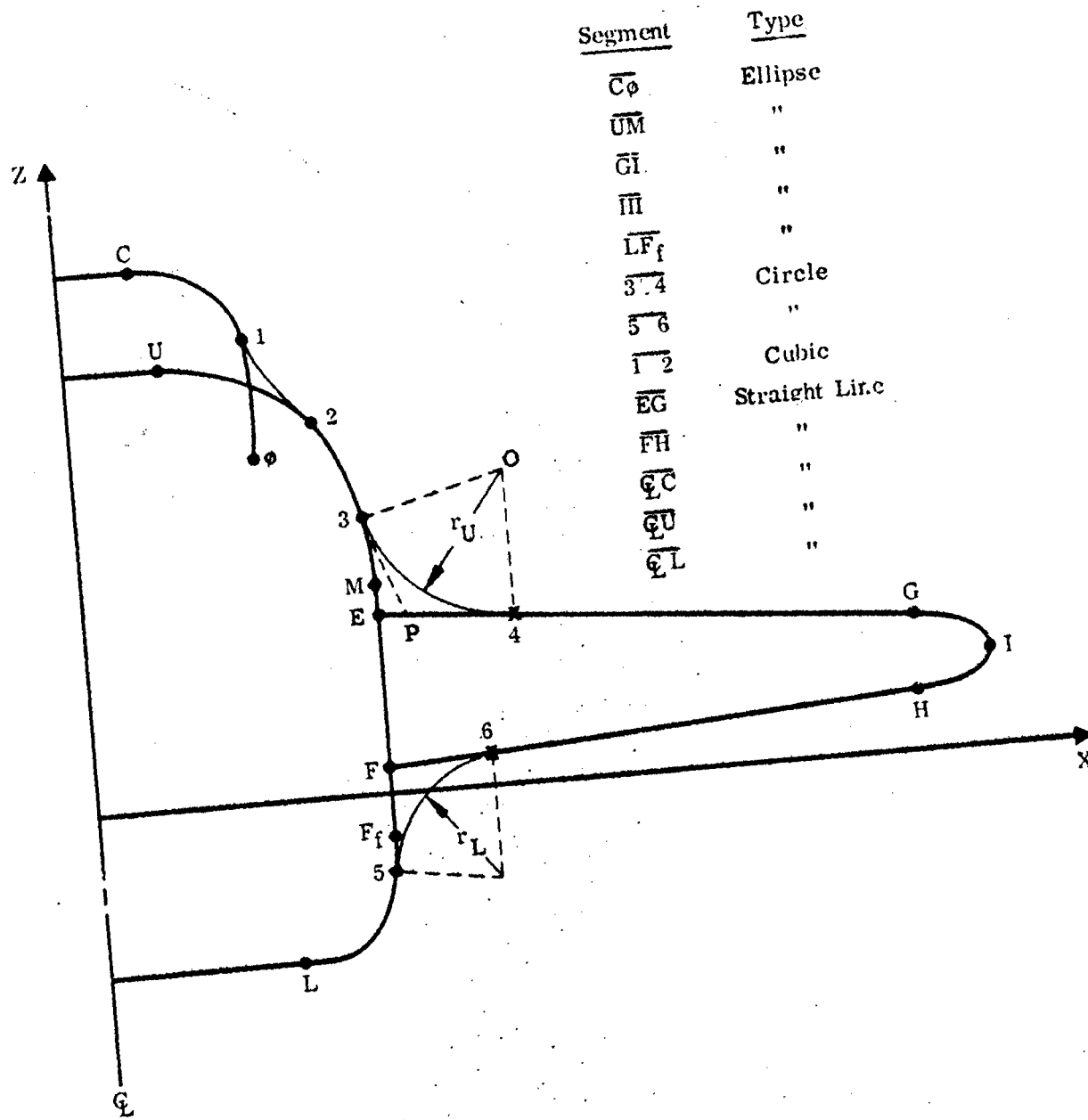


FIGURE 1. Schematic of Fuselage and Wing Cross Sections Description

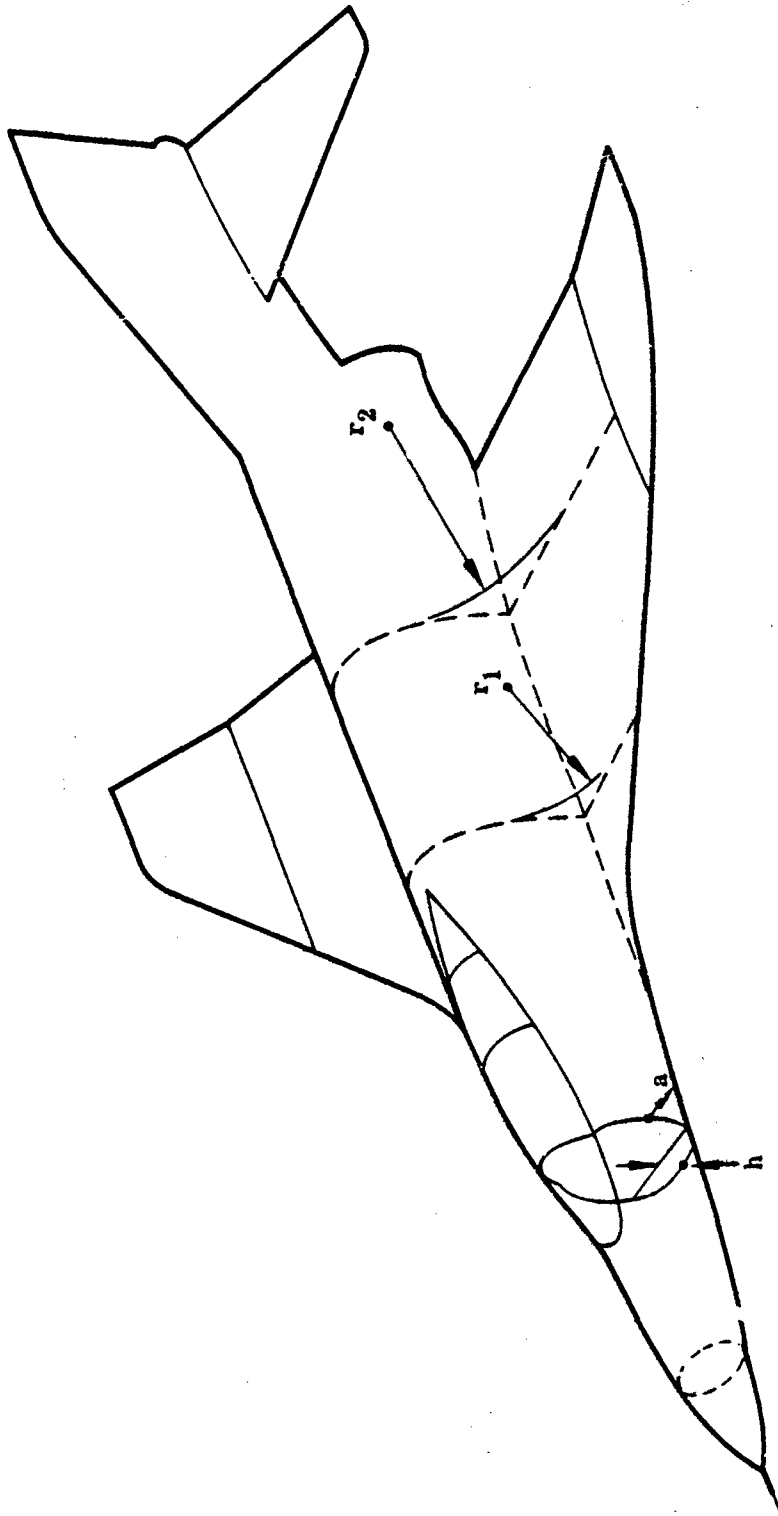


FIGURE 2. Geometric Variables for Fuselage Variation and Wing-Body Blending

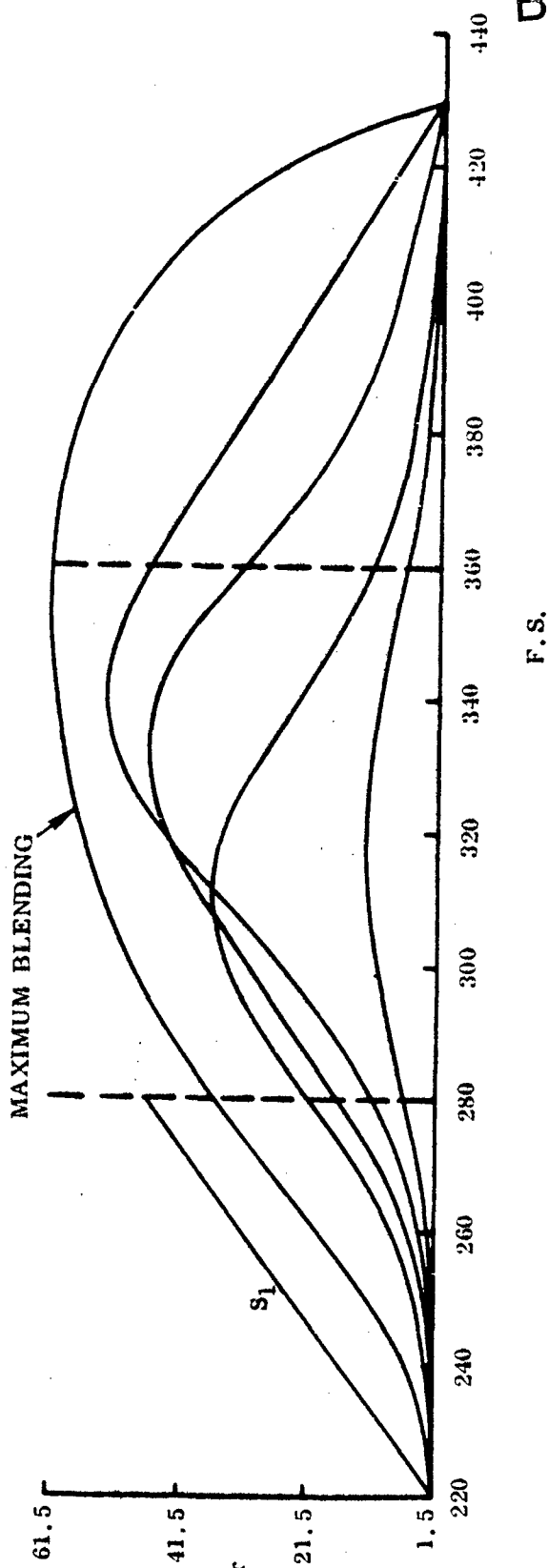
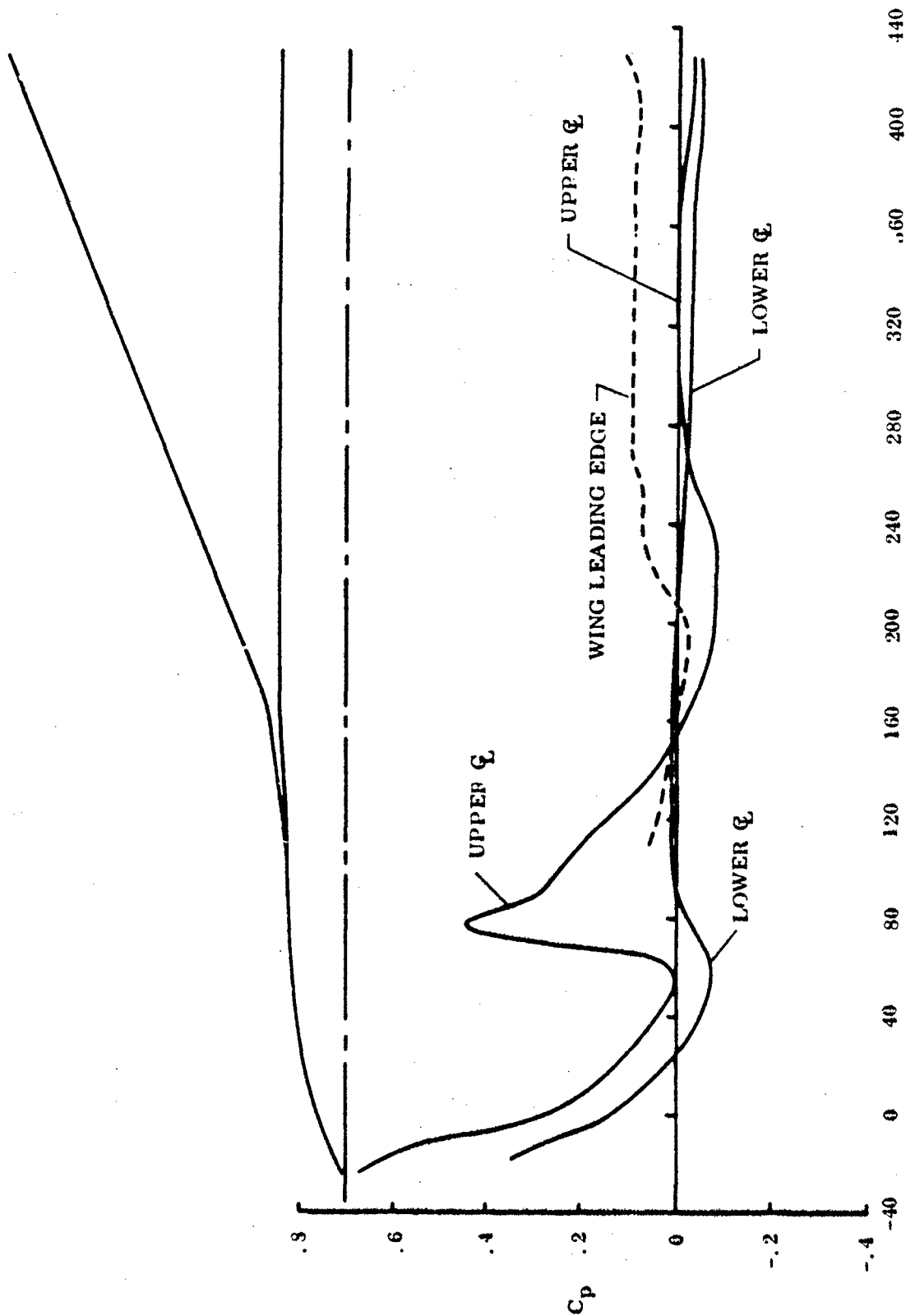


FIGURE 3. Sample Distributions of Blending Radius r



F. S.

FIGURE 4 Pressure Distributions Along Contourlines and

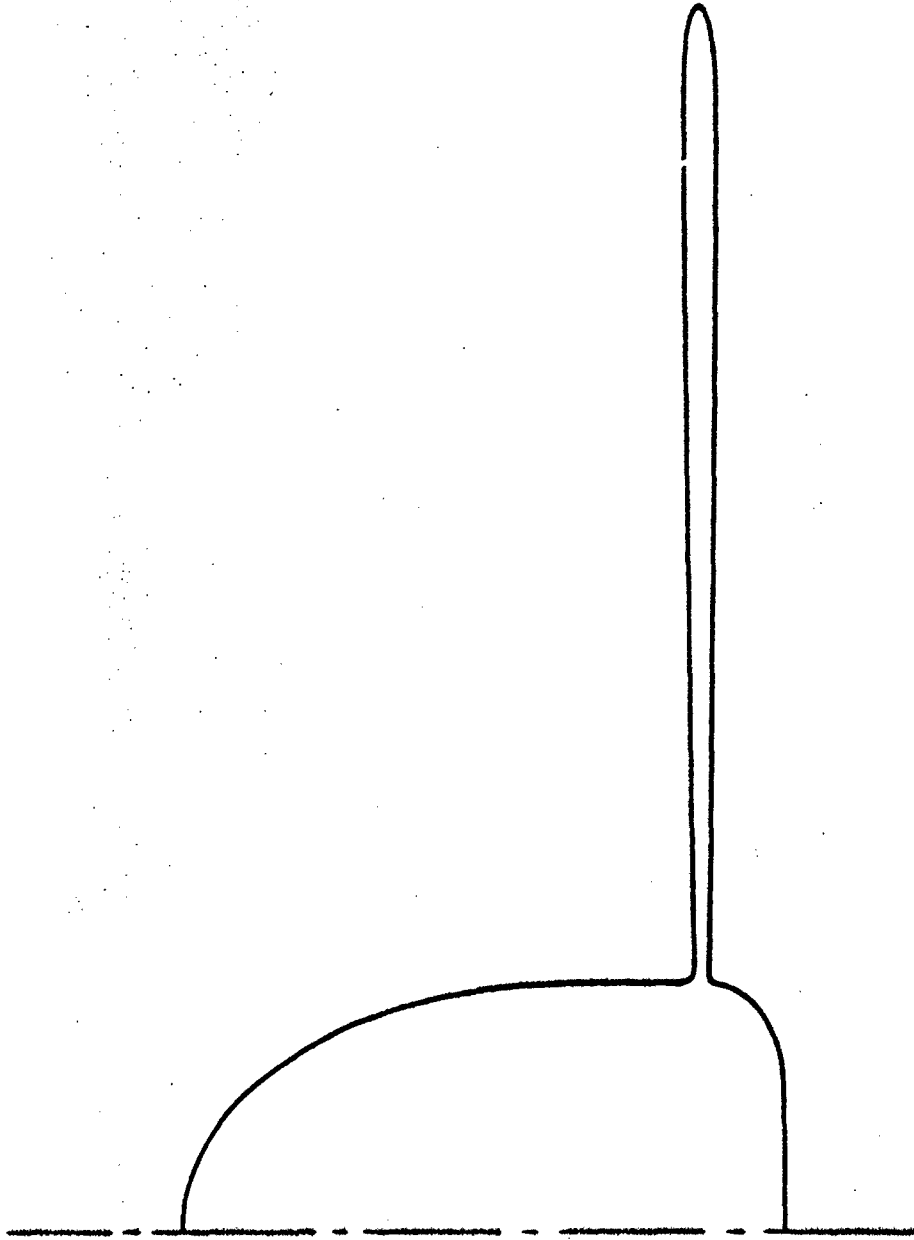


FIGURE 5. Cross Section of F-4 Type Baseline at Fuselage Station 430

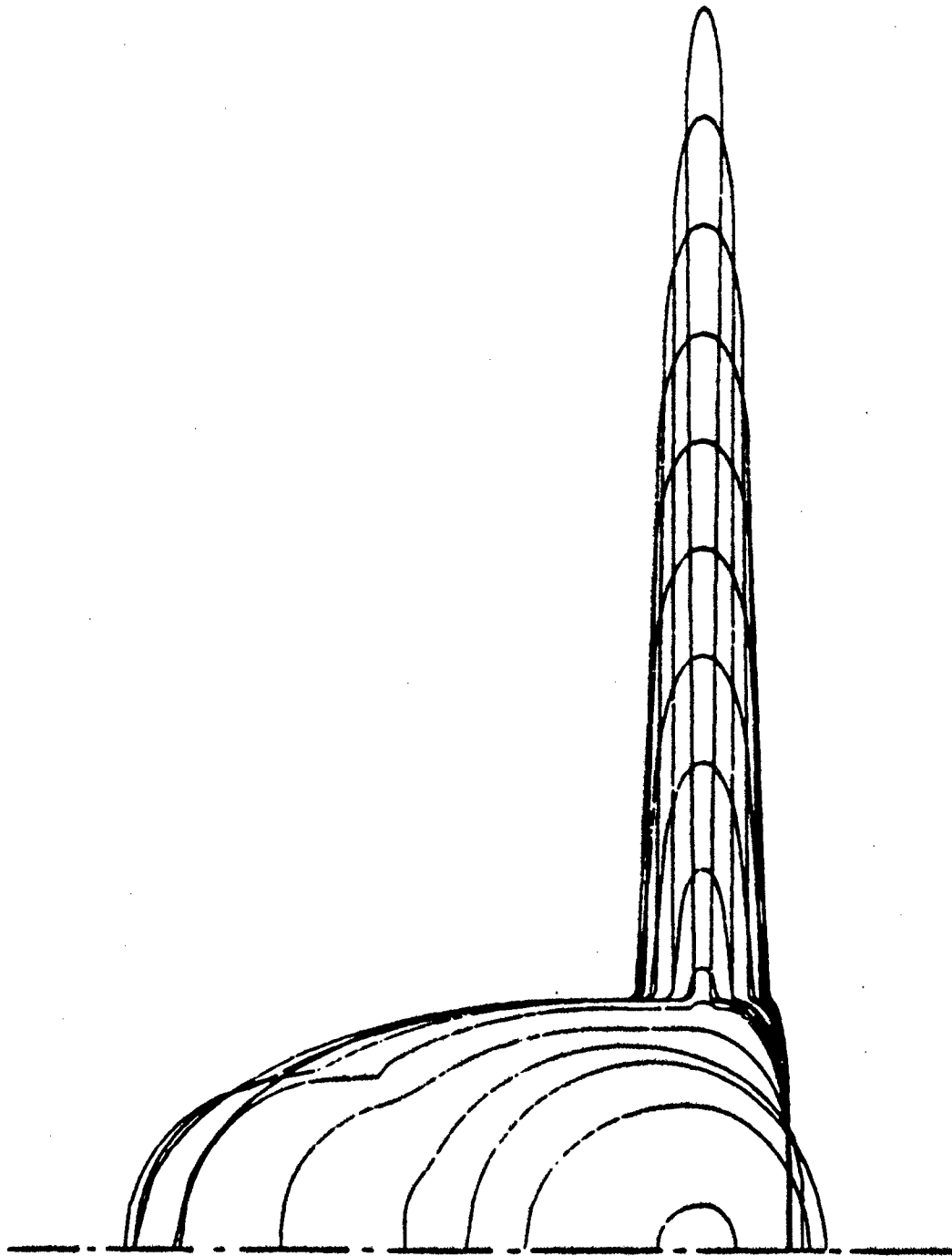


FIGURE 6. Front Views of F-4 Type Baseline Cross Sections

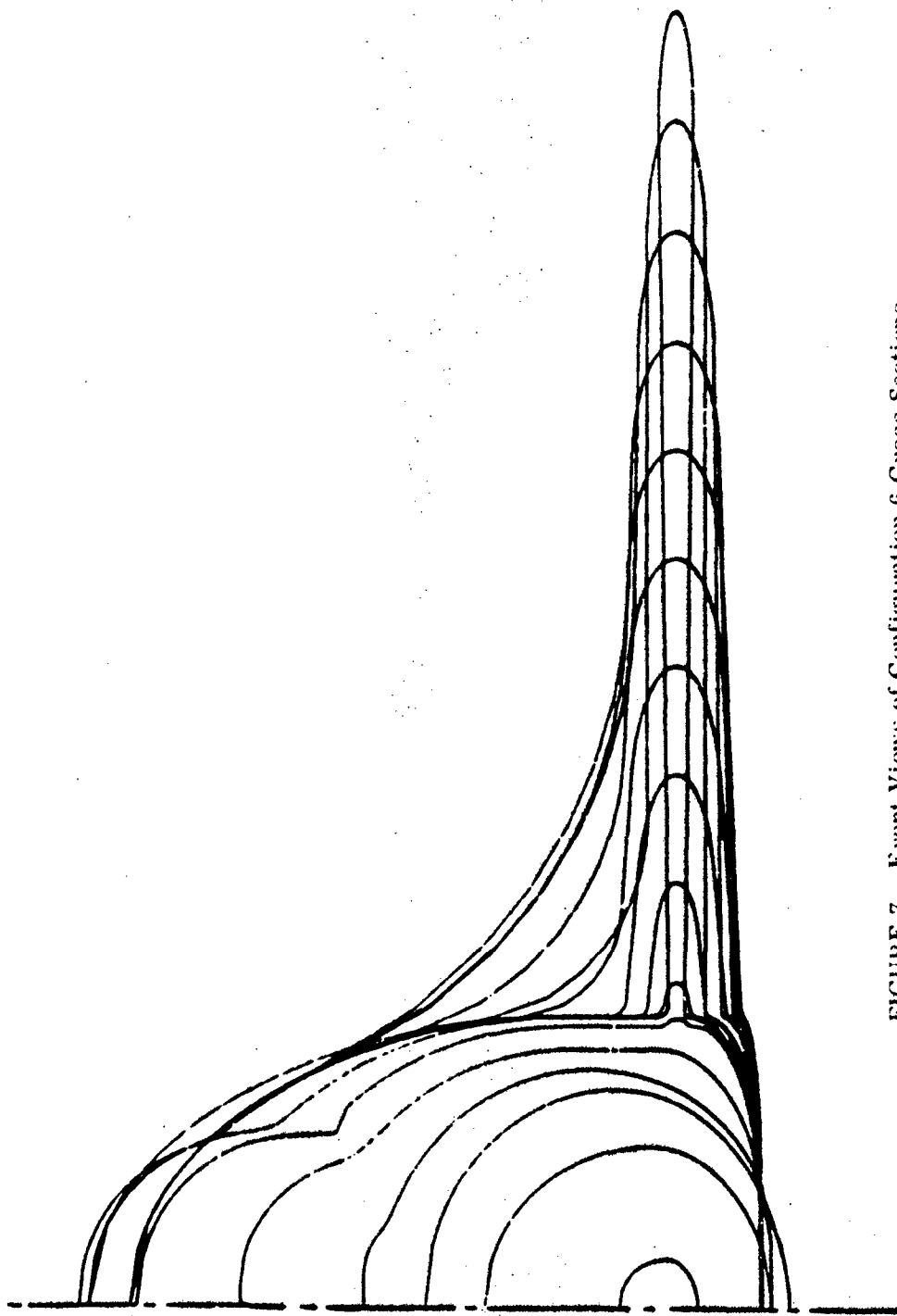


FIGURE 7. Front Views of Configuration 6 Cross Sections

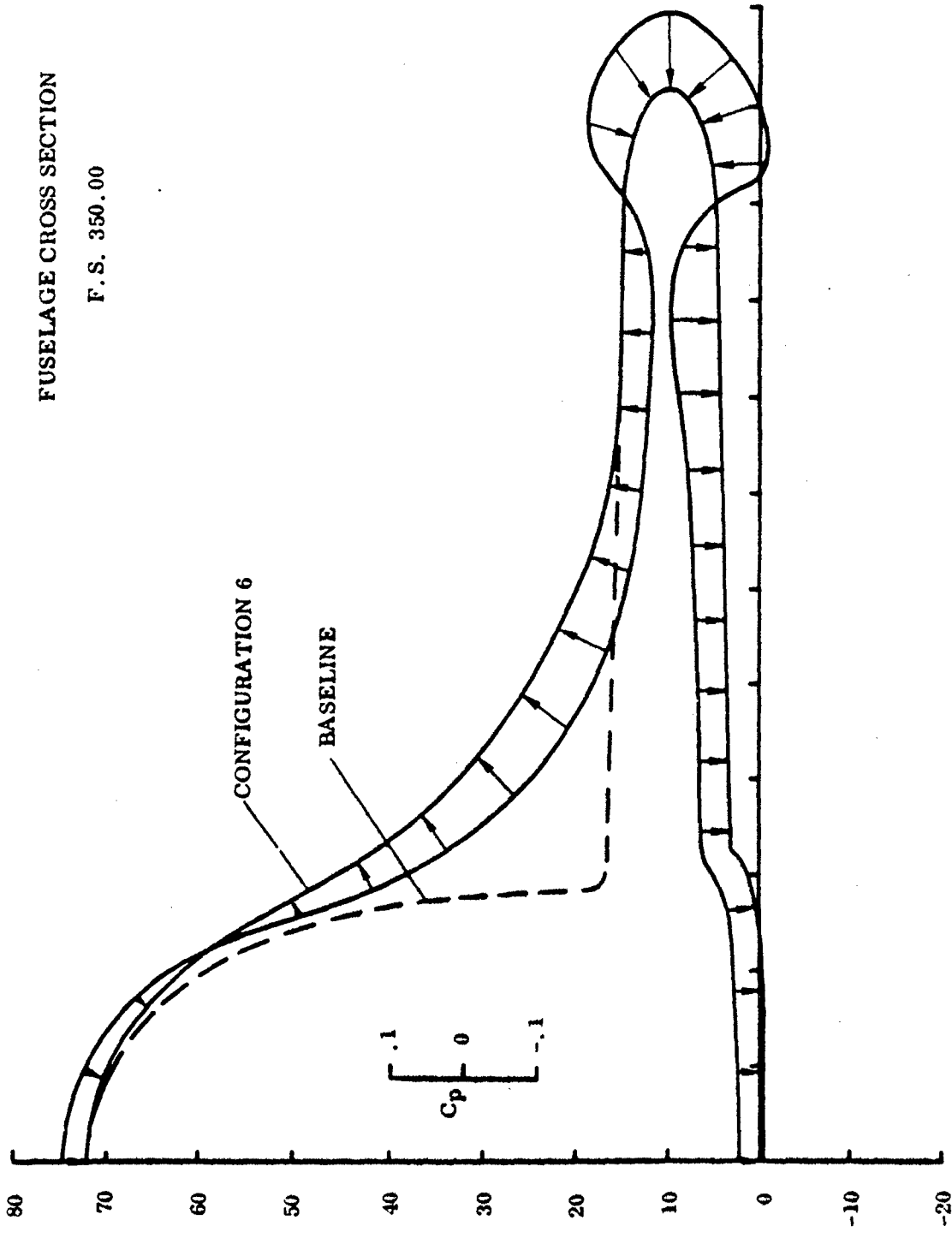


FIGURE 8. Cross Section and Pressure Distribution at F. S. 350 of Blended Wing Configuration 6

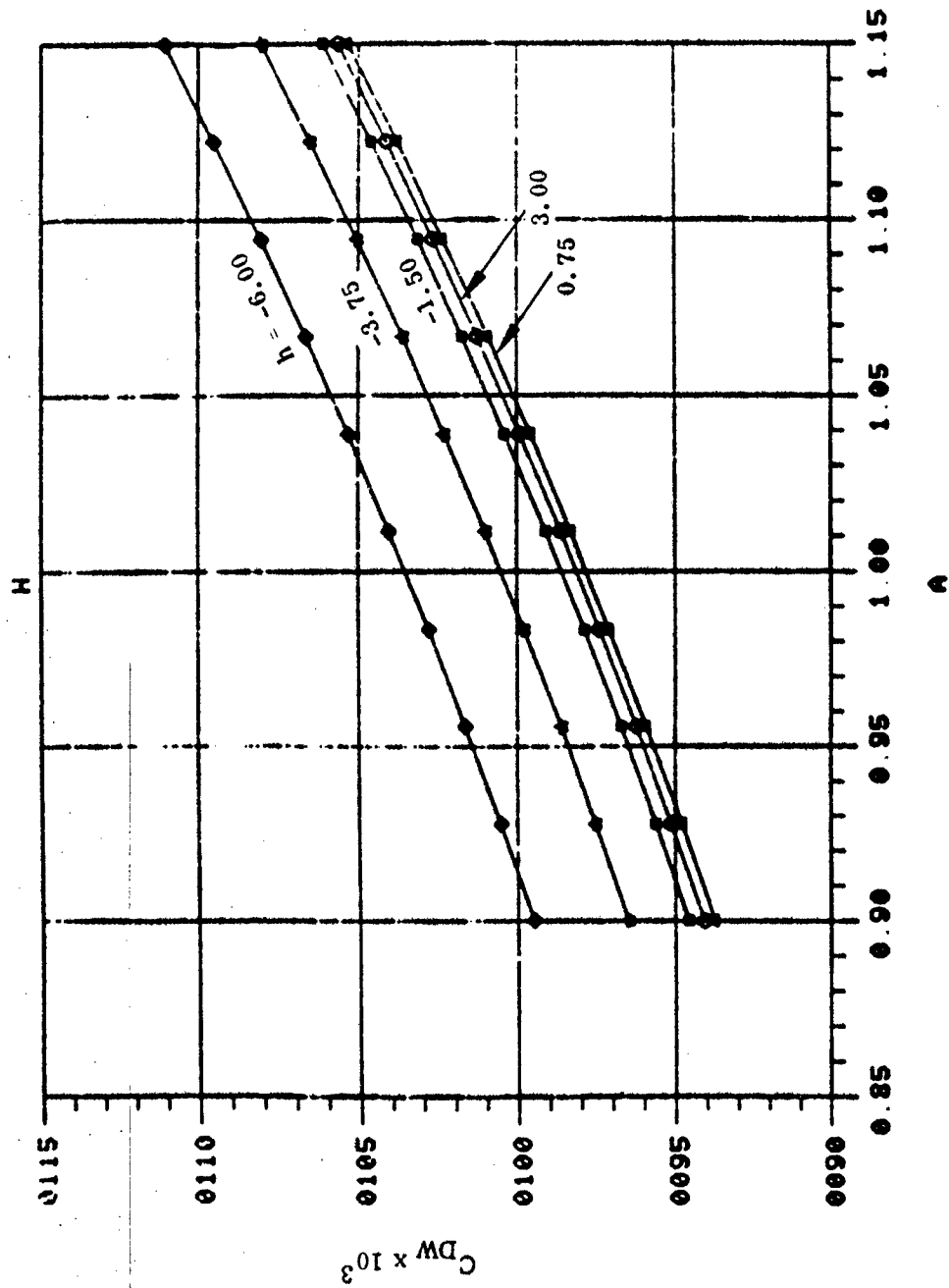


FIGURE 9. Variation of Wave Drag Coefficient  $C_{DW}$  vs  $a$  ( $r_1 = 1.5, r_2 = 1.5$ )

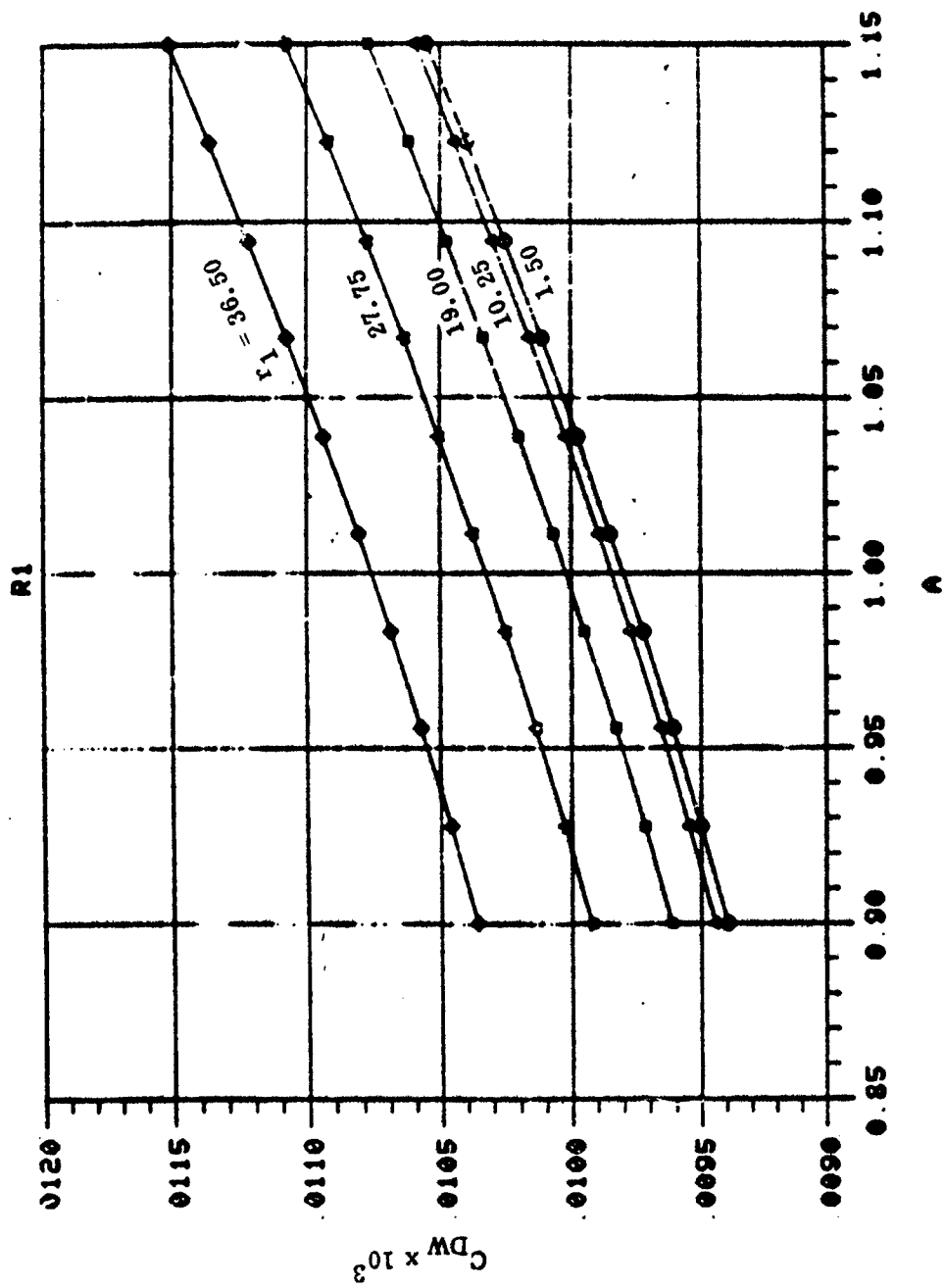


FIGURE 10. Variation of Wave Drag Coefficient  $C_{DW}$  vs  $a$  ( $r_2 = 1.5$ ,  $h = 0$ )

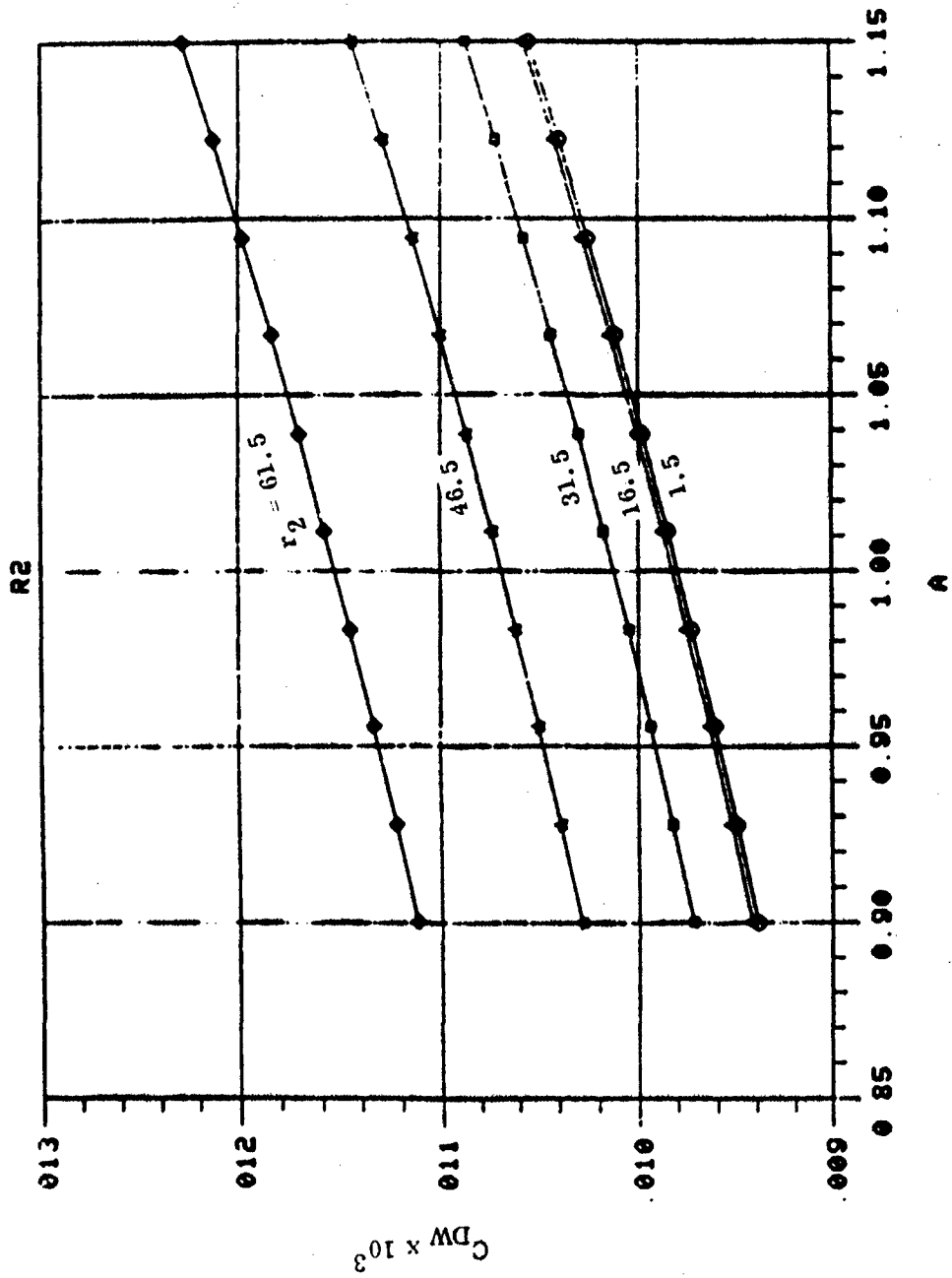


FIGURE 11. Variation of Wave Drag Coefficient  $C_{DW}$  vs  $a$  ( $r_1 = 1.5, h = 0$ )

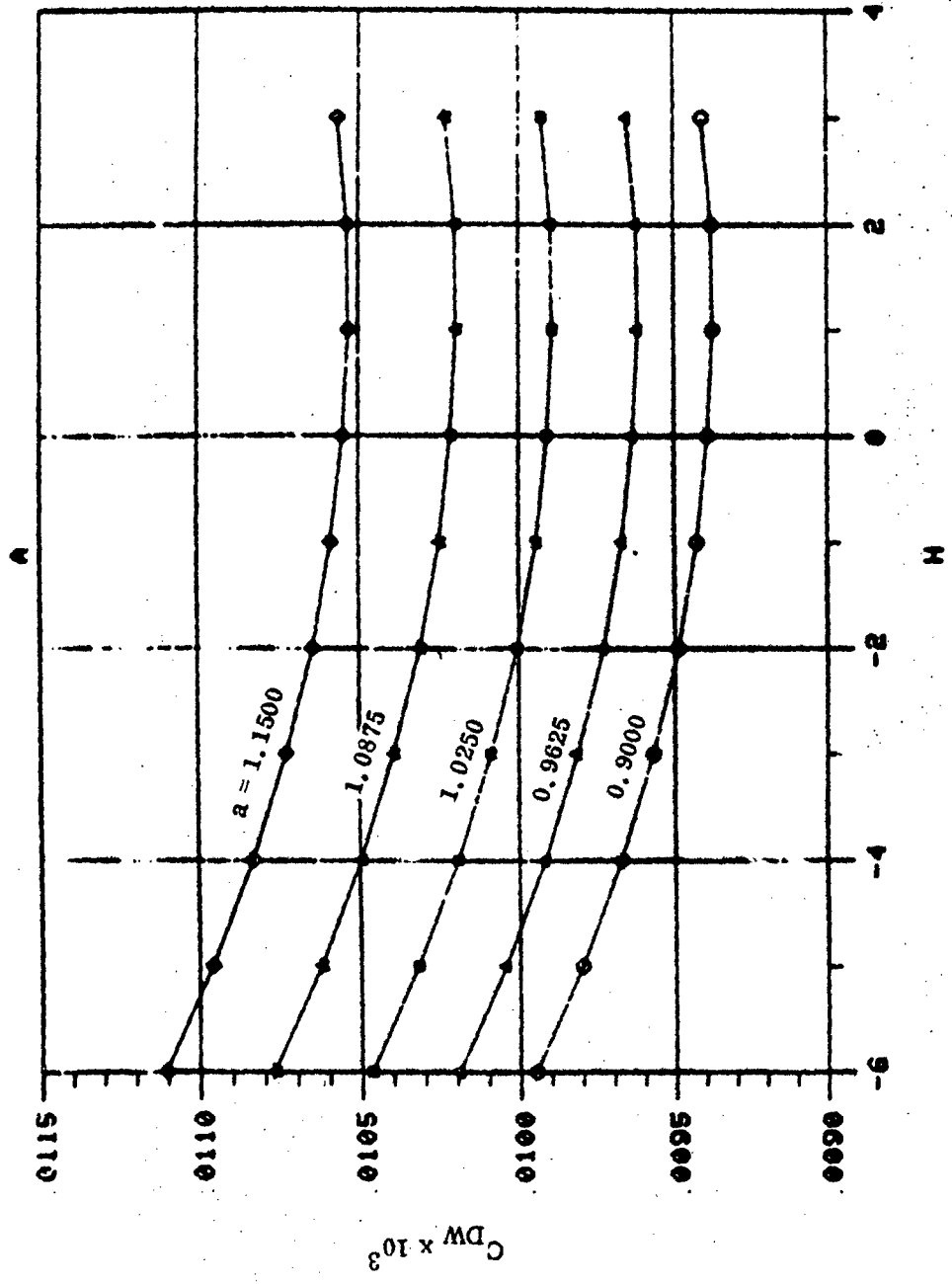


FIGURE 12. Variation of Wave Drag Coefficient  $C_{DW}$  vs  $h$  ( $r_1 = 1.5, r_2 = 1.5$ )

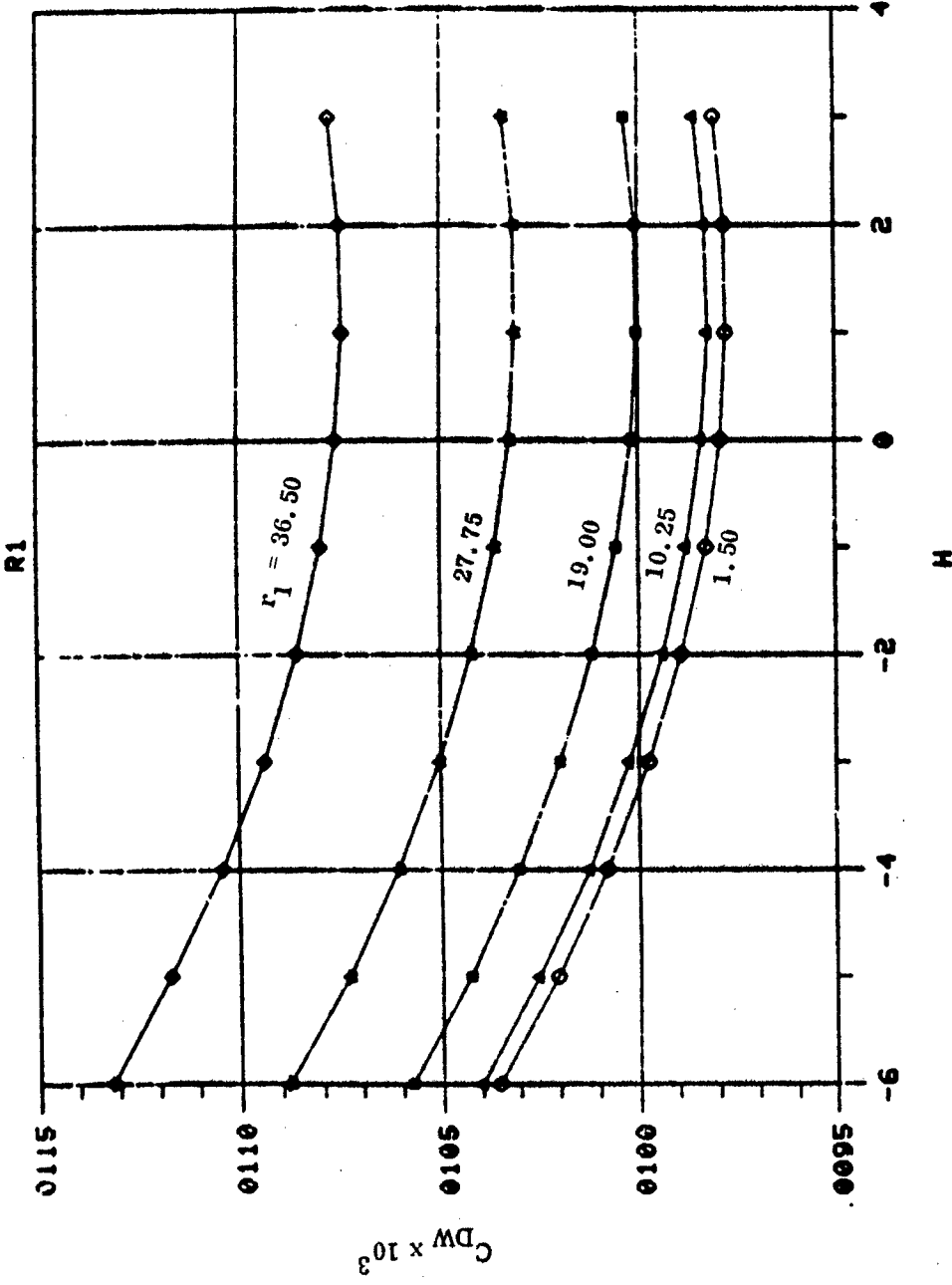


FIGURE 13. Variation of Wave Drag Coefficient  $C_{DW}$  vs  $h$  ( $a = 1.0, r_2 = 1.5$ )

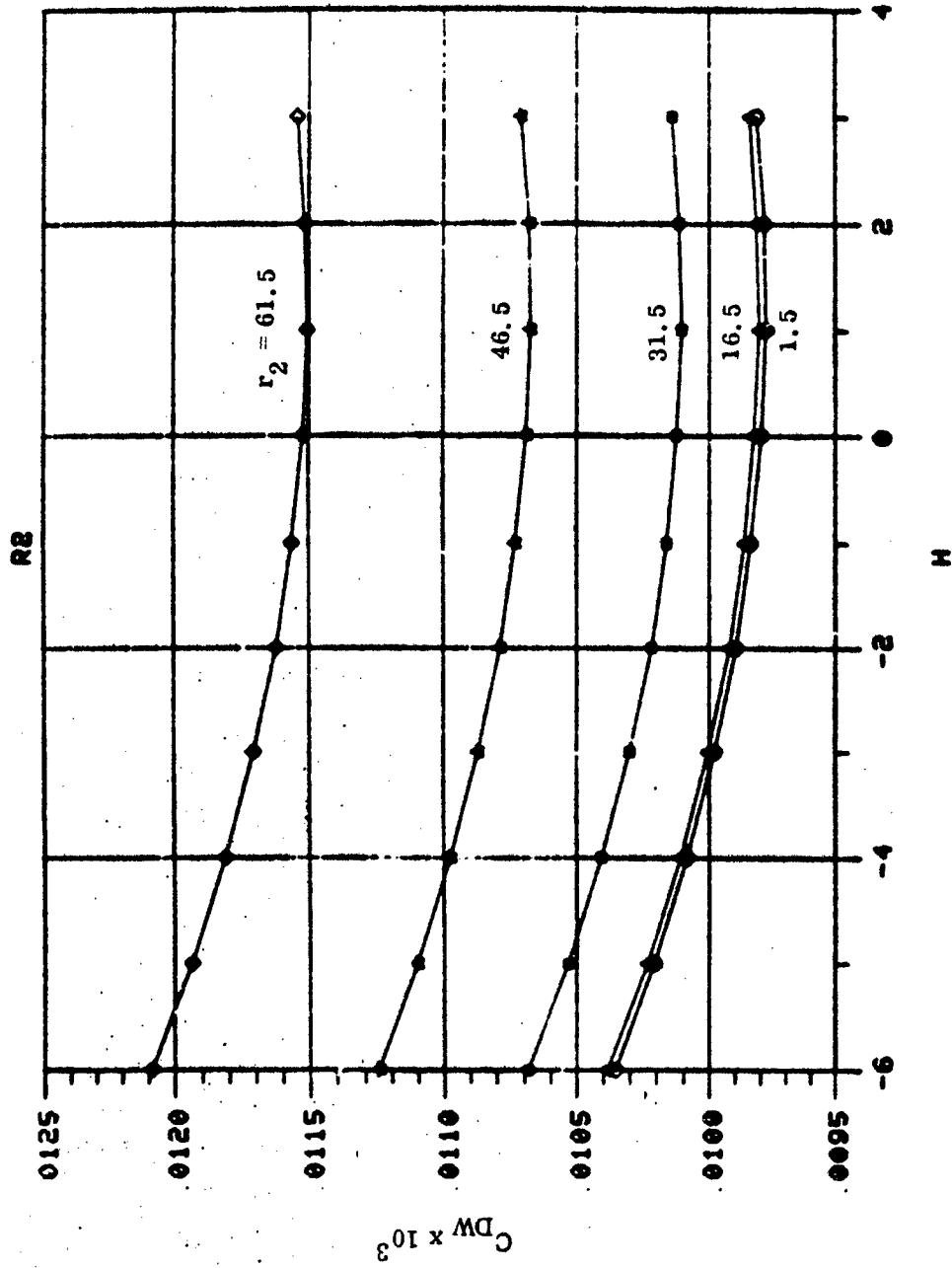


FIGURE 14. Variation of Wave Drag Coefficient  $C_{DW}$  vs  $h$  ( $a = 1.0$ ,  $r_1 = 1.5$ )

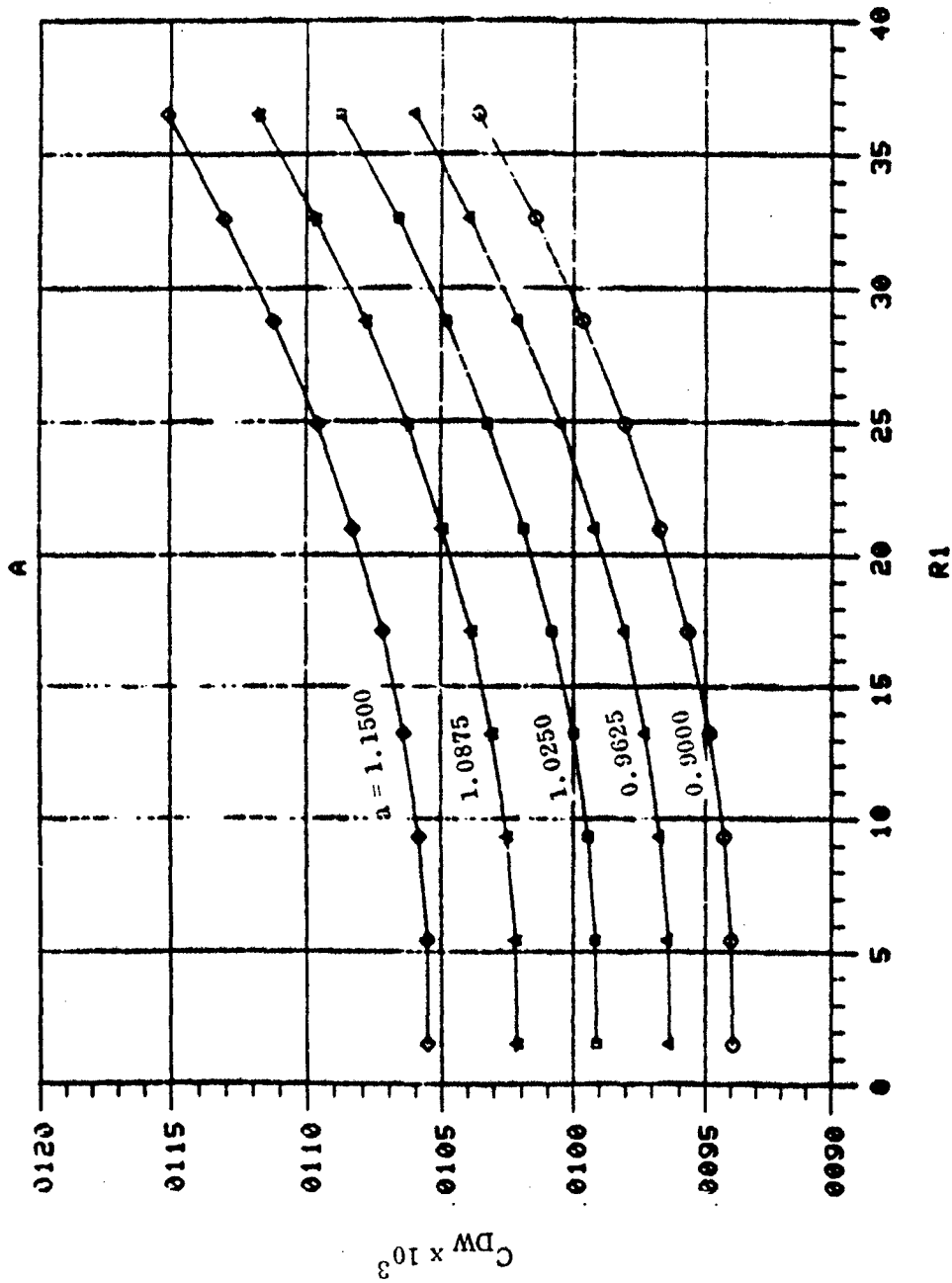


FIGURE 15. Variation of Wave Drag Coefficient  $C_{DW}$  vs  $r_1$  ( $r_2 = 1.5, h, 0$ )

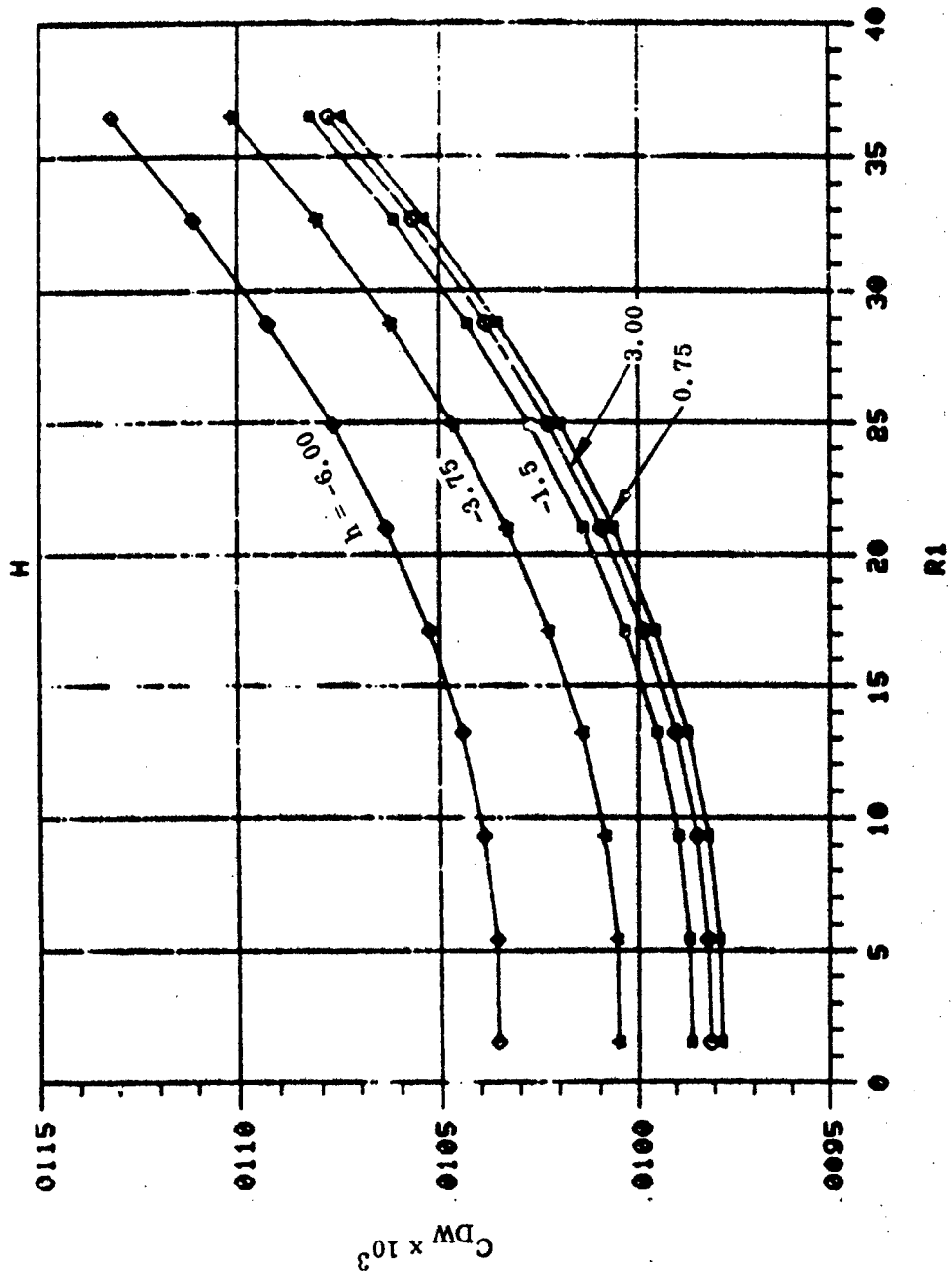


FIGURE 16. Variation of Wave Drag Coefficient  $C_{DW}$  vs  $r_1$  ( $a = 1.0, r_2 = 1.5$ )

Best Available Copy

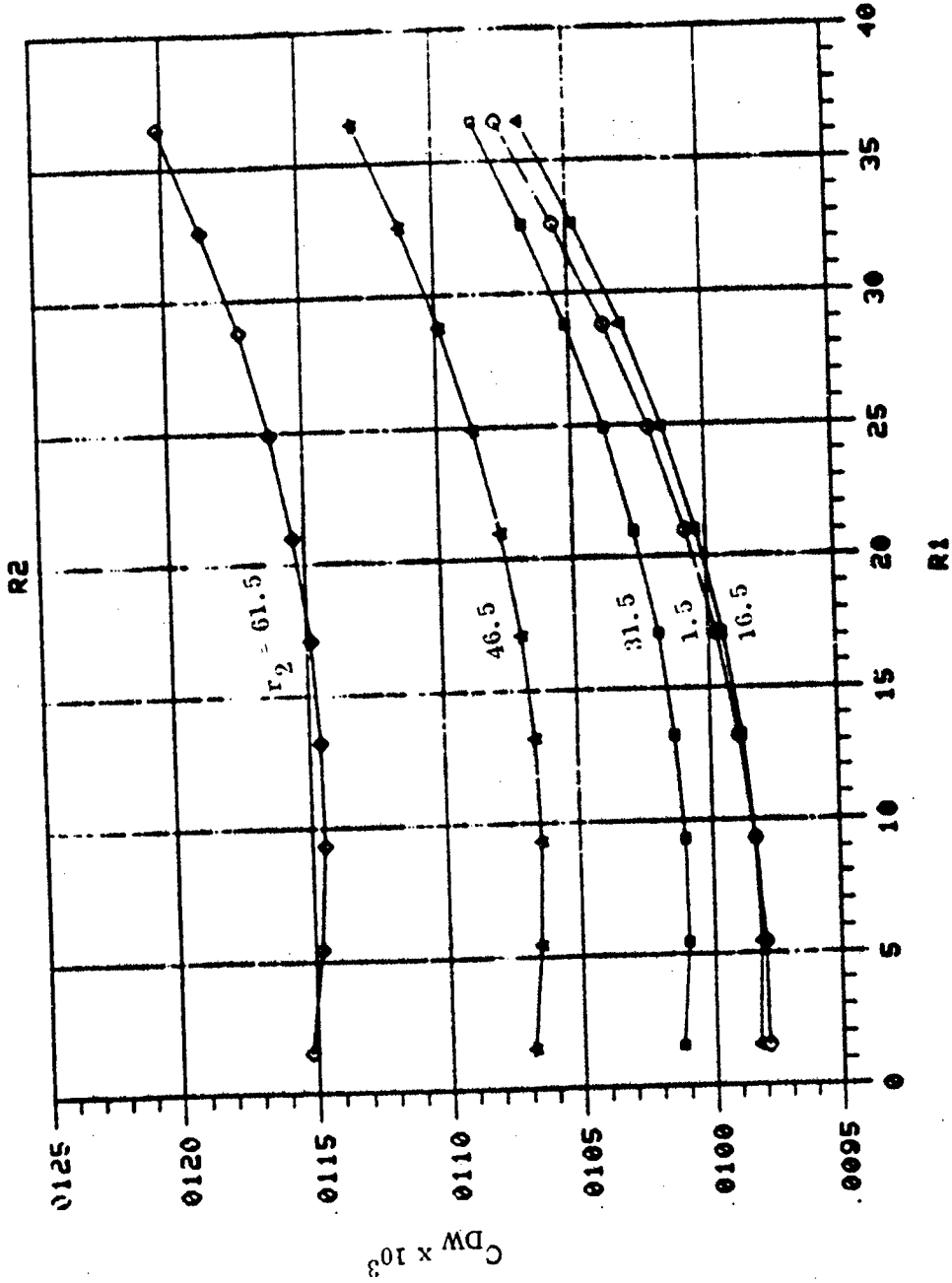


FIGURE 17. Variation of Wave Drag Coefficient  $C_{DW}$  vs  $R_1$  (a 1.0, h = 0)

Best Available Copy

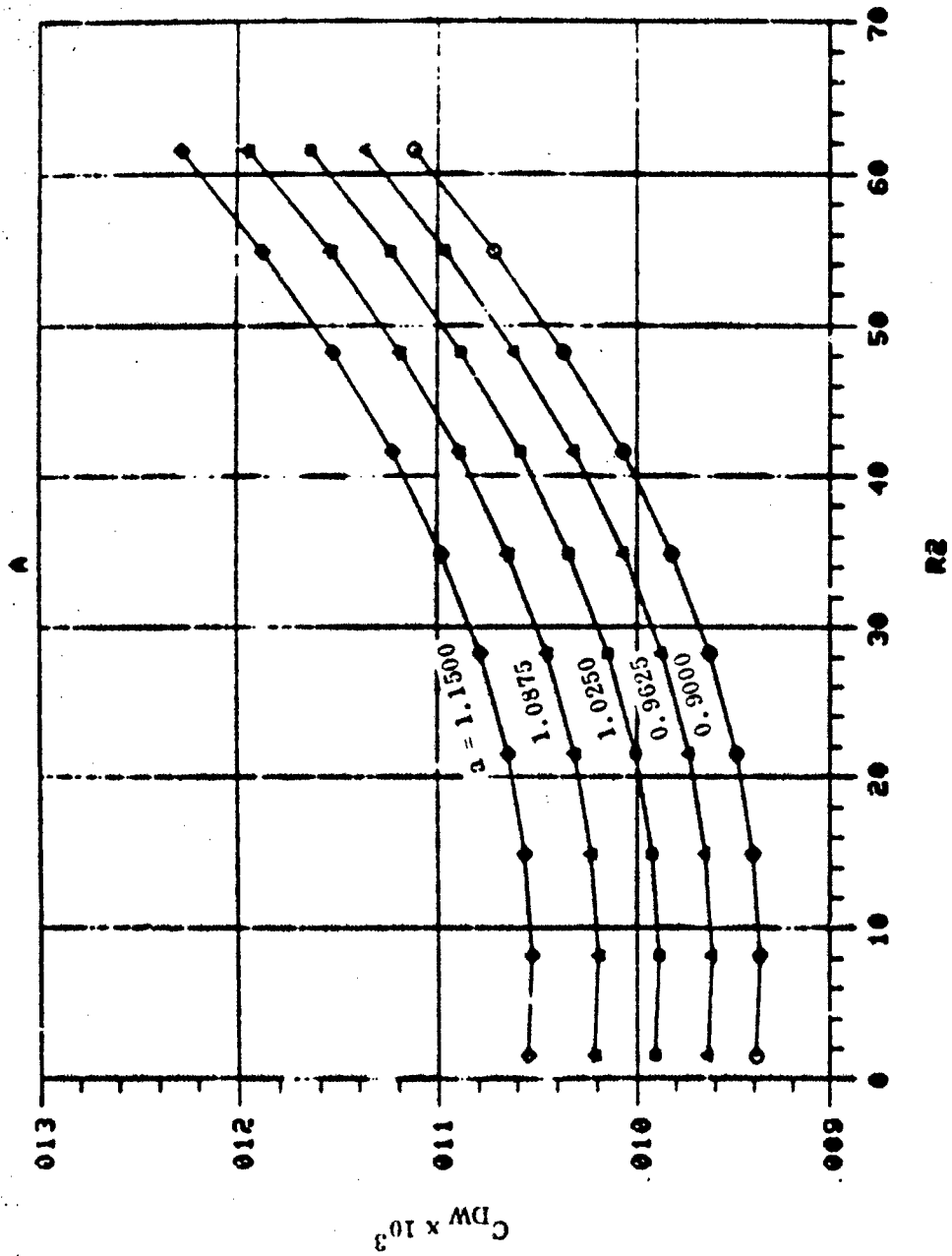


FIGURE 18. Variation of Wave Drag Coefficient  $C_{DW}$  vs  $r_2$  ( $r_1 = 1.5, h = 0$ )

Best Available Copy

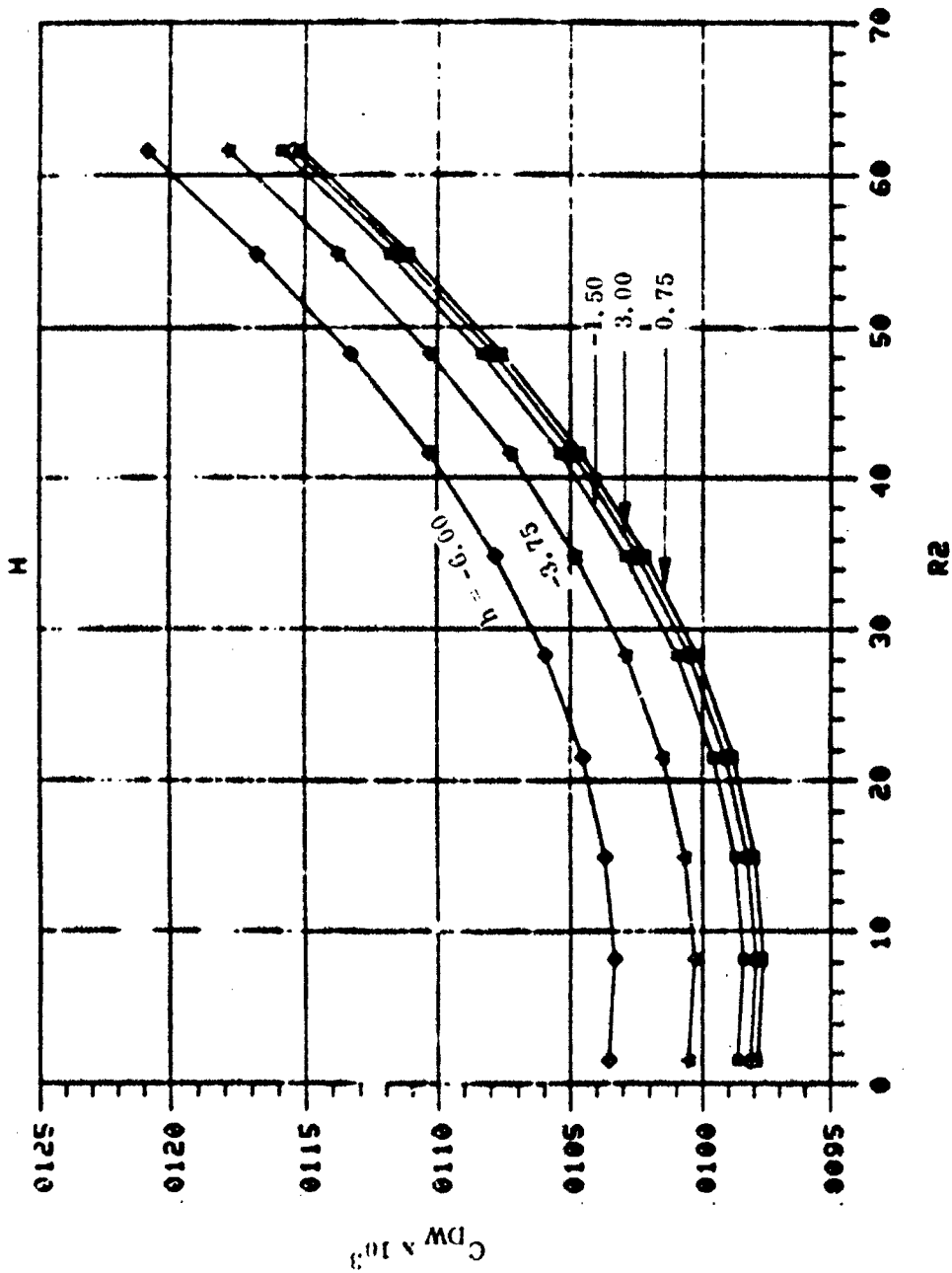


FIGURE 19. Variation of Wave Drag Coefficient  $C_{DW}$  vs  $r_2$  ( $a = 1.0, r_1 = 1.5$ )

Best Available Copy

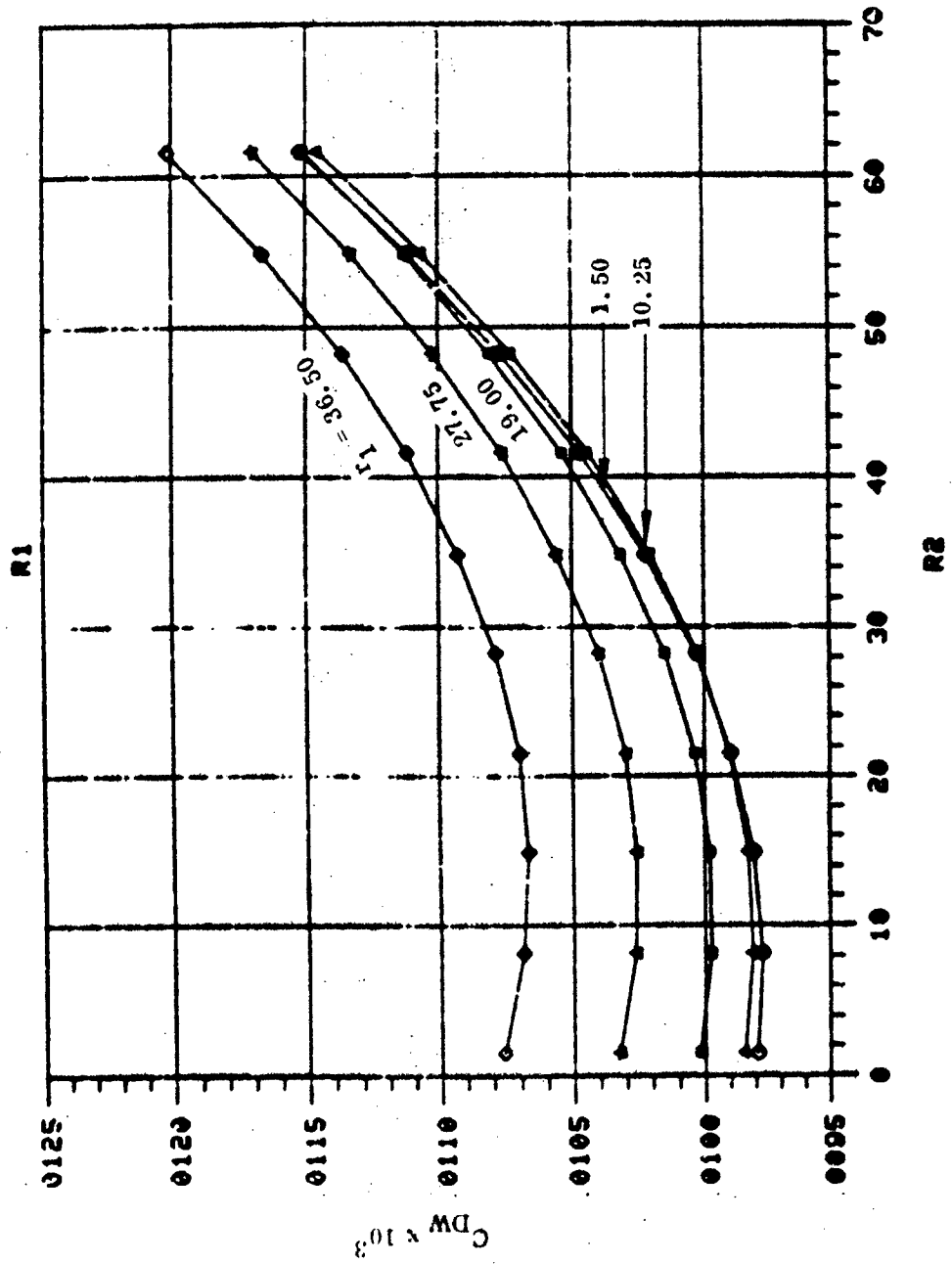
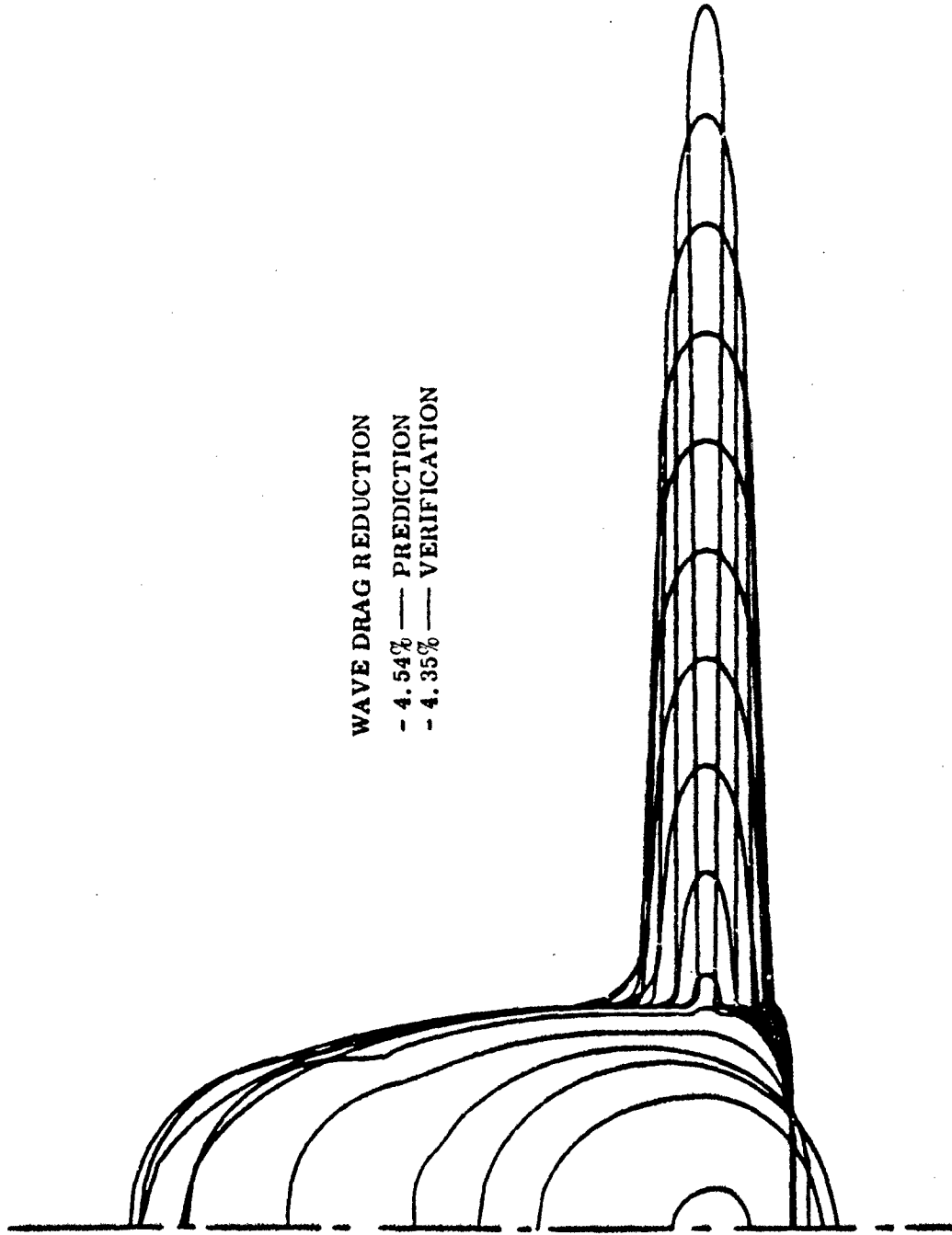


FIGURE 20. Variation of Wave Drag Coefficient  $C_{DW}$  vs  $r_2$  ( $a = 1.0, h = 0$ )



WAVE DRAG REDUCTION  
- 4.54% --- PREDICTION  
- 4.35% --- VERIFICATION

FIGURE 21. Front View of a Minimum Wave Drag Configuration

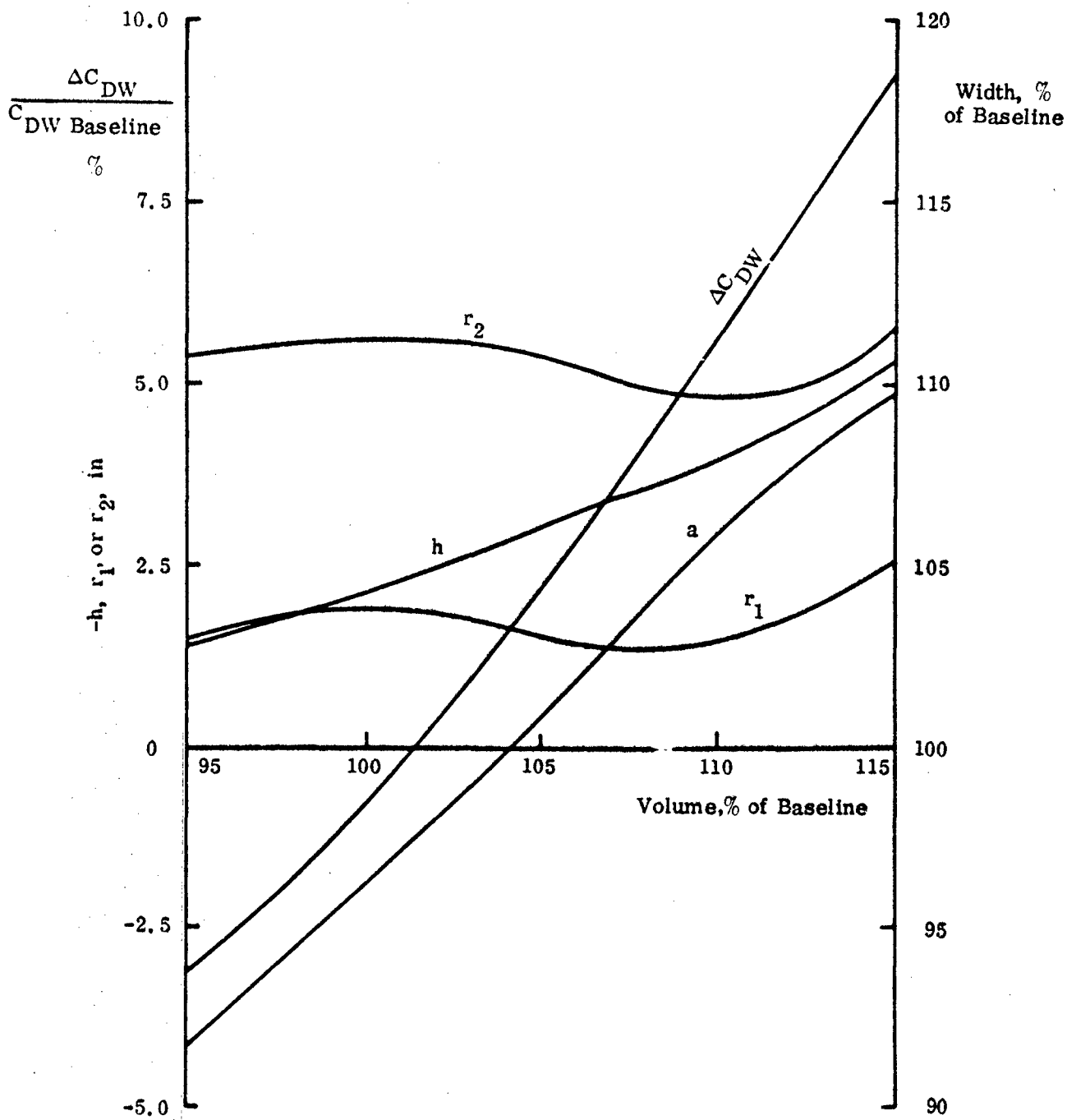


FIGURE 22. Minimum Wave Drag Configurations for Various Volumes (% of Baseline Volume)

## APPENDIX A

### WAVE DRAG REDUCTION FOR FORWARD FUSELAGES

#### 1. INTRODUCTION

The complete wave drag reduction program has been carried out in two phases. In the first phase, a procedure was developed for minimizing the wave drag of a forward fuselage and canopy configuration. In the second phase, the procedure was expanded to account for the influence of the wing and wing-body blending on the overall wave drag. In this appendix, the research performed in the first phase of the program is presented. The basic approach is given first, which consists of the formulation of the problem and a brief account of the two basic methods. It is followed by a discussion of the method of describing the body and the selection of geometric variables and their ranges for defining a family of configurations. Then the flow field calculation and the wave drag equation are presented. Sample results of the calculated flow fields are given, and calculated wave drag coefficients are tabulated. These coefficients were used to derive the wave drag equation which expresses the wave drag as a function of the geometric variables. A new concept which enables the wave drag equation to "learn" from experience to improve its performance is also presented. This concept proved very useful in achieving successful results during the Phase I work and can be applied to improve other optimization procedures using Latin Square sampling. Then the wave drag reduction procedure and the types of geometric constraints imposed by design requirements considered in the procedure are presented, followed by the discussion of the wave drag equation and the new concept for improvement. Various aspects of the wave drag reduction procedure are demonstrated using the F-4 fuselage as the baseline; the results are presented and discussed. Some characteristics of the wave drag equation are plotted, and concluding remarks are made for the Phase I work.

## 2. APPROACH

In this section the formulation of the wave drag reduction problem is outlined, and the two basic methods to be used in this study are introduced.

### a. Formulation

The baseline configuration can be described by a set of geometric variables. A family of configurations including the baseline can be generated by assigning different values to some or all of the geometric variables. If the wave drag can be expressed as a function of these variables, a particular set of values of these variables that gives the least wave drag can be found by minimizing the function. This set of values then produces the minimum wave drag configuration.

The key to this problem is how to obtain such a functional expression for the wave drag. In this study, six geometric variables are considered in defining the family of configurations. If each variable assumes five values, the evaluation of the partial derivatives with respect to these six variables for a Taylor-series type expression would require  $5^6$  or 15,625 wave drag calculations. This is obviously not feasible. In the present approach the wave drag coefficient  $C_{DW}$  is first assumed to be of the form

$$C_{DW} = a_0 + \sum_{i=1}^6 a_i x_i + \sum_{j=1}^5 \sum_{i=2}^5 a_{ij} x_i x_j \quad (1)$$

where  $x_i$  ( $i = 1, 6$ ) are the geometric variables and  $a_i$  and  $a_{ij}$  are to be determined. The Latin Square sampling technique<sup>1</sup> is used to sample 25 sets of values of  $x_i$  out of the total population of 15,625 sets. The wave drag coefficients for the configurations defined by each of the 25 sets are then calculated by the Three-Dimensional Method of Characteristics.<sup>2,3</sup> When the 25 calculated wave drag coefficients  $C_{DW}$  and the corresponding values of the geometric variables  $x_i$  are substituted into Eq. (1), 25 linear equations for the 17 unknowns  $a_i$  and  $a_{ij}$  are obtained. A least-squares procedure is used to solve these equations for the  $a_i$  and  $a_{ij}$ , which are then substituted back into

Eq. (1) to produce the functional expression for the wave drag in terms of the geometric variables. By minimizing  $C_{DW}$  in Eq. (1) subject to a given set of constraints, e. g., a given length and width of the fuselage, the minimum wave drag configuration corresponding to the given set of constraints is determined. In the present study, a numerical search procedure is used to find the minimum wave drag configuration (Appendix D).

b. Latin Square Sampling Technique

The Latin Square method, which has mostly been used in agriculture and biological research, is a very efficient sampling technique and is much better than random sampling. For this study a particular type of Latin Square (the orthogonal squares) suitable for a variety of technical problems<sup>1</sup> is adopted. With this type of Latin Square arrangement, a 5X5 square is the correct size for six geometric variables  $x_i$ , each taking five values. It is convenient to introduce the reduced variables  $z_i$ , which are related to the geometric variable  $x_i$  through

$$x_i = \frac{x_{i\max} + x_{i\min}}{2} + \frac{z_i (x_{i\max} - x_{i\min})}{4} \quad (2)$$

where subscripts max and min denote the maximum and minimum values, respectively. Corresponding to the five values of the geometric variables  $x_i$ , the reduced variables  $z_i$  always assume the five levels of 0, +1, +2. The 5X5 Latin Square arrangement in terms of the levels of the reduced variables is shown in Table 1.\* It is seen that in this way the Latin Square arrangement remains the same whatever the values of the geometric variables. At first glance, it appears that the roles of  $z_1$  and  $z_6$  are unique since their levels are arranged regularly in Table 1 and their nonlinear terms are excluded from Eq. (1). This is true for the conventional approach. However, it is shown in Appendix B that by rearranging Table 1 any pair of the reduced variables can have their levels arranged regularly as  $z_1$  and  $z_6$ , and it will be shown later in this

---

\* A discussion of the Latin Square construction is given in Appendix B.

TABLE 1. A 5x5 LATIN SQUARE ARRANGEMENT

CELL CODE

$z_1$	$z_6$
$z_2$	$z_5$
$z_3$	$z_4$

-2	-2	-1	-2	0	-2	1	-2	2	-2
1	0	2	1	-2	2	-1	-2	0	-1
-1	2	0	-2	1	-1	2	0	-2	1
-2	-1	-1	-1	0	-1	1	-1	2	-1
2	-1	-2	0	-1	1	0	2	1	-2
1	0	2	1	-2	2	-1	-2	0	-1
-2	0	-1	0	0	0	1	0	2	0
-2	-2	-1	-1	0	0	1	1	2	2
-2	-2	-1	-1	0	0	1	1	2	2
-2	1	-1	1	0	1	1	1	2	1
-1	2	0	-2	1	-1	2	0	-2	1
0	1	1	2	2	-2	-2	-1	-1	0
-2	2	-1	2	0	2	1	2	2	2
0	1	1	2	2	-2	-2	-1	-1	0
2	-1	-2	0	-1	1	0	2	1	-2

appendix that some or all nonlinear terms of  $z_1$  and  $z_6$  can be included in the wave drag equation.

c. Three-Dimensional Method of Characteristics

In this study the Three-Dimensional Method of Characteristics<sup>2,3</sup> is used to calculate the wave drag coefficients for the fuselage-canopy configurations sampled by the Latin Square technique.

### 3. DESCRIPTION AND VARIATION OF FORWARD FUSELAGE

Three-dimensional body description requires a great deal of effort which at times becomes extremely tedious. Basically, two types of description can be made, analytical and numerical. The latter can describe complicated geometry accurately, but is cumbersome for preparing input data. The former is much simpler to input and can define a family of configurations based on a few geometric variables. Hence, analytical description is chosen for the present study.

#### a. Body Description

Every configuration has a number of generating lines, such as the upper profile, the lower profile, the maximum breadth line, or the wing leading edge. In the present body description procedure, each generating line is divided into a number of segments to permit each segment to be described by a conic-section curve. At each cross section of the configuration, simple analytic curves, e.g., the ellipse or cubic, connect any two adjacent generating lines to form the contour of the cross section. The configuration is thus described analytically by simple low-order curves. For a smooth body a unique normal to the surface exists everywhere, and this condition usually requires slope continuity at the junctures between two contour curves or two segments of a generating line.

The fuselage is located in a right-handed coordinate system where the Y-axis is aligned with the fuselage axis; the X-axis is spanwise and the Z-axis is up. A schematic of the fuselage-canopy configuration is shown in Figure 1 and a typical cross section, in Figure 2. All generating lines are represented by a general curve fit of conic sections in several segments. The conic-section curves take the form

$$\begin{pmatrix} Z_j \\ X_j \end{pmatrix} = P_j Y + Q_j + \left( R_j Y^2 + S_j Y + T_j \right)^{1/2} \quad (3)$$

where  $j = 1, 5$ . A straight line is a special case with  $R = S = T = 0$ . Each curve can be divided into as many segments as necessary to provide adequate body description.

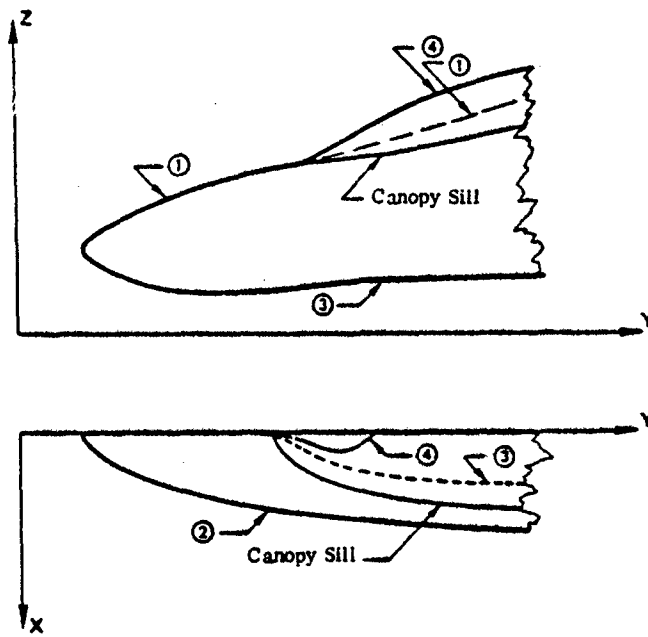


FIGURE 1. FUSELAGE-CANOPY SCHEMATIC

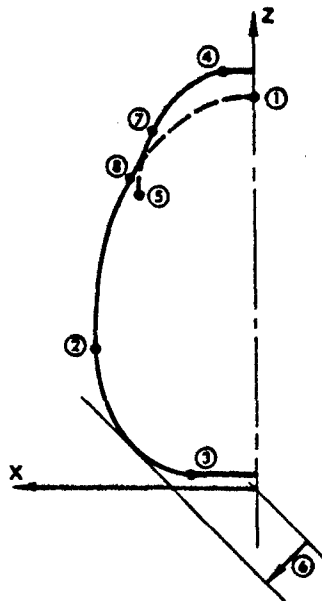


FIGURE 2. A TYPICAL CROSS SECTION

Each segment must be continuous with the previous segment and with very few exceptions the slope must be continuous at the junctures to satisfy the requirement of a unique normal to the surface. Unlike others, line 6 is not a true generating line. It is actually a shape factor which expresses the distance to a tangent line as a function of Y and is discussed in Section 3b. For lines 7 and 8, only  $Z_7$  and  $Z_8$  are fitted by conic section curves while  $X_7$  and  $X_8$  are given by Eq. (10a) in Section 3c.

As shown in Figure 2, the contour of the cross section begins with a straight line representing the canopy flat. The canopy contour from points 4 to 5 is circular but can be elliptic in general. The upper fuselage is represented by an elliptic curve from points 1 to 2. The lower fuselage is represented by a general conic-section curve from points 2 to 3; the bottom flat, by a straight line from point 3 to the centerline. The intersection between the canopy and the fuselage is faired by a cubic from points 7 to 8. The derivation of the cubic equation is presented in Section 3c. The equation for the canopy is given by

$$\left[ \frac{Z - Z_5(Y)}{Z_4(Y) - Z_5(Y)} \right]^2 + \left[ \frac{X - X_4(Y)}{X_5(Y) - X_4(Y)} \right]^2 - 1 = 0 \quad (4)$$

If it is a circular arc, then  $(Z_4 - Z_5)^2 = (X_5 - X_4)^2$ . The equation for the upper fuselage is

$$\left[ \frac{Z - Z_2(Y)}{Z_1(Y) - Z_2(Y)} \right]^2 + \left[ \frac{X - X_1(Y)}{X_2(Y) - X_1(Y)} \right]^2 - 1 = 0 \quad (5)$$

#### b. Shape Factor

Referring to Figure 2, the contour curve from points 2 to 3 has a zero slope at point 3 and the slope approaches infinity at point 2. As in aircraft lofting practice, the shape of this contour curve is determined by specifying the distance from the origin to one of its tangent lines that makes a 45° angle with the x-axis. Hence, this distance, which is designated by b in the following derivation of the equation for the contour curve, may be regarded as a shape factor for this curve.

This equation for the 45° tangent line is

$$X = Z - \sqrt{2} b$$

which, when the origin is translated to point 3, becomes

$$X' = Z' + H \quad (6)$$

where  $Z' = Z - Z_3$ ,  $X' = X - X_3$ , and  $H = Z_3 - X_3 - \sqrt{2} b$ . In the new coordinate system, the general quadric equation, satisfying the conditions  $Z' (X'_2) = Z'_2$ ,  $X' (0) = 0$ ,

$\left(\frac{dX'}{dZ'}\right)_2 = 0$ , and  $\left(\frac{dZ'}{dX'}\right)_3 = 0$ , reduces to

$$K(Z'_2 X' - X'_2 Z')^2 + Z' (X' - X'_2) = 0 \quad (7)$$

which represents a family of curves with  $K$  as a parameter. To determine  $K$ .

Eq. (6) is substituted into Eq. (7) to yield a quadratic equation in the form

$$AZ'^2 + BZ' + C = 0 \quad (8)$$

and the condition for Eq. (6) to be a tangent line is that Eq. (8) should have a double root; i. e.,  $B^2 - 4AC = 0$ , which leads to

$$K = \frac{(H - X'_2)^2}{4HZ'_2 X'_2 (H + Z'_2 - X'_2)} \quad (9)$$

Equation (7) with  $K$  given by Eq. (9) is the equation for the contour curve from points 2 to 3. The range of variation of this curve obtainable by applying this equation is illustrated in Figure 3, where a family of conic-section curves is given for different values of  $b$ . By increasing the distance  $b$ , the curve is seen to vary from almost a straight line to a sharply bending curve approaching the two sides of a right triangle.

### c. Fairing Curve

The intersection between the canopy and fuselage is faired by a cubic from points 7 to 8 (Figure 2). The projections  $Z_7(Y)$  and  $Z_8(Y)$  of lines 7 and 8 on the  $Y-Z$  plane are given by Eq. (3) where the coefficients  $P$ ,  $Q$ ,  $R$ ,  $S$ ,  $T$  are input quantities. The

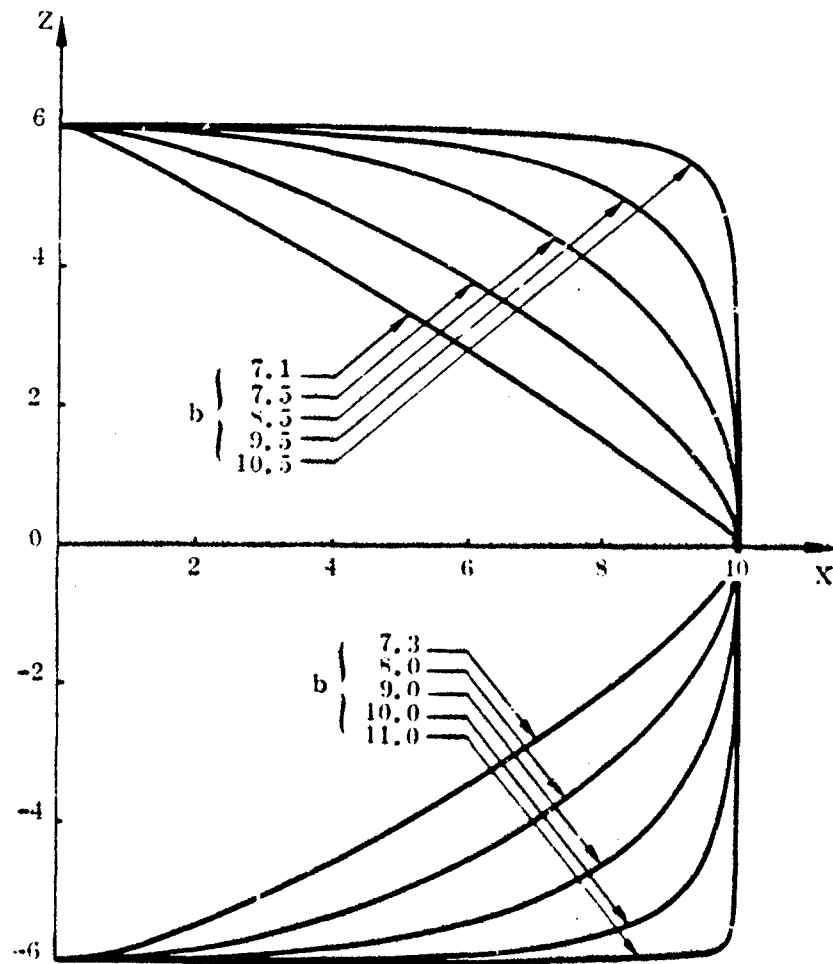


FIGURE 3. A FAMILY OF CONIC-SECTION CURVES

projections  $X_7(Y)$  and  $X_8(Y)$  on the X-Y plane are obtained by solving Eqs (4) and (5), respectively.

$$X_7(Y) = X_4 + (X_5 - X_4) \left[ 1 - \frac{(Z_7 - Z_5)^2}{Z_4 - Z_5} \right]^{1/2} \quad (10a)$$

$$X_8(Y) = X_1 + (X_2 - X_1) \left[ 1 - \frac{(Z_8 - Z_2)^2}{Z_1 - Z_2} \right]^{1/2}$$

The fairing curve matches the slopes of the ellipses at both end points 7 and 8. The slopes are obtained by differentiation of Eqs. (4) and (5)

$$X'_7(Y) = \left( \frac{cX}{cZ} \right)_7 = - \frac{(Z_7 - Z_5)}{(X_7 - X_4)} \left( \frac{X_4 - X_5}{Z_4 - Z_5} \right)^2 \quad (10b)$$

$$X'_8(Y) = \left( \frac{cX}{cZ} \right)_8 = - \frac{(Z_8 - Z_2)}{(X_8 - X_1)} \left( \frac{X_1 - X_2}{Z_1 - Z_2} \right)^2$$

The cubic equation that satisfies the first conditions of Eqs. (10a) and (10b) can be written

$$X = X_7 + X'_7 (Z - Z_7) + c \left( \frac{Z - Z_7}{Z_8 - Z_7} \right)^2 + d \left( \frac{Z - Z_7}{Z_8 - Z_7} \right)^3 \quad (11)$$

The coefficients  $c$  and  $d$  are obtained by applying the last conditions of Eqs. (10a) and (10b)

$$c = 3 (X_8 - X_7) - (X'_8 + 2X'_7) (Z_8 - Z_7) \quad (12)$$

$$d = -2 (X_8 - X_7) + (X'_8 + X'_7) (Z_8 - Z_7)$$

Equation (11) with  $c$  and  $d$  given by Eq. (12) is then the cubic equation for the fairing curve from points 7 to 8. The quantities  $X_7$ ,  $X_8$ ,  $X'_7$  and  $X'_8$  are given by Eqs. (10a) and (10b) while  $X_1$ ,  $X_2$ ,  $X_4$ ,  $X_5$ ,  $Z_1$ ,  $Z_2$ ,  $Z_4$ ,  $Z_5$ ,  $Z_7$  and  $Z_8$  are obtained from Eq. (3) where coefficients  $P_j$ ,  $Q_j$ ,  $R_j$ ,  $S_j$  and  $T_j$  are input quantities.

d. Geometric Variables and Ranges of Variation

Six geometric variables were selected to generate a family of forward fuselages including the F-4 baseline. As illustrated in Figure 4, these variables are the length  $l$  of the fuselage nose, the horizontal displacement  $a$  and vertical displacement  $a'$  of the maximum horizontal breadth line, the shape factor  $b$ , the lower deck height,  $h$ , and the bottom flat width  $f$ . As discussed previously the shape factor  $b$  is the distance from the origin to the  $45^\circ$  tangent line which is tangent to a contour curve of the lower fuselage cross section. All configurations generated by these variables have the same canopy as the F-4 and must satisfy the over-the-nose and over-the-side view line limitations.

The correspondence between the geometric variables and the reduced variables defined in Eq. (2), the ranges of variation of these geometric variables, and the baseline values of these variables are tabulated in Table 2. The variety of configurations that can be obtained using these geometric variables within their ranges of variation is illustrated in Figures 5 and 6. Figure 5 shows the top and side views of the configurations. The solid lines show the baseline configuration of the F-4. The dash-dot lines describe two extreme variations of the fuselage shape. The variation of the fuselage shape ahead of the canopy has to satisfy the over-the-nose view constraint, and the width of the fuselage is subject to the over-the-side view constraint. The radar installation imposes a minimum requirement for the width and limits the amount by which the lower profile can be moved upward. Notice that the figure shows only two extreme examples of the variations. The long nose version can be combined with a wide fuselage or the short nose version can be combined with a slender fuselage to yield other intermediate configurations. Figure 6 demonstrates the type of configuration variation that can be achieved through the chosen variables. Cross-sectional views at the three fuselage stations indicated in Figure 5 are shown in Figure 6. The solid lines describe the baseline configuration while the dashed lines describe two extreme variations of the cross sections. The circle at F.S. 50, which represents

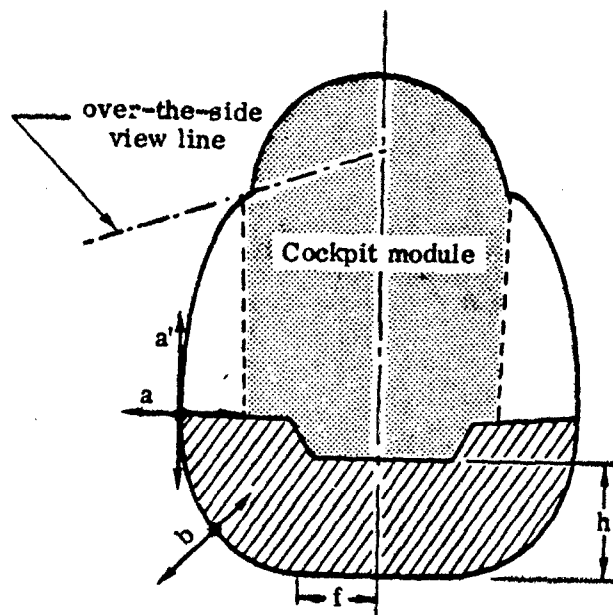
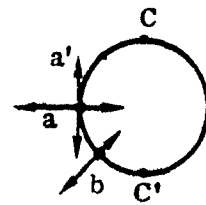
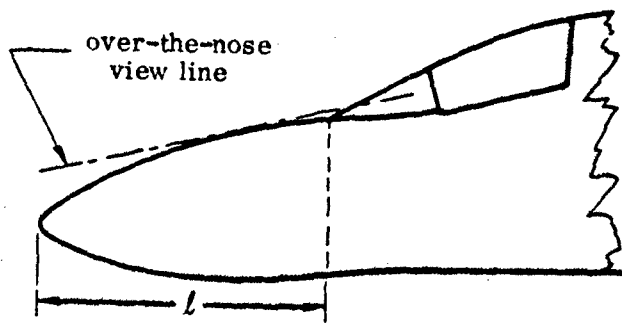


FIGURE 4. GEOMETRIC VARIABLES FOR WAVE DRAG REDUCTION

TABLE 2. VARIABLES, RANGES, AND BASELINE VALUES

Reduced Variables $z_i$	Geometric Variables $x_i$	Ranges of $x_i$		Baseline Values	
		$x_{i\min}$	$x_{i\max}$	$z_i$	$x_i$
$z_1$	$l$	84	104	-1.38	87.1
$z_2$	$b$	-2/3	2/3	0	*
$z_3$	$f$	0.	1.5	2/3	1.
$z_4$	$h$	5.	-10.	-2/3	0.
$z_5$	$a'$	0.6	1.2	2/3	1.
$z_6$	$a$	0.9	1.15	-0.4	1.

\*Baseline values for  $x_i$  vary from station to station.  $x_{i\min}$  is taken to be the local baseline value minus 2/3 of the difference between the baseline value and the local minimum value and  $x_{i\max}$  is taken to be the local baseline value plus 2/3 of the difference between the baseline value and the local maximum value.

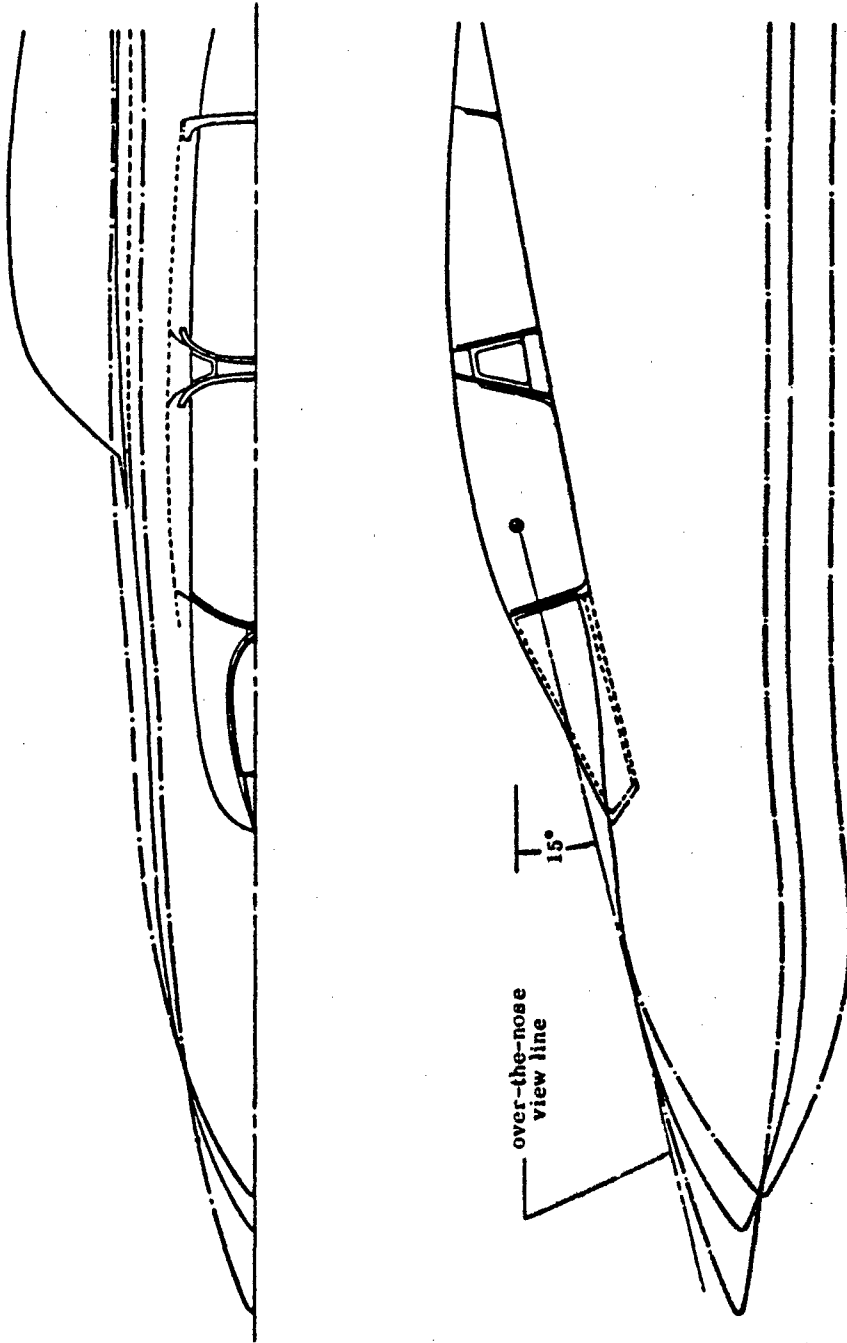
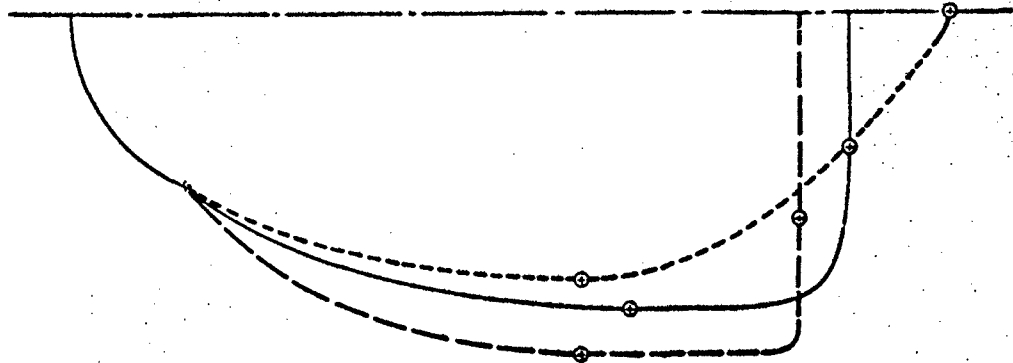
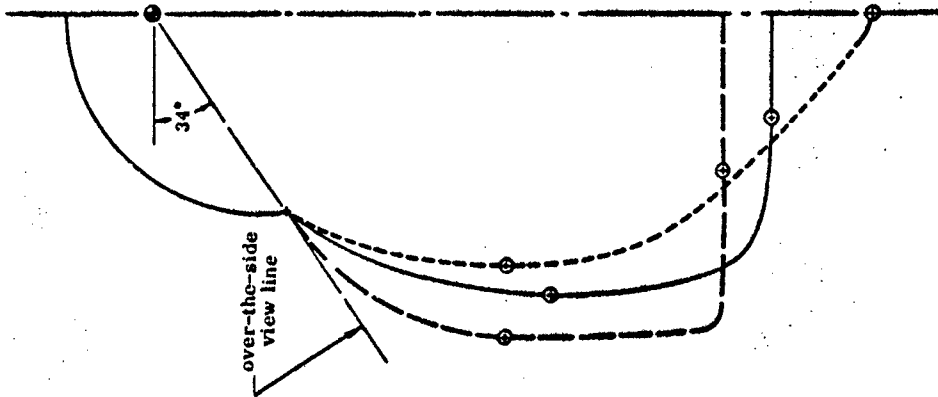


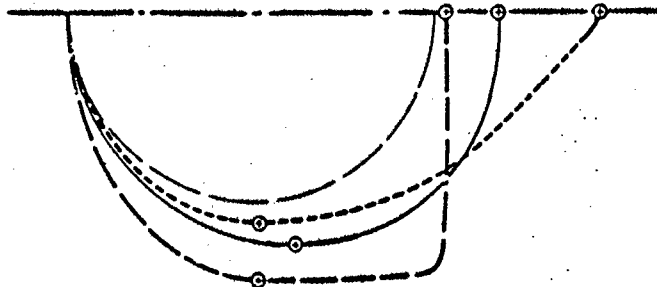
FIGURE 5. VARIATION OF FUSELAGE PROFILES AND BREADTH



FS 203



FS 123



FS 50

FIGURE 6. VARIATION OF FUSELAGE CROSS SECTIONS

the minimum area for the radar, limits the amount by which the maximum breadth line can move in or the lower profile can move up. The over-the-side view line governs how far the maximum breadth line can move out and up. Again only two extreme examples are given. Other configurations can be easily constructed. The important variable for the cross-sectional variation is the shape factor  $b$  which drastically alters the shape of the lower fuselage between the maximum breadth line and the lower surface flat.

It should be fairly obvious that the choice of geometric variables and their ranges of variation are somewhat arbitrary. The present selection allows a fairly wide range of variation of configurations which are similar to the baseline configuration. Other selections can be made such that the range of variation is more limited or the family of configurations is less similar to the baseline.

Some guidelines for the selection of geometric variables and their ranges can be given.

- (1) The two linear variables should be selected if their effects on the wave drag are small or if they affect the wave drag nearly linearly and their interactions with other variables are very small. The interaction between two variables is the influence of either variable on the wave drag contribution of the other. Nonlinear effects, however, can be included through a new concept which will be discussed in Section 4c.
- (2) The four remaining nonlinear variables should be selected in such a way that their interactions with each other are small or nearly linear.
- (3) The range of each variable should be as small as necessary, just wide enough to serve the particular purpose.
- (4) In general the nonlinear variables and their ranges should be selected in such a way that their influences on the wave drag are of the same order of magnitude.

#### 4. FLOW FIELD CALCULATION AND WAVE DRAG EQUATION

The wave drag coefficients of the baseline configuration and the 25 configurations picked by the Latin Square technique are calculated by applying the Three-Dimensional Method of Characteristics. The resulting wave drag coefficients are then used to obtain the wave drag equation.

##### a. Flow Over F-4 Baseline

As an example of the flow fields calculated by using the Three-Dimensional Method of Characteristics, the flow over the F-4 baseline at Mach 2.5 and zero angle of attack is presented here. Figure 7 shows the top and front views of the configuration, four cross-sectional views, and the upper and lower centerline pressure distributions. Along the upper centerline of the configuration, the pressure rises sharply as the flow hits the canopy-fuselage juncture. This signifies the existence of an embedded shock wave created by the canopy. At the pressure peak the local Mach number drops to 1.17. As the flow spreads over the canopy flat section, the pressure drops although the canopy profile is almost straight. A sudden drop of pressure is experienced as the canopy profile curves back after the flat section. Along the lower centerline the  $C_p$  first drops to a negative value due to further expansion. It recovers somewhat and eventually comes close to zero, consistent with the condition of zero angle of attack.

Figure 8 shows polar plots of the pressure distributions at four fuselage stations with cross sections shown in Figure 7. Since the forward fuselage ahead of the canopy droops somewhat, the pressure is higher on the upper fuselage than that on the lower fuselage at zero angle of attack. At F.S. 35.4 the  $C_p$  increases monotonically from a slightly negative value at the bottom to a positive value at the top. A noticeable pressure rise can be seen at F.S. 85.3 near the fuselage-canopy juncture. A similar pressure peak is visible at F.S. 145, at which  $C_p$  has become negative except near

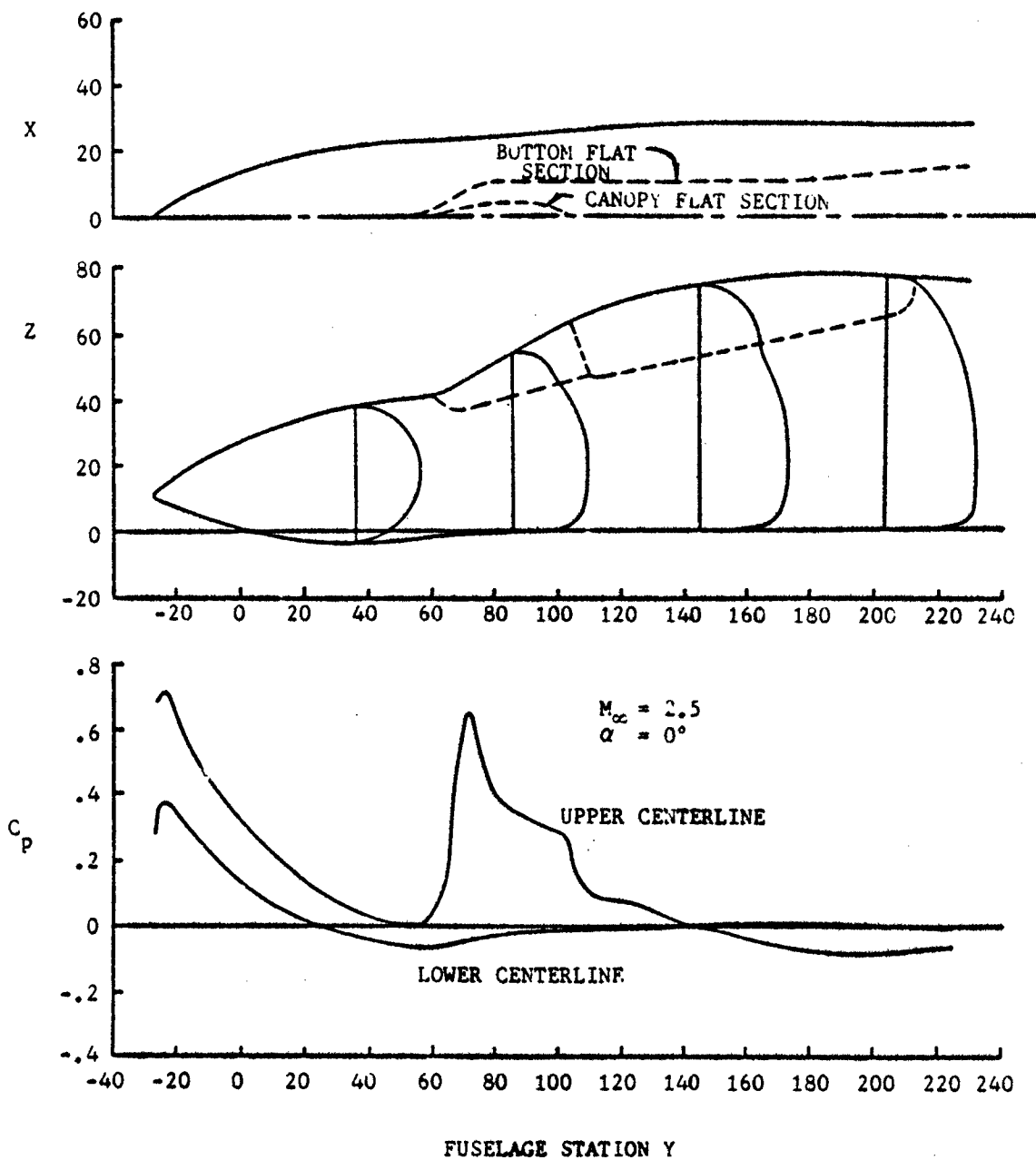
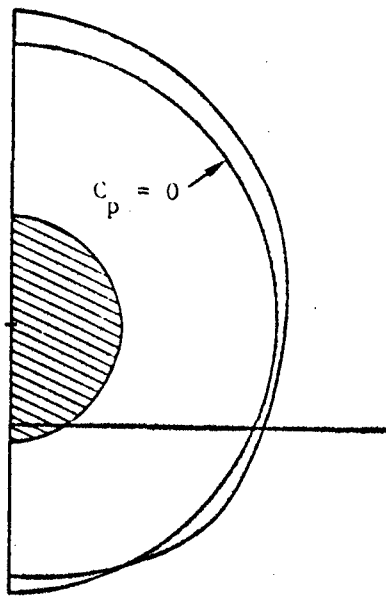
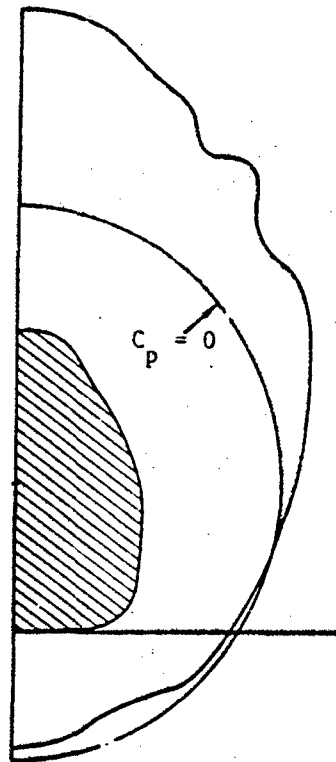
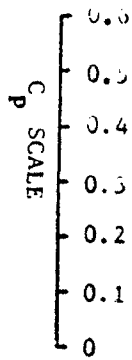


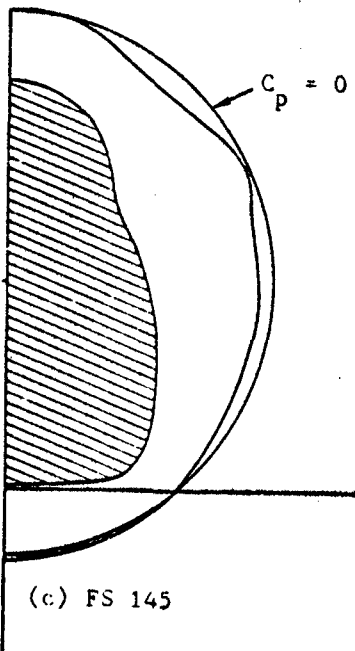
FIGURE 7. F-4 FUSELAGE AND CALCULATED CENTERLINE PRESSURE DISTRIBUTIONS



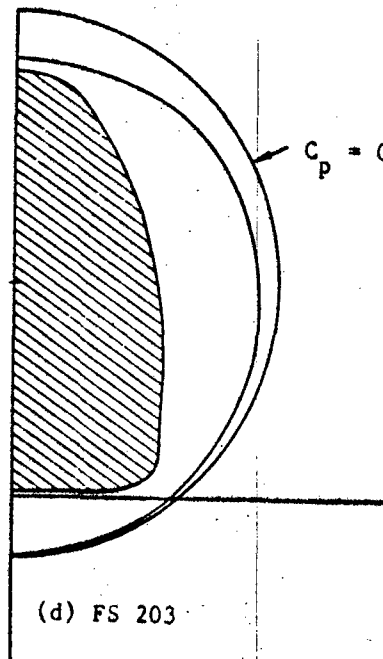
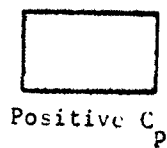
(a) FS 35.4



(b) FS 85.3



(c) FS 145



(d) FS 203

FIGURE 8. POLAR GRAPHS OF PRESSURE DISTRIBUTIONS AT FOUR FUSELAGE STATIONS

the bottom flat. In general the flow continues to expand downstream. By F.S. 203 the pressure everywhere has become slightly less than the free-stream pressure, and the variation of  $C_p$  is small and nearly monotonic.

b. Calculation of Wave Drag Coefficients

As shown in Eq. (1), for a given Mach number and angle of attack, the wave drag coefficient  $C_{DW}$  is assumed to be a quadric function of the six chosen geometric variables  $x_1, \dots, x_6$  with the coefficients  $a_i$  and  $a_{ij}$  to be determined. The reduced variables  $z_i$ , which take the levels of 0,  $\pm 1$ ,  $\pm 2$  according to the Latin Square arrangement shown in Table 1, assign corresponding values to the geometric variables  $x_i$ . For instance, according to the first cell,  $z_1$  and  $z_6$  are assigned level -2, which corresponds to the minimum values of the geometric variables  $x_1$  and  $x_6$  while  $z_4$  is assigned level 2, which corresponds to the maximum value of  $x_4$ . The other three reduced variables are assigned levels corresponding to intermediate values of the geometric variables. Thus the first cell specifies a set of values for the geometric variables which in turn defines a configuration whose wave drag coefficient can then be calculated by the method of characteristics program. In this way, each cell leads to one equation for the determination of the  $a_i$  and  $a_{ij}$  in the wave drag equation.

Since the method of characteristics is based on hyperbolic equations, the complete flow field must be supersonic in order to apply the method. As mentioned above, the local Mach number dropped to 1.17 near the fuselage canopy juncture of the F-4 at free-stream Mach 2.5 and zero angle of attack. Local subsonic regions would likely occur for some of the 25 variation configurations if the free-stream Mach number should be lowered. Hence the wave drag coefficients for the F-4 fuselage and the 25 variations, each corresponding to a cell of the Latin Square, were calculated using the Three-Dimensional Method of Characteristics program at Mach 2.5 and zero angle

of attack. The calculated wave drag coefficients (based on a wing area of 530 sq. ft.) are tabulated in Table 3. The mean value of the 25 coefficients is slightly higher than the baseline coefficient.

c. Wave Drag Equation

In the wave drag equation, Eq. (1), two of the geometric variables, i.e.,  $x_1$  and  $x_6$ , have only linear terms while other variables have nonlinear terms. In this way there are only 17 coefficients  $a_i$  and  $a_{ij}$  while there are 25 equations available for their evaluation. It therefore seems logical to include nonlinear terms of  $x_1$  and  $x_6$  in the equation as well. However, a preliminary numerical study suggested that the matrix of coefficients of the system of 25 equations has a rank of 17 and consequently only 17 unknowns  $a_i$  and  $a_{ij}$  can be determined.

It is more convenient to express the wave drag equation in terms of the reduced variables  $z_i$ . Since the reduced variables always take the levels 0, -1, -2, the least square fitting procedure once developed can be applied to any other values of the geometric variables without modification. Also, since all reduced variables are of the same order of magnitude, the coefficient of each term in the wave drag equation is a measure of the contribution of that term to the total wave drag. In terms of the reduced variables the original wave drag equation takes the form

$$C_{DW} = b_0 + \sum_{i=1}^6 b_i z_i + \sum_{j=1}^5 \sum_{i=2}^5 b_{ij} z_i z_j \quad (13)$$

When the coefficients  $b_i$  and  $b_{ij}$  were evaluated using the calculated wave drag coefficients of the 25 cells and the baseline in a least-square procedure, Eq. (13) was

TABLE 3. WAVE DRAG COEFFICIENTS  $C_{DW} \times 10^3$   
 (FOR FORWARD FUSELAGE UP TO FS 230)

8.72259	5.97017	5.72492	5.88469	5.95256
7.62580	7.25404	7.10510	5.43938	5.76062
6.52684	6.67305	6.59154	6.86143	7.61059
8.21773	8.68830	6.43817	6.61810	5.93960
7.63046	8.22275	8.62522	7.24846	5.87617

Baseline value  $C_{DW} = 6.69437 \times 10^{-3}$

used for some preliminary investigation of minimum wave drag configurations. One of the predicted configurations was obtained when the fuselage length was set to that of the baseline and no other constraints were imposed. The predicted cross section at F.S. 50 is shown in Figure 9 by a dash-dot line. Also shown are the radar dish by a dashed line and the baseline cross section by a thin solid line. While it was interesting to note that the radome requirement was fortuitously satisfied, it was suspected that the wrong trend was predicted since a reduction in the shape factor  $b$  would reduce the cross-sectional areas all the way from the nose to F.S. 230. Subsequent verification runs by the method of characteristics program showed that the wave drag equation was under-predicting the wave drag and the predicted trend in  $b$  was incorrect. This poor prediction was attributed to the rather wide ranges of the variables. In order to increase the prediction accuracy, the three calculated wave drag coefficients by the verification runs and their corresponding levels of the reduced variables (cells 27, 28, and 29 of Table 4) were used to provide three more equations for the determination of the coefficients  $b_1$  and  $b_{11}$ , which are tabulated in Table 5. From Table 5 it is seen that in general  $b_0$  is one order of magnitude greater than  $b_1$  which is one order of magnitude greater than  $b_{11}$ . Eq. (13) with the improved  $b_1$  and  $b_{11}$  was again used to predict the minimum wave drag configuration when the fuselage length was set to that of the baseline and the radome constraint was imposed. The resulting cross section of the minimum wave drag configuration at F.S. 50 is shown in Figure 9 by a heavy solid line. Both the predicted trend and wave drag coefficient were verified by the method of characteristics program, as presented in the next section.

A new concept has therefore been introduced to the optimization procedure using Latin Square sampling. This concept enables the prediction equation to "learn" from experience in order to improve its prediction. After each or several verification calculations of the predicted configurations, the resulting equations corresponding to

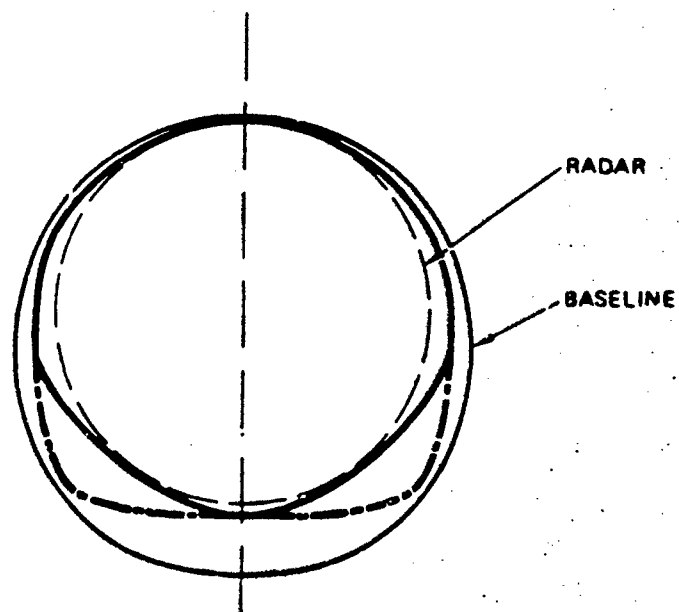


FIGURE 9. FUSELAGE CROSS SECTIONS AT F.S. 50

TABLE 4. ADDITIONAL WAVE DRAG COEFFICIENTS AND CORRESPONDING SETS OF REDUCED VARIABLES

Cell No.	$z_1$	$z_2$	$z_3$	$z_4$	$z_5$	$z_6$	$C_{DW} \times 10^3$
26*	-1.35	0	2/3	-2/3	2/3	-0.4	6.67437
27	-1.35	1.5	2	-2/3	2	-2	6.57260
28	-1.35	2	2	-2	2	-2	6.09569
29	-1.35	0	2	-2	2	-2	5.95529
30	-1.35	-1.71	-2	-2	0.54	-2	5.56343
31	-1.35	2	2	-2	1.91	0.5325	6.51449
32	-0.35	2	2	-2	1.5	0.415	6.11554

\*Cell 26 corresponds to the baseline.

TABLE 5. COEFFICIENTS OF WAVE DRAG EQUATION

$$b_0 = 6.677233 \times 10^{-3}$$

VALUE OF  $b_i \times 10^4$

i	1	2	3	4	5	6
$b_i \times 10^4$	-3.960518	2.010588	0.035260	4.557457	-0.191512	2.672168

VALUE OF  $b_{ij} \times 10^5$

i \ j	2	3	4	5
2	2.450636	-6.113357	7.665063	-0.727027
3		0.134838	-1.613047	-2.356471
4			5.565432	1.405971
5				4.228010

the verification runs are included in the least-square procedure to obtain improved coefficients  $b_i$  and  $b_{ij}$  of the prediction equation. In general one or two applications of this process should yield satisfactory results. The improved prediction for one set of constraints may or may not lead to improvement for other sets of constraints. However, the same process can be applied wherever needed.

An additional advantage of this new concept is that nonlinear terms involving  $z_1$  and  $z_6$  can also be taken into account. With each addition of an equation due to a verification, the rank of the matrix of coefficients usually increases by one. That means one more  $b_{ij}$  of a nonlinear term involving  $z_1$  or  $z_6$  can be included. This process can be repeated, if necessary, until all quadric terms are accounted for.

## 5. GEOMETRIC CONSTRAINTS AND WAVE DRAG REDUCTION

The wave drag equation can now be investigated to reduce the wave drag. In the process of determining the minimum wave drag configuration, certain geometric constraints, such as minimum cross-sectional area or maximum fuselage length, must be satisfied. For each set of geometric constraints there exists a minimum wave drag configuration. In this section the optimization procedure and some minimum wave drag configurations are presented and discussed.

### a. Optimization Procedure and Geometric Constraints

The simplest and surest way to find the minimum wave drag configuration subject to a given set of geometric constraints is to use Eq. (13) to calculate the wave drag coefficients for all allowable sets of levels of the variables and pick the set that gives the least wave drag. The optimization procedure consists of the following steps.\*

- (1) Make a numerical search through the ranges of all six variables, using the wave drag equation to calculate the wave drag coefficients for those sets of levels that satisfy the constraints.
- (2) Identify the set of levels of the variables that yields the least wave drag.
- (3) Prepare body description input data for the minimum wave drag configuration.
- (4) Use the Three-Dimensional Method of Characteristics program to verify the wave drag coefficient predicted by Eq. (13).

The coefficients  $b_i$  and  $b_{ij}$  of Eq. (13) were obtained by applying a least square procedure to fit the hypersurface represented by Eq. (13) over the 25 wave drag coefficients given in Table 3 and the first four coefficients of Table 4. The standard deviation of the fit was about  $1.02 \times 10^{-4}$  which corresponds to an error of about 1.5%

---

\*The Numerical Search Procedure is presented in Appendix D.

based on the mean wave drag coefficient. The maximum error of the fit over the 29 data points was about 2.4%. Hence step 5 of the optimization procedure is necessary for wave drag reduction of 4-5% or less as predicted by Eq. (13).

Four types of geometric constraints are considered in order to satisfy most design needs. These are:

- (1) One or more of the six geometric variables take assigned values within the ranges of variation. For instance, the length can be kept the same as that of the baseline or the width can take 90% of the baseline width.
- (2) At one or more fuselage stations the configuration cross sections contain geometric curves prescribed by tabulated data of widths versus elevations. This type of constraint is useful for the placement of particular equipment, for instance, the radome.
- (3) At one or more fuselage stations the configuration cross sections satisfy minimum area requirements. The minimum area can be either a given area or a certain percentage of the baseline cross-sectional area.
- (4) The configuration satisfies a minimum volume requirement between two given stations. A given volume or a certain percentage of the baseline volume can be imposed.

#### b. Minimum Wave Drag Configurations

Several minimum wave drag configurations subject to various geometric constraints are presented to illustrate the application of this program. These configurations were obtained by using the optimization procedure, and the predicted wave drag coefficients were verified by the Three-Dimensional Method of Characteristics (3DMoC) program in some cases.

Within the ranges of variation of the six variables (when the only constraint was implicitly imposed by the ranges under consideration), a 34.8% reduction of the wave drag coefficient was predicted by Eq. (13). The configuration corresponds to the longest nose, as might be expected. When the length was set to be equal to that of the baseline, a 15% reduction was predicted by the equation. The percentage reduction of the wave drag in relation to the increase of fuselage length is plotted in Figure 10. It is seen that for every inch the fuselage is lengthened the wave drag equation predicts a wave drag reduction slightly over 1%. Since no constraint other than the nose length was imposed, these minimum wave drag configurations have the least cross-sectional areas attainable within the ranges of variation of the remaining five geometric variables. Consequently these configurations cannot contain the radar dish which is represented by a dashed circle at F.S. 50 in Figures 6 and 9. When the fuselage length was set to that of the baseline and the radome constraint was imposed, the wave drag equation predicted a 14% reduction of the wave drag coefficient. The cross section of this minimum wave drag configuration at F.S. 50 is shown by the heavy solid line in Figure 9. It is seen that the lower fuselage cross section barely contains the radar dish. This predicted trend that the wave drag decreases with the shape factor  $b$  in the neighborhood of this minimum wave drag configuration was verified by calculations using the Three-Dimensional Method of Characteristics program. Calculation of the wave drag of this configuration also resulted in a wave drag reduction of 12.6%, which agrees fairly well with the 14% reduction predicted by the wave drag equation, considering that the standard deviation of the least square fit is 1.5%. The front view of this minimum wave drag configuration is presented in Figure 11, which shows the contours of the cross sections from F.S. 20 to F.S. 230 at intervals of 10. The front view of the baseline is presented in Figure 12 for comparison. It is seen that this substantial reduction of the wave drag was accomplished at the expense of reduced fuselage volume.

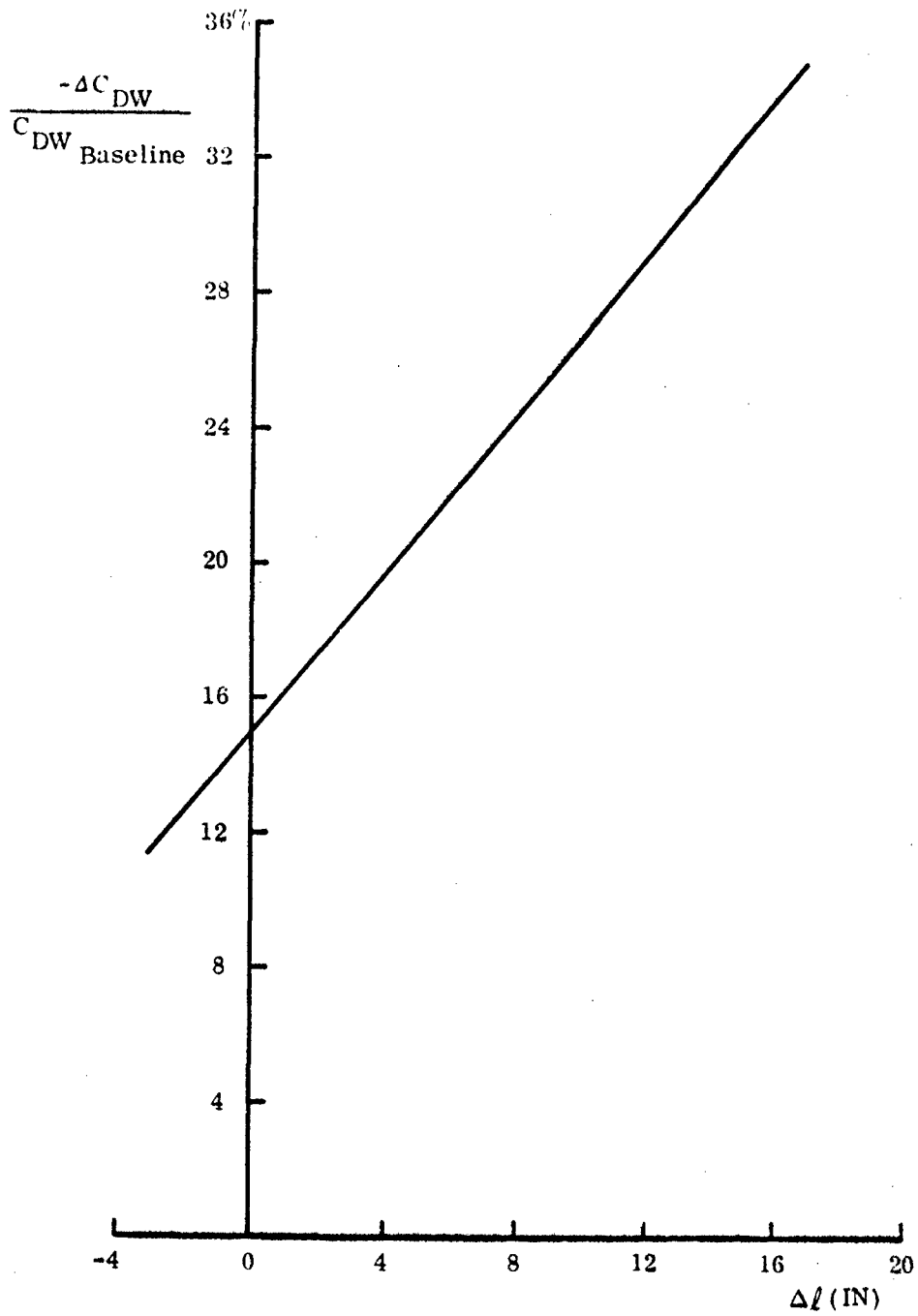


FIGURE 10. REDUCTION OF WAVE DRAG VS INCREASE OF FUSELAGE LENGTH

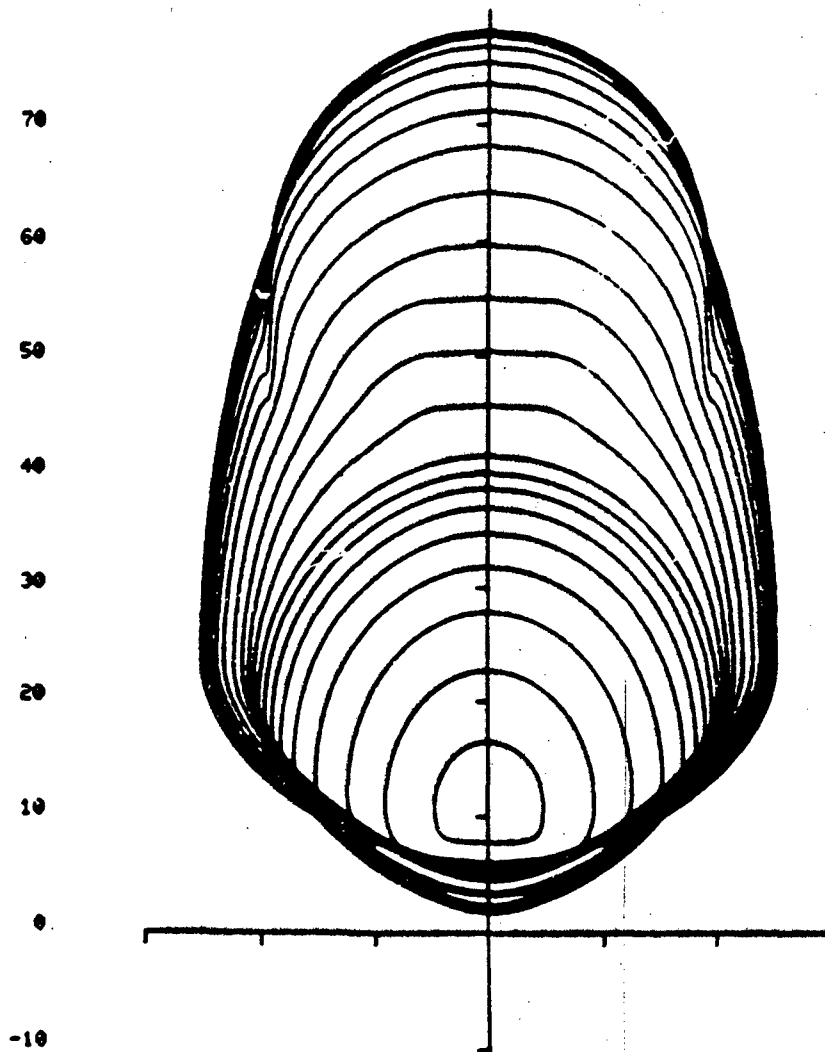


FIGURE 11. FRONT VIEW OF A MINIMUM WAVE DRAG CONFIGURATION  
SATISFYING THE RADOME REQUIREMENT

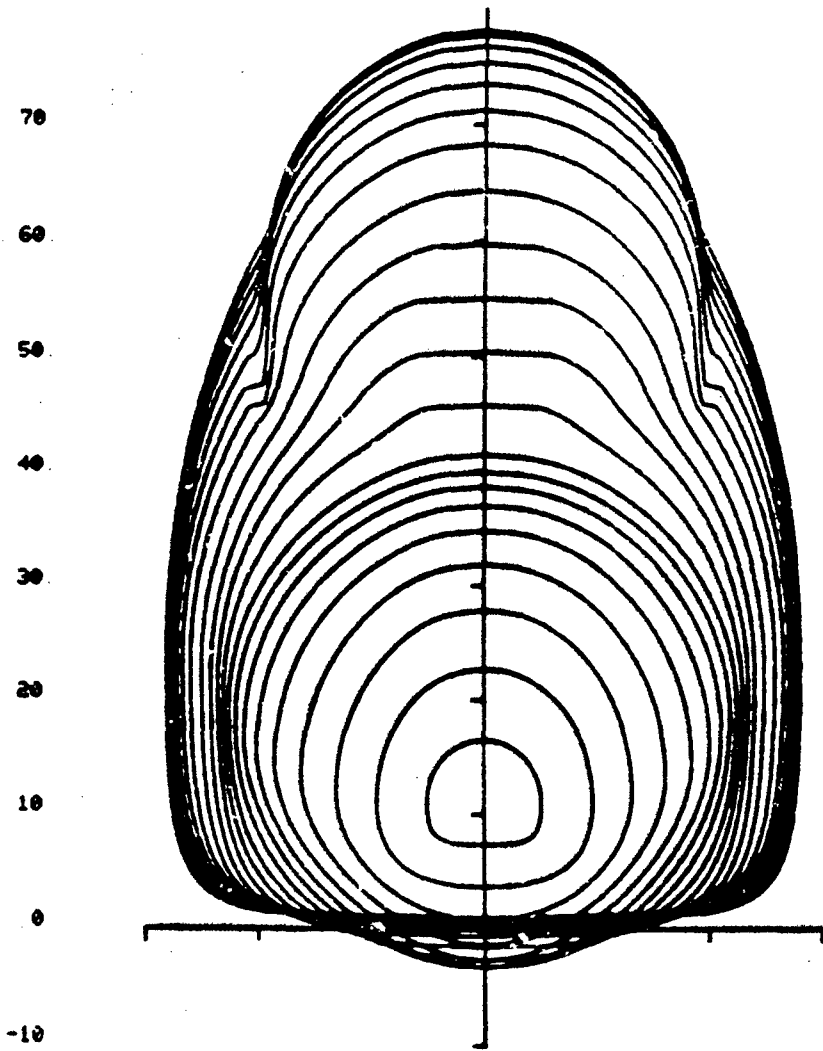


FIGURE 12. FRONT VIEW OF THE BASELINE CONFIGURATION

Two important general constraints that strongly affect the wave drag are the fuselage nose length and the fuselage volume. Therefore, the optimization procedure was used to determine a number of minimum wave drag configurations for various nose lengths and fuselage volumes. Since the horizontal displacement of the maximum breadth line has an important effect on the fuselage volume, nonlinear terms of the displacement  $a$  and the nose length  $l$  should be included in the wave drag equation for accurate prediction of the influence of these two geometric variables on the wave drag. Equation (13) was first used to obtain two preliminary minimum wave drag configurations which are tabulated in Table 4 as cells 31 and 32. The 30th cell in Table 4 corresponds to the minimum wave drag configuration subject to the radome constraint, which was discussed in the preceding paragraph. These 32 cells provided 32 equations which allowed 23 terms (or 23 coefficients  $b_i, b_{ij}$ ) to be included in an improved wave drag equation. All important nonlinear terms involving  $a$  and  $l$  were included.

The final improved wave drag equation, with six additional terms, is expanded into the form:

$$\begin{aligned}
 C_{DW} = & b_0 + b_1 Z_1 + b_2 Z_2 + b_3 Z_3 + b_4 Z_4 + b_5 Z_5 + b_6 Z_6 \\
 & + b_{11} Z_1^2 + b_{22} Z_2^2 + b_{33} Z_3^2 + b_{44} Z_4^2 + b_{55} Z_5^2 + b_{66} Z_6^2 \\
 & + b_{21} Z_2 Z_1 + b_{32} Z_3 Z_2 + b_{41} Z_4 Z_1 + b_{42} Z_4 Z_2 + b_{43} Z_4 Z_3 \\
 & + b_{52} Z_5 Z_2 + b_{53} Z_5 Z_3 + b_{54} Z_5 Z_4 + b_{62} Z_6 Z_2 + b_{64} Z_6 Z_4
 \end{aligned} \tag{14}$$

The coefficients of Eq. (14) are tabulated in Table 6. The optimization procedure using the improved wave drag equation was then applied to determine the dependence of the wave drag on the nose length and fuselage volume. The predicted percentage reduction of the wave drag coefficient is plotted against the increase of the fuselage nose length in Figure 13 for various fuselage volumes (expressed as % of the baseline volume). The two circles mark the calculated percentage reductions of the wave drag

TABLE 6. COEFFICIENTS OF IMPROVED WAVE DRAG EQUATION

$$b_0 = 6.559250 \times 10^{-3}$$

VALUE OF  $b_i \times 10^4$

i	1	2	3	4	5	6
$b_i \times 10^4$	-3.965690	1.952752	0.020646	4.552590	-0.205050	2.655061

VALUE OF  $b_{ij} \times 10^5$

j \ i	1	2	3	4	5	6
1	*4.236247	*1.614632		*-4.901642		
2		3.790654	-2.450446	5.690593	1.303169	*2.562793
3			-0.045254	-1.453514	-2.052481	
4				4.179456	-0.470882	*0.183437
5					2.906675	
6						*1.710665

\*Additional terms added to the original wave drag equation

using the Three-Dimensional Method of Characteristics for the two selected configurations. Excellent agreement between the predicted and calculated wave drag reduction is seen. When the nose length and fuselage volume were set to the baseline values, very little wave drag reduction was obtained within the variations of the six geometric variables as selected. This set of geometric variables and their ranges were chosen to illustrate the wave drag reduction procedure in such generality that a wide range of configurations similar to the baseline was covered and various illustrations could be made. No specific effort was made to tailor the variables to the wave drag reduction of the baseline configuration. The baseline wave drag could conceivably be further reduced by some appropriately selected variables. Referring to Figure 13 again, some rule-of-thumb percentage reductions of the wave drag can be observed. On the average one inch increase in the fuselage length reduces the wave drag by slightly over one percent while one percent decrease in the fuselage volume reduces the wave drag by about 3/4 percent.

The characteristics of the improved wave drag equation are shown in Figures 14 through 18. Each of the figures shows the variations of the wave drag coefficient with respect to two of the six geometric variables, where the remaining four are set equal to the values of the baseline. Although it is difficult to plot the present wave drag function in a six-dimensional space, these figures at least enable one to isolate and study the interacting characteristics between any two of the six variables. The effects of volume are also shown by plotting symbols on the curves to indicate various fuselage volume limits. Since the geometric variable  $b$  is different for different fuselage stations, the parameter  $b$  used in these figures is actually the reduced variable which is constant for each given configuration.

Figures 14a through 14e show the variations of the drag coefficient with respect to the height of the lower deck  $h$  for families of  $l$ ,  $b$ ,  $a'$ ,  $a$  and  $f$ , respectively. Within the ranges of variables studied,  $C_{DW}$  decreases monotonically with  $h$ . Figure 14a

# Best Available Copy

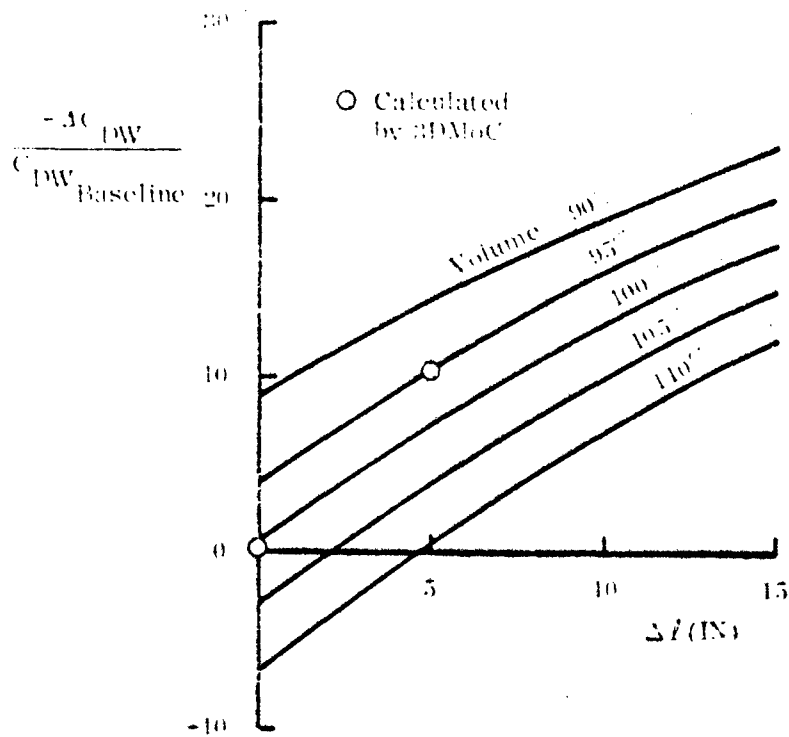


FIGURE 13. REDUCTION OF WAVE DRAG VS INCREASE OF FUSELAGE LENGTH FOR VARIOUS FUSELAGE VOLUMES (% OF BASELINE VOLUME)

Symbol	$\frac{\text{Vol}}{\text{Vol}_{BL}}$
X	.98
Δ	.99
○	1.00
□	1.01
★	1.02

$f = 1$   
 $a' = 1$   
 $a = 1$   
 $b$ , baseline

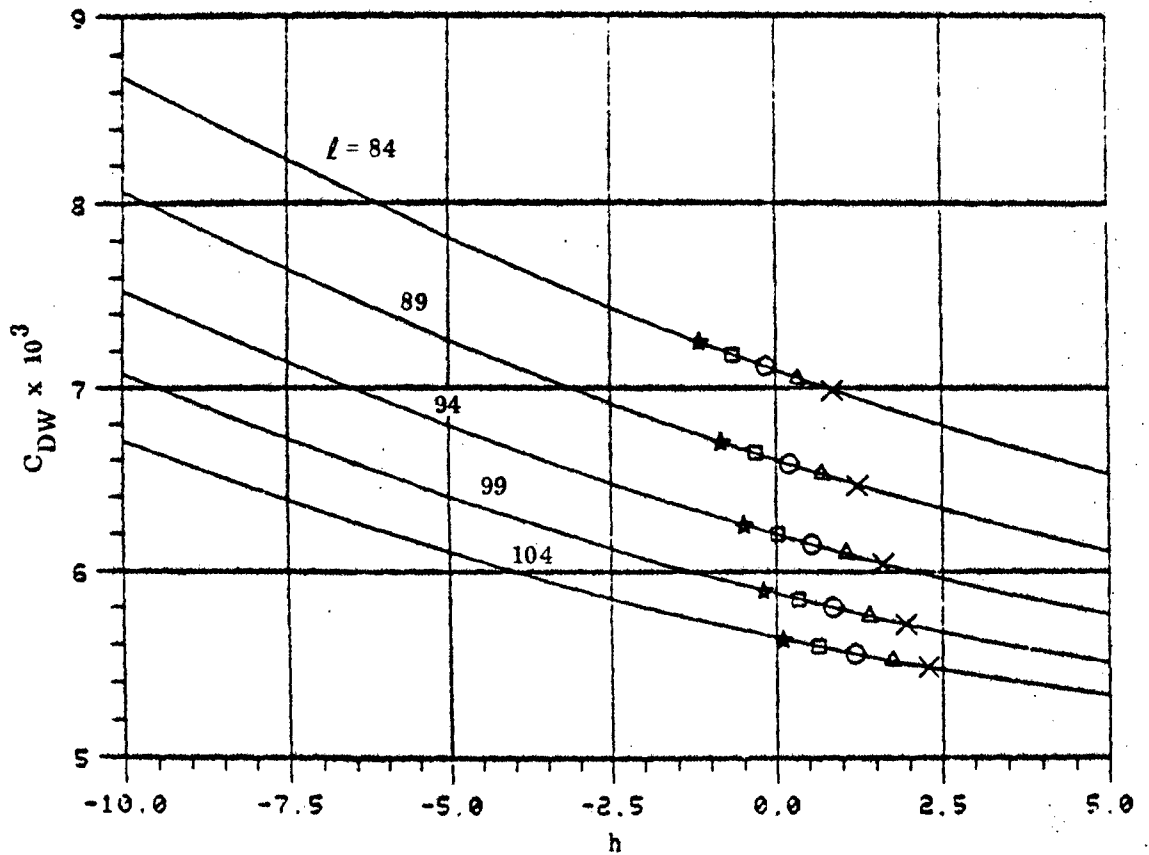


FIGURE 14a. CHARACTERISTICS OF THE WAVE DRAG EQUATION -  $C_{DW}$  VS  $h$  (FOR CONSTANT  $l$ )

Symbol	$\frac{\text{Vol}}{\text{Vol}_{BL}}$
×	.98
△	.99
○	1.00
□	1.01
★	1.02

$l = 87.1$

$f = 1$

$a' = 1$

$a = 1$

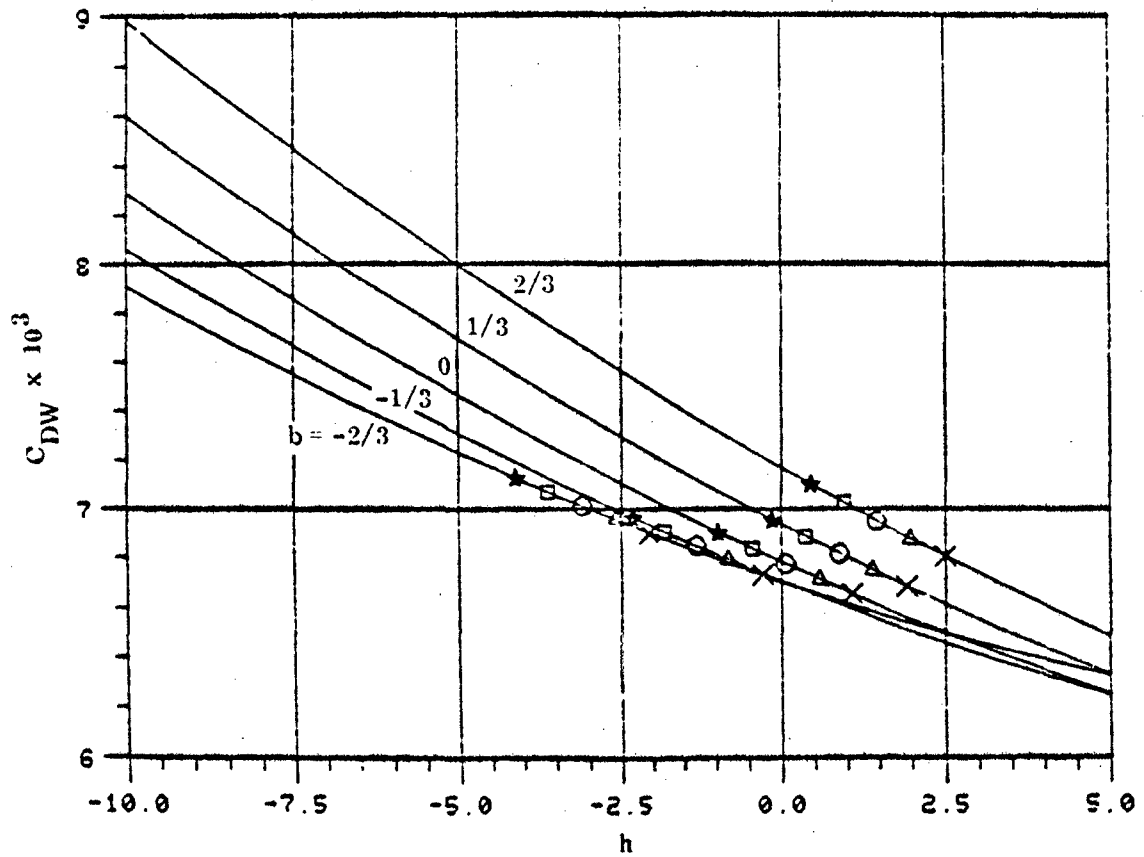


FIGURE 14b. CHARACTERISTICS OF THE WAVE DRAG EQUATION -  $C_{DW}$  VS  $h$  (FOR CONSTANT  $b$ )

Symbol	$\frac{\text{Vol}}{\text{Vol}_{BL}}$
×	.98
△	.99
○	1.00
□	1.01
★	1.02

$l = 87.1$   
 $f = 1$   
 $a = 1$   
 b, baseline

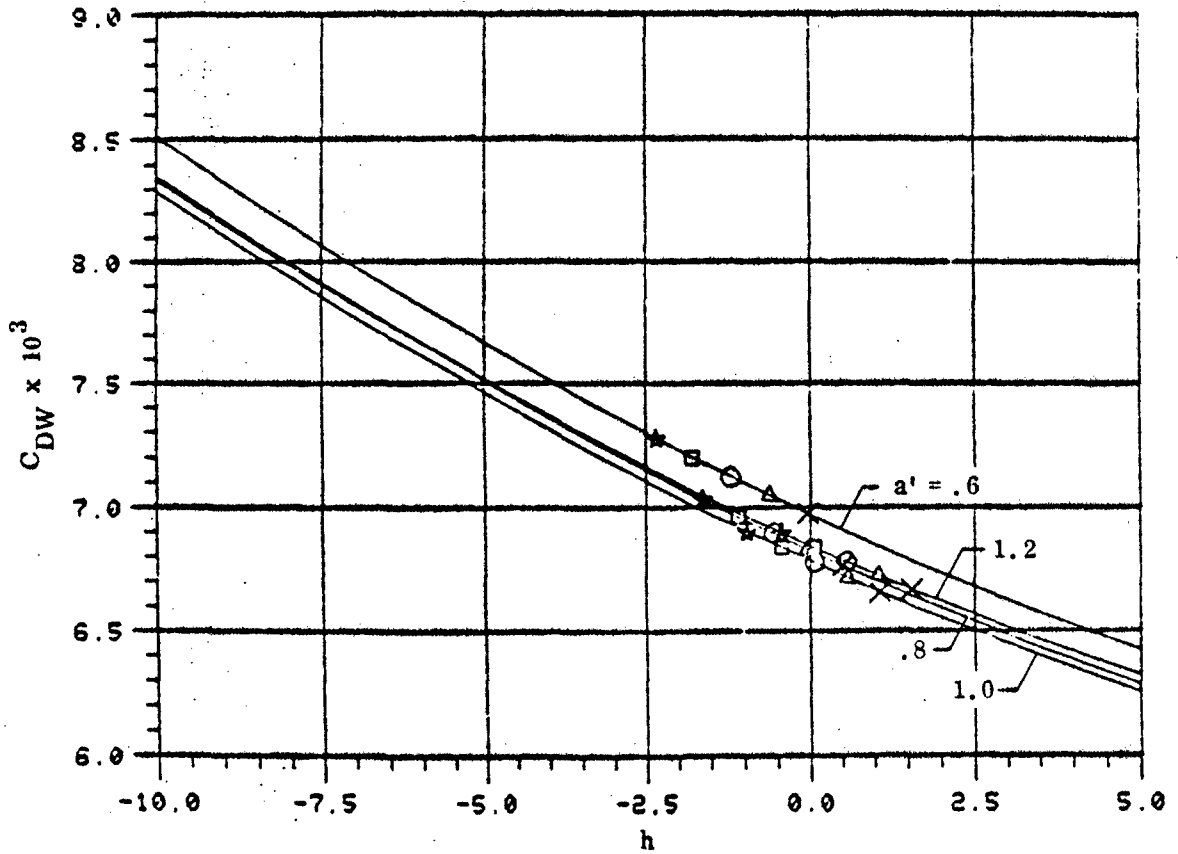


FIGURE 14c. CHARACTERISTICS OF THE WAVE DRAG EQUATION -  $C_{DW}$  VS  $h$  (FOR CONSTANT  $a'$ )

Symbol	$\frac{Vol}{Vol_{BL}}$
×	.98
△	.99
○	1.00
□	1.01
★	1.02

$l = 87.1$   
 $f = 1$   
 $a' = 1$   
 $b$ , baseline

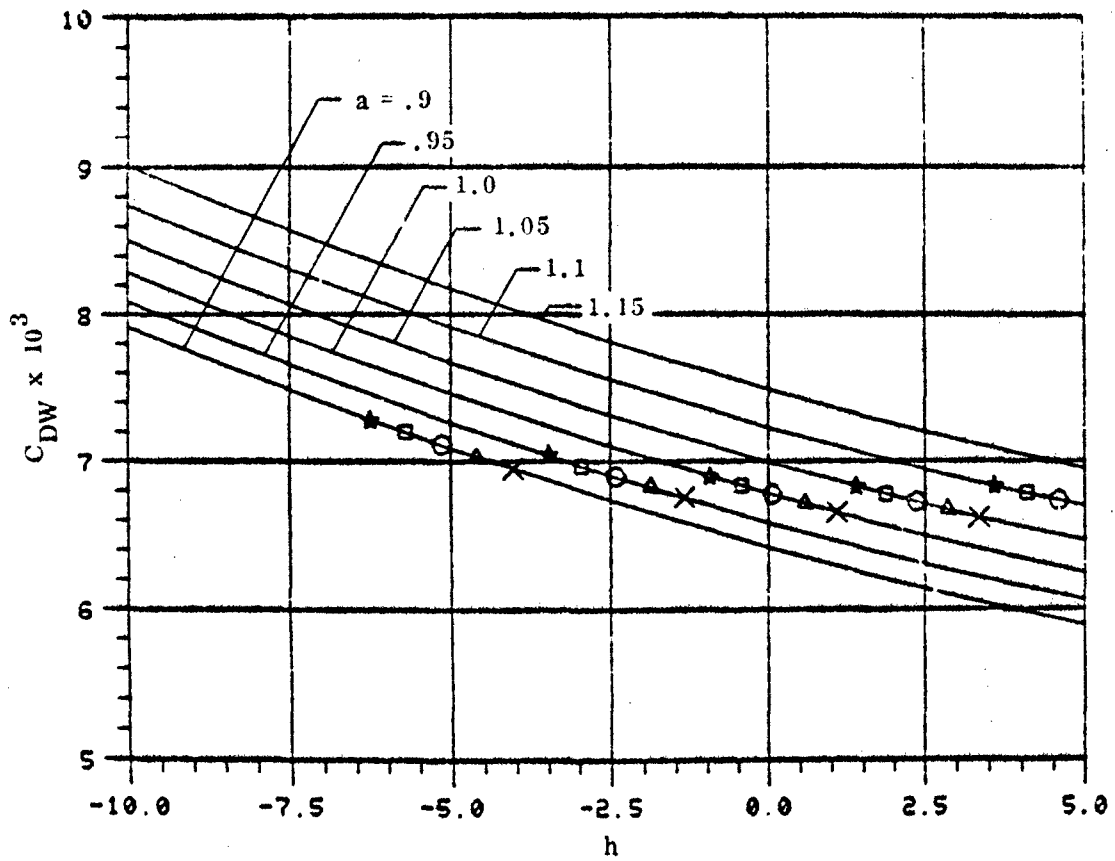


FIGURE 14d. CHARACTERISTICS OF THE WAVE DRAG EQUATION -  $C_{DW}$  VS  $h$  (FOR CONSTANT  $a$ )

Symbol	$\frac{\text{Vol}}{\text{Vol}_{\text{BL}}}$
×	.98
△	.99
○	1.00
□	1.01
★	1.02

$l = 87.1$   
 $a' = 1$   
 $a = 1$   
 b, baseline

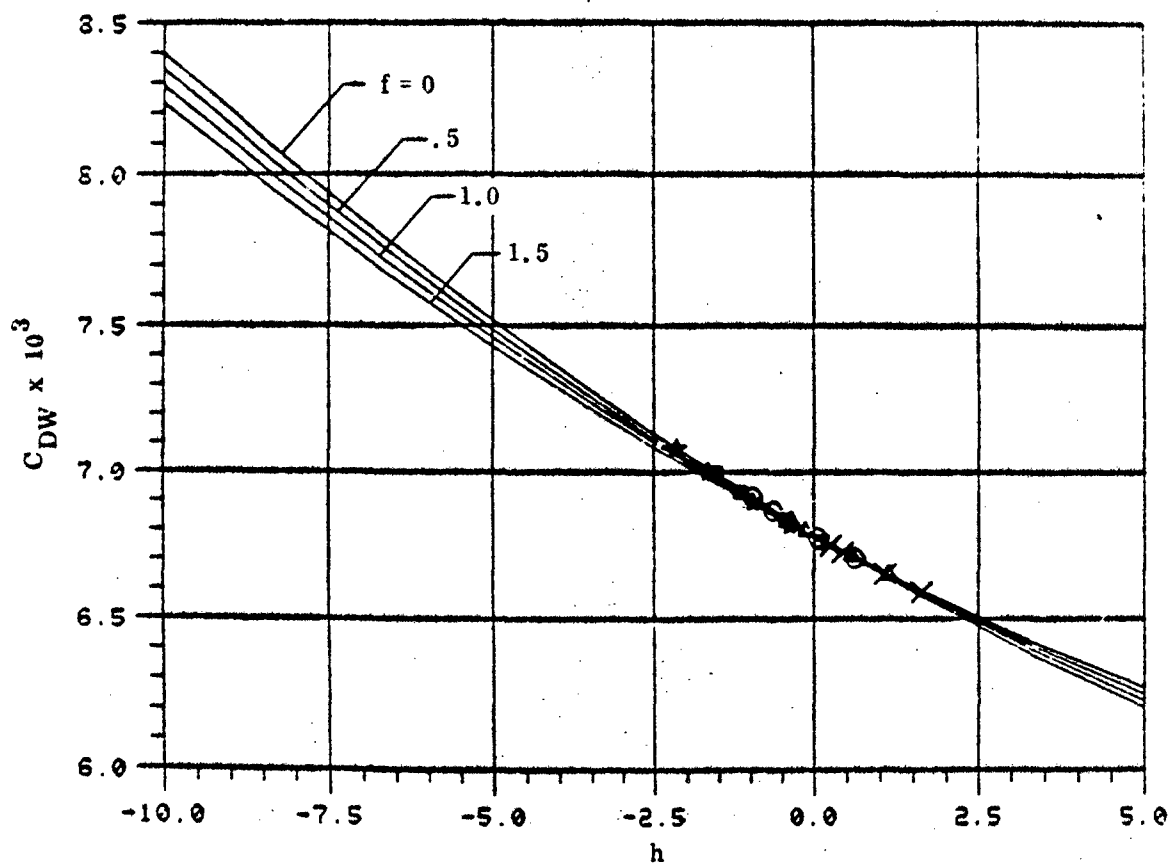


FIGURE 14e. CHARACTERISTICS OF THE WAVE DRAG EQUATION -  $C_{DW}$  VS  $h$  (FOR CONSTANT  $f$ )

## Best Available Copy

indicates that for a given volume,  $C_{DW}$  decreases with the length of the fuselage nose  $l$ . Along values of constant volume, Figures 14b, 14c and 14d show that when each of the respective variables ( $b$ ,  $a'$  and  $a$ ) interacts with  $h$ , there is a definite combination of variables which yields a configuration of minimum wave drag. For a volume equal to the baseline value ( $Vol/Vol_{BL} = 1$ ), for example, Figure 14b shows that a minimum occurs near  $b = h = 0$  which are equal to the baseline values. The occurrence of the minimum near the baseline configuration verifies the results obtained from the numerical search where little reduction of wave drag from the baseline was obtained within the variations of the selected geometric variables. Lines of constant  $a'$  and  $a$  in Figures 14c and 14d respectively are nearly parallel, indicating that the interaction between  $a'$  and  $h$  and the interaction between  $a$  and  $h$  are weak. This fact is also revealed by examining the magnitude of the coefficients of the wave drag equation tabulated in Table 6. The magnitude of these interaction terms, although included in the formulation of the wave drag equation, is one order of magnitude smaller than the average of the remaining interaction terms. Figures 15a and 15b show the variations with respect to the length of the nose  $l$  for families of  $a'$  and  $f$ , respectively. Again, the trend shows that  $C_{DW}$  decreases with  $l$ , but minima for given constant volumes are not definitely shown. Figure 15b shows that the width of the fuselage bottom flat section has little effect on the drag coefficient when the remaining four variables are set equal to the values of the baseline. Figures 16a through 16d show the variations with respect to the horizontal displacement of the maximum breadth line  $a$  for families of  $l$ ,  $b$ ,  $a'$  and  $f$ , respectively. Here, the figures show that the drag coefficient increases monotonically with  $a$ . Similar to the results shown in Figures 14a through 14e, for constant volume the drag coefficient decreases with  $l$ , and when the volume is equal to that of the baseline, minima occur at or near the baseline. In Figure 16b, for example, the minimum occurs at  $a = 1.01$  and  $b = 1/6$  approximately for  $Vol/Vol_{BL} = 1$ . The curves in Figures 16a, 16c, and 16d are parallel since interaction terms between each of the variables with  $a$  are not included in the present wave

Symbol	$\frac{\text{Vol}}{\text{Vol}_{BL}}$
×	.98
△	.99
○	1.00
□	1.01
★	1.02

$f = 1$   
 $h = 0$   
 $a = 1$   
 b, baseline

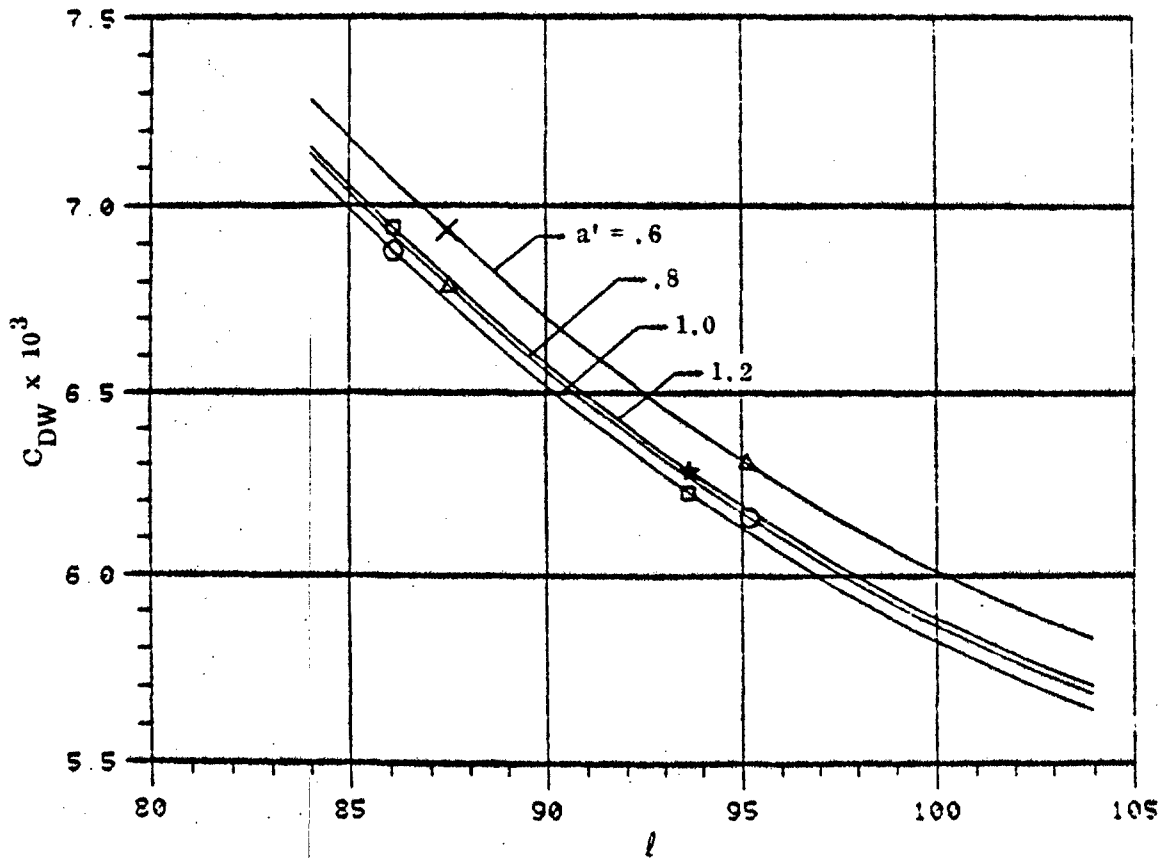


FIGURE 15a. CHARACTERISTICS OF THE WAVE DRAG EQUATION -  $C_{DW}$  VS  $l$  (FOR CONSTANT  $a'$ )

Symbol	$\frac{\text{Vol}}{\text{Vol}_{\text{BL}}}$
×	.98
△	.99
○	1.00
□	1.01
★	1.02

$h = 0$   
 $a' = 1$   
 $a = 1$   
 $b$ , baseline

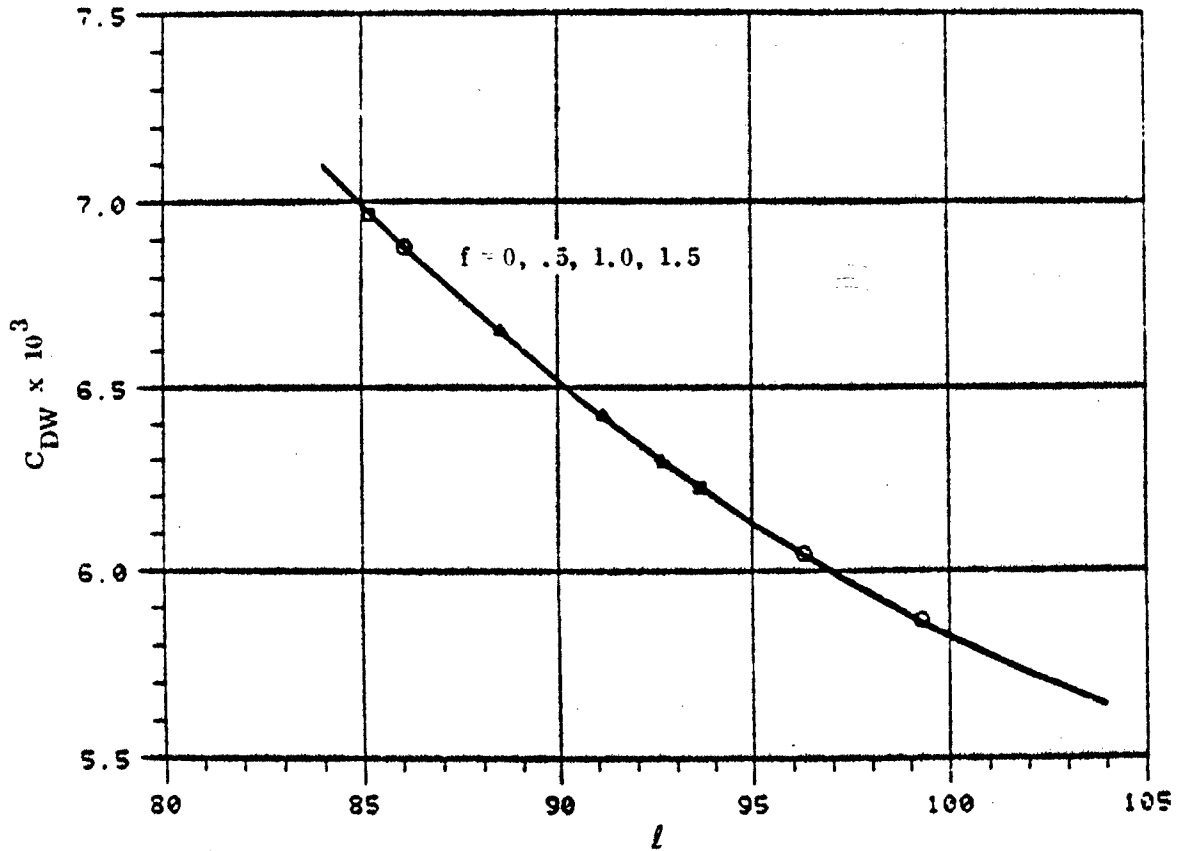


FIGURE 15b. CHARACTERISTICS OF THE WAVE DRAG EQUATION -  $C_{DW}$  VS  $l$  (FOR CONSTANT  $f$ )

Symbol	$\frac{\text{Vol}}{\text{Vol}_{BL}}$
×	.98
△	.99
○	1.00
□	1.01
★	1.02

f 1  
h 0  
a' = 1  
b, baseline

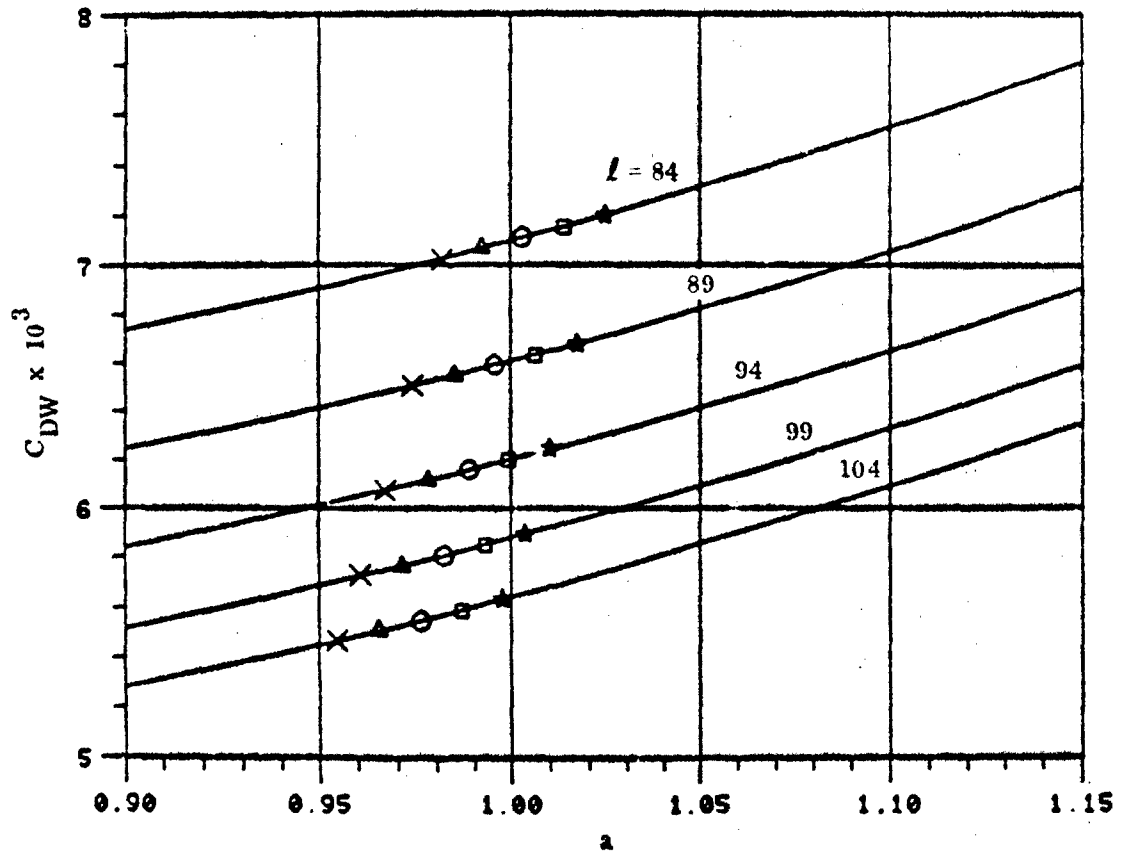


FIGURE 16a. CHARACTERISTICS OF THE WAVE DRAG EQUATION -  $C_{DW}$  VS  $a$  (FOR CONSTANT  $l$ )

Symbol	$\frac{Vol}{Vol_{BL}}$
×	.98
△	.99
○	1.00
□	1.01
★	1.02

$\lambda = 87.1$   
 $f = 1$   
 $h = 0$   
 $a' = 1$

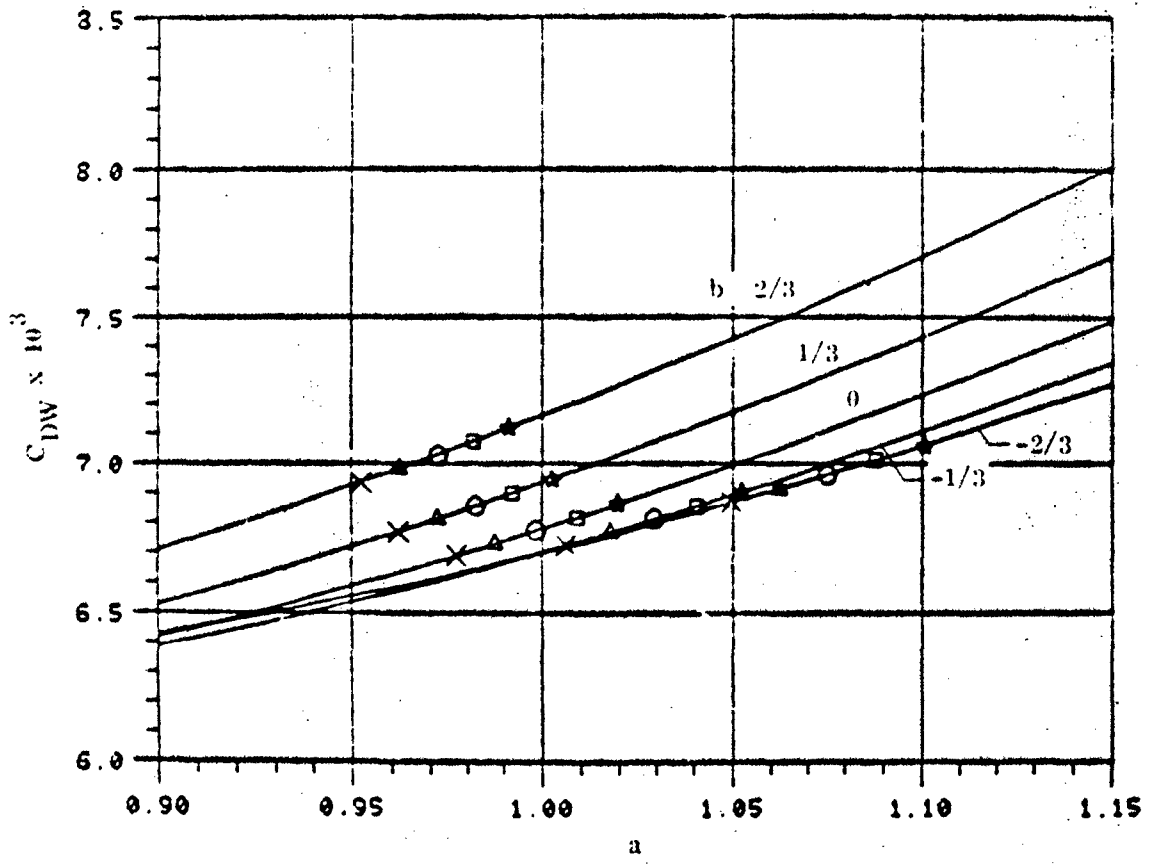


FIGURE 16b. CHARACTERISTICS OF THE WAVE DRAG EQUATION -  $C_{DW}$  VS  $a$  (FOR CONSTANT  $b$ )

Symbol	$\frac{\text{Vol}}{\text{Vol}_{\text{BL}}}$
×	.98
△	.99
○	1.00
□	1.01
★	1.02

$\beta = 87.1$   
 $f = 1$   
 $h = 1$   
 $h, \text{ baseline}$

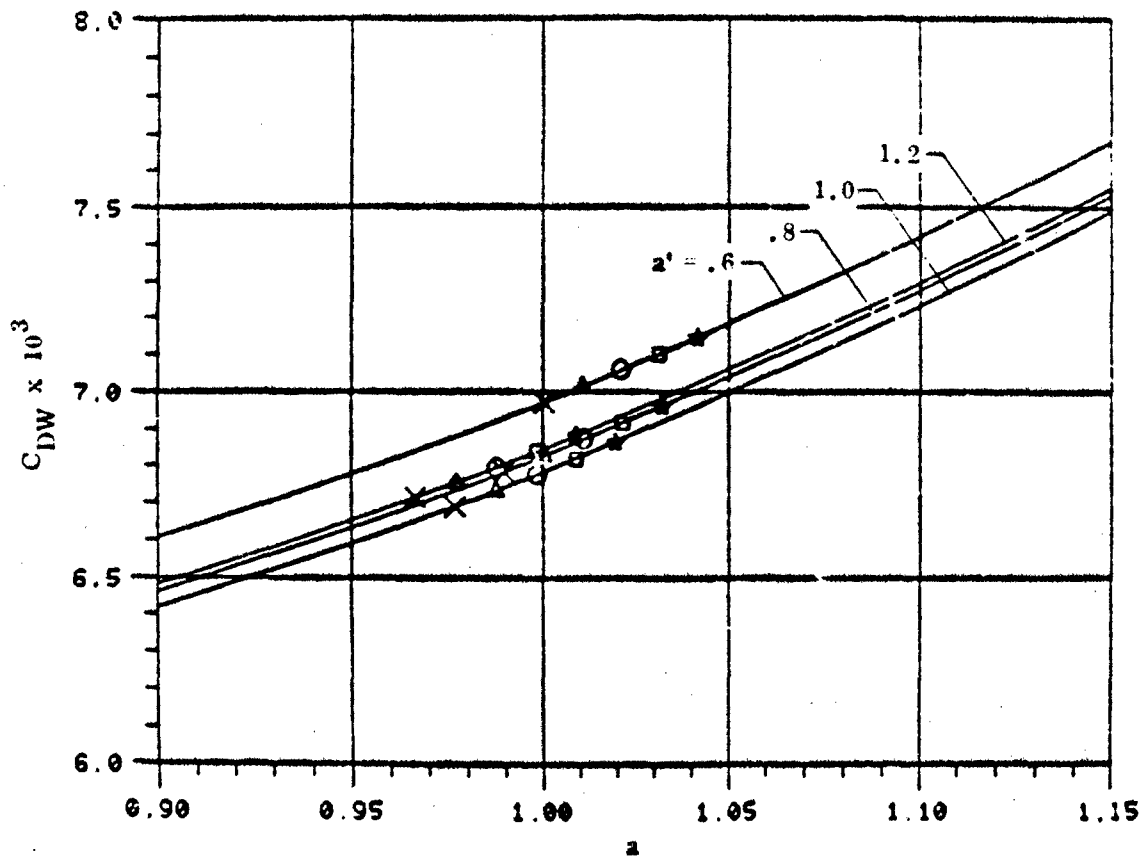


FIGURE 16c. CHARACTERISTICS OF THE WAVE DRAG EQUATION -  $C_{DW}$  VS  $a$  (FOR CONSTANT  $a'$ )

Symbol	Vol Vol <sub>BL</sub>
×	.98
△	.99
○	1.00
□	1.01
★	1.02

$f = 87.1$   
 $h = 0$   
 $a' = 1$   
 $b$ , baseline

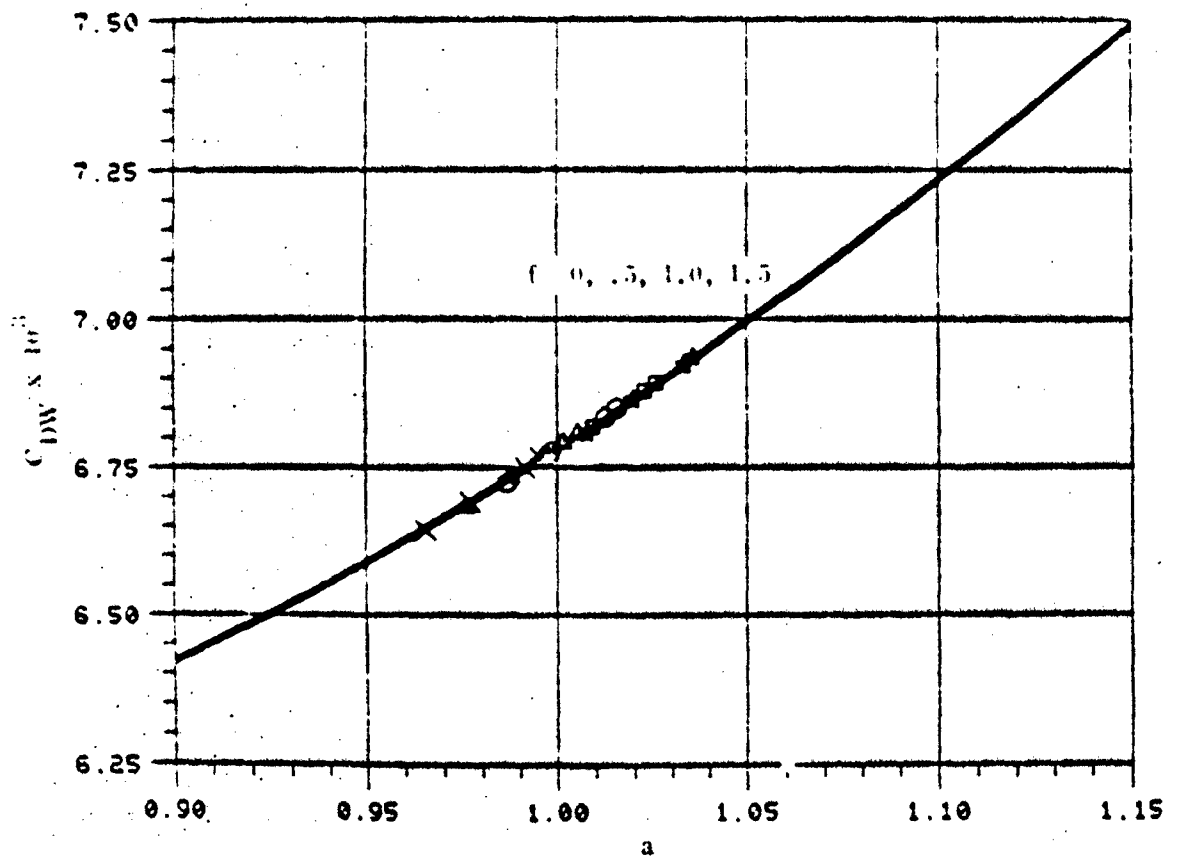


FIGURE 16L. CHARACTERISTICS OF THE WAVE DRAG EQUATION -  $C_{DW}$  VS  $a$  (FOR CONSTANT  $f$ )

drag equation. Similar to the results shown in Figure 15b,  $C_{DW}$  varies little with  $f$ . Figures 17a and 17b show the variations with respect to the vertical displacement of the maximum breadth line for families of  $b$  and  $f$ , respectively. Here, a minimum configuration for a given volume constraint cannot be determined graphically but a minimum can be located for each constant  $b$  or  $f$ . Figure 17a shows that the drag coefficient increases with  $b$ , except when  $a'$  is below the value of the baseline ( $a' = 1$ ) and when  $b$  is less than about  $-1/3$ . Figure 17b shows that the drag coefficient increases with  $f$  when  $a'$  is below the baseline value ( $a' = 1$ ) and the trend reverses when  $a'$  is above the baseline value. Figures 18a and 18b show the variation with respect to the shape factor  $b$  for families of  $f$  and  $f$ , respectively. Again, Figure 18a shows that the drag coefficient decreases with  $f$ . Similar to the characteristics of  $C_{DW}$  vs.  $a'$  shown in Figure 17b, the trend of the wave drag coefficient reverses from increasing with  $f$  when  $b$  is below the baseline value ( $b = 0$ ) to decreasing with  $f$  above the baseline value. Along the constant baseline volume line, Figure 18b shows a slight reduction of the drag coefficient from the baseline when  $f = 1.5$  and  $b = -.25$ .

Best Available Copy

Symbol	$\frac{\text{Vol}}{\text{Vol}_{BL}}$
×	.98
△	.99
○	1.00
□	1.01
★	1.02

$l = 87.1$   
 $f = 1$   
 $h = 0$   
 $a = 1$

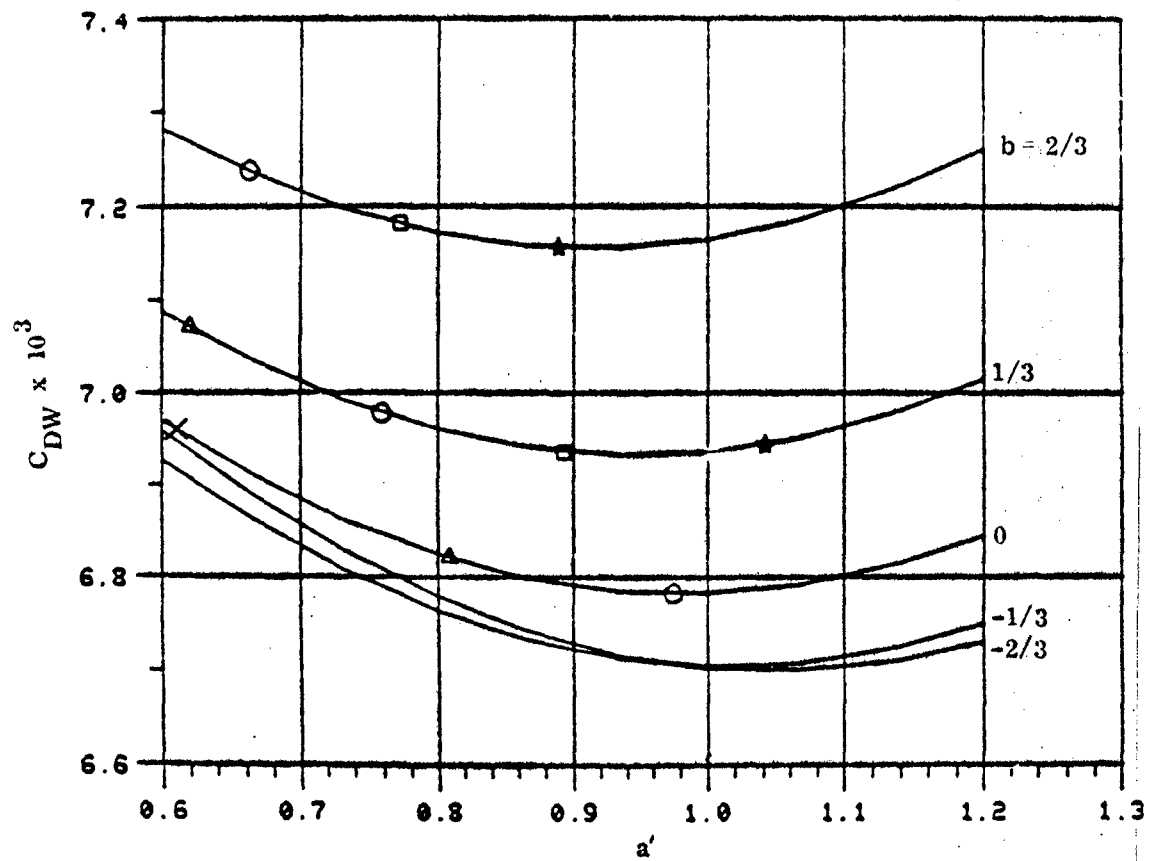


FIGURE 17a. CHARACTERISTICS OF THE WAVE DRAG EQUATION -  $C_{DW}$  VS  $a'$  (FOR CONSTANT  $b$ )

Symbol	$\frac{\text{Vol}}{\text{Vol}_{BL}}$
×	.98
△	.99
○	1.00
□	1.01
★	1.02

$\ell = 87.1$   
 $h = 0$   
 $a = 1$   
 $b$ , baseline

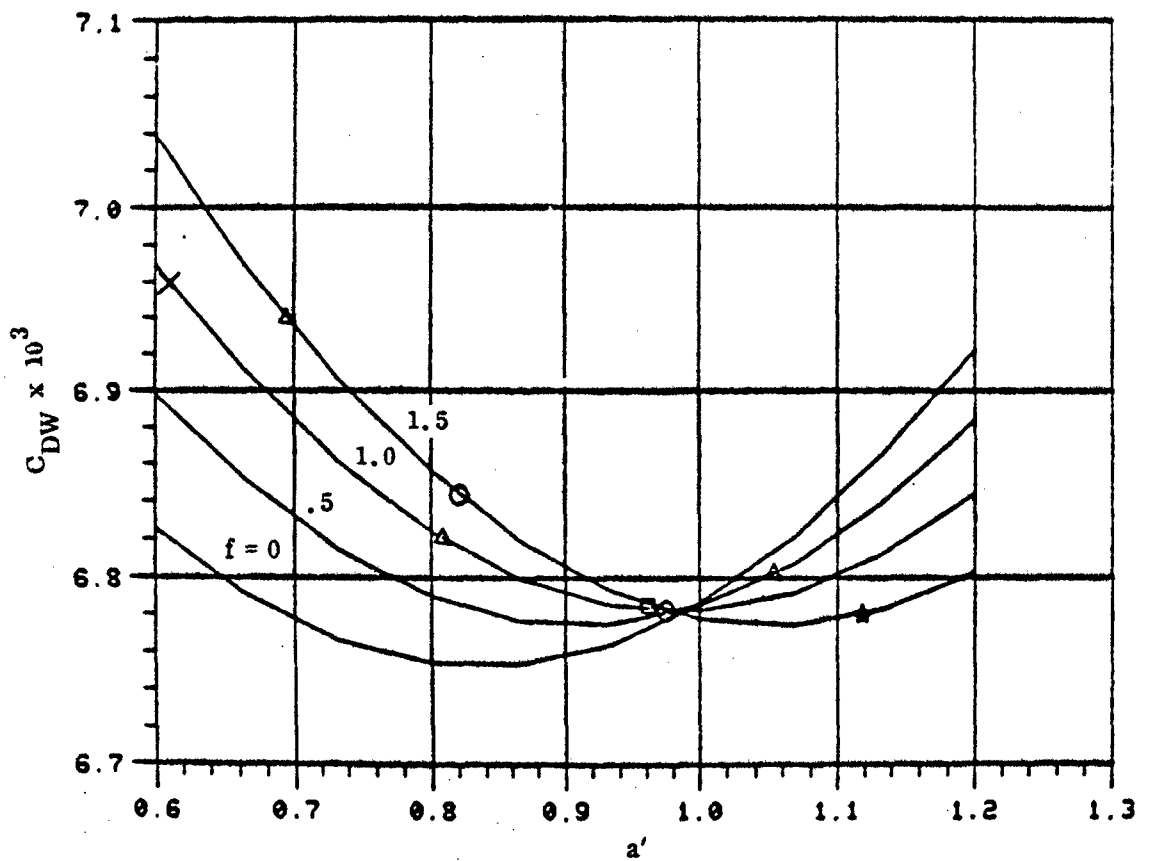


FIGURE 17b. CHARACTERISTICS OF THE WAVE DRAG EQUATION -  $C_{DW}$  VS  $a'$  (FOR CONSTANT  $f$ )

Symbol	$\frac{\text{Vol}}{\text{Vol}_{BL}}$
×	.98
△	.99
○	1.00
□	1.01
★	1.02

$f = 1$   
 $h = 0$   
 $a' = 1$   
 $a = 1$

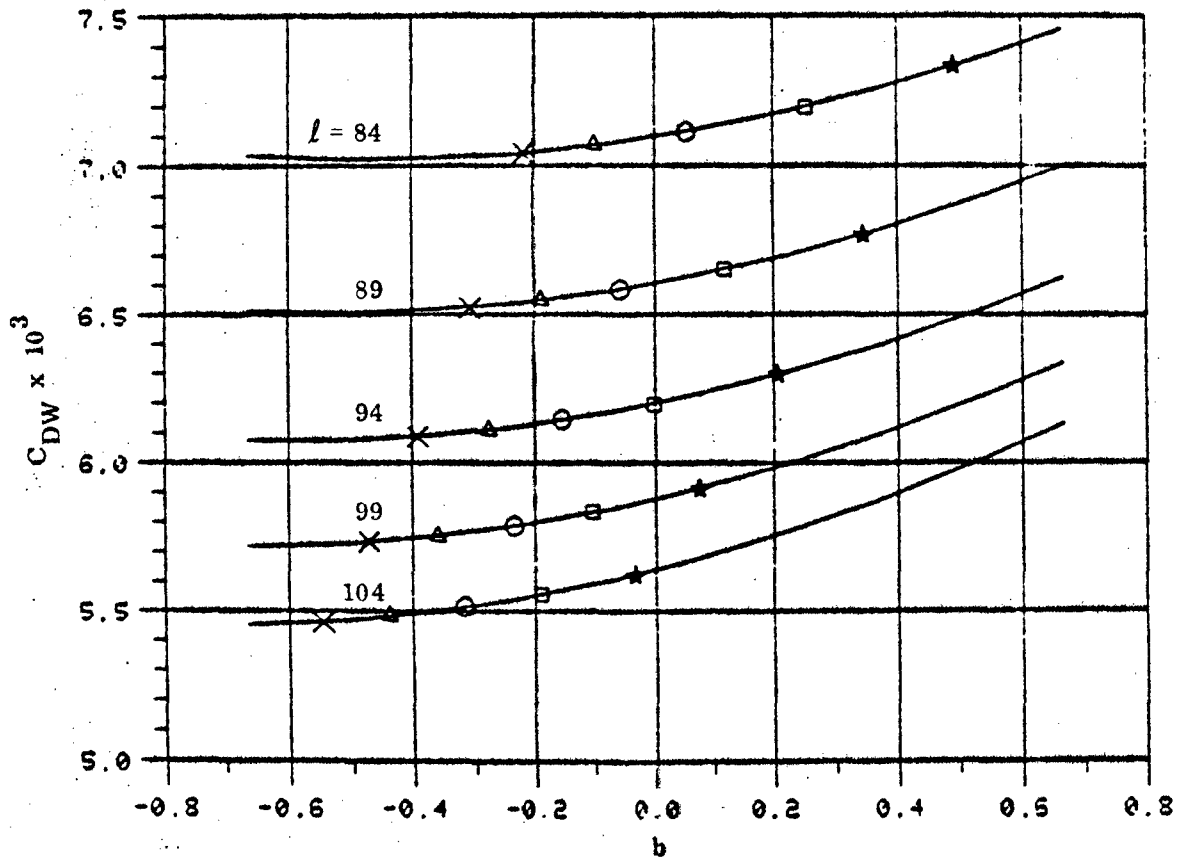


FIGURE 18a. CHARACTERISTICS OF THE WAVE DRAG EQUATION -  $C_{DW}$  VS  $b$  (FOR CONSTANT  $l$ )

Symbol	$\frac{\text{Vol}}{\text{Vol}_{BL}}$
×	.98
△	.99
○	1.00
□	1.01
★	1.02

$l = 87.1$   
 $h = 0$   
 $a' = 1$   
 $a = 1$

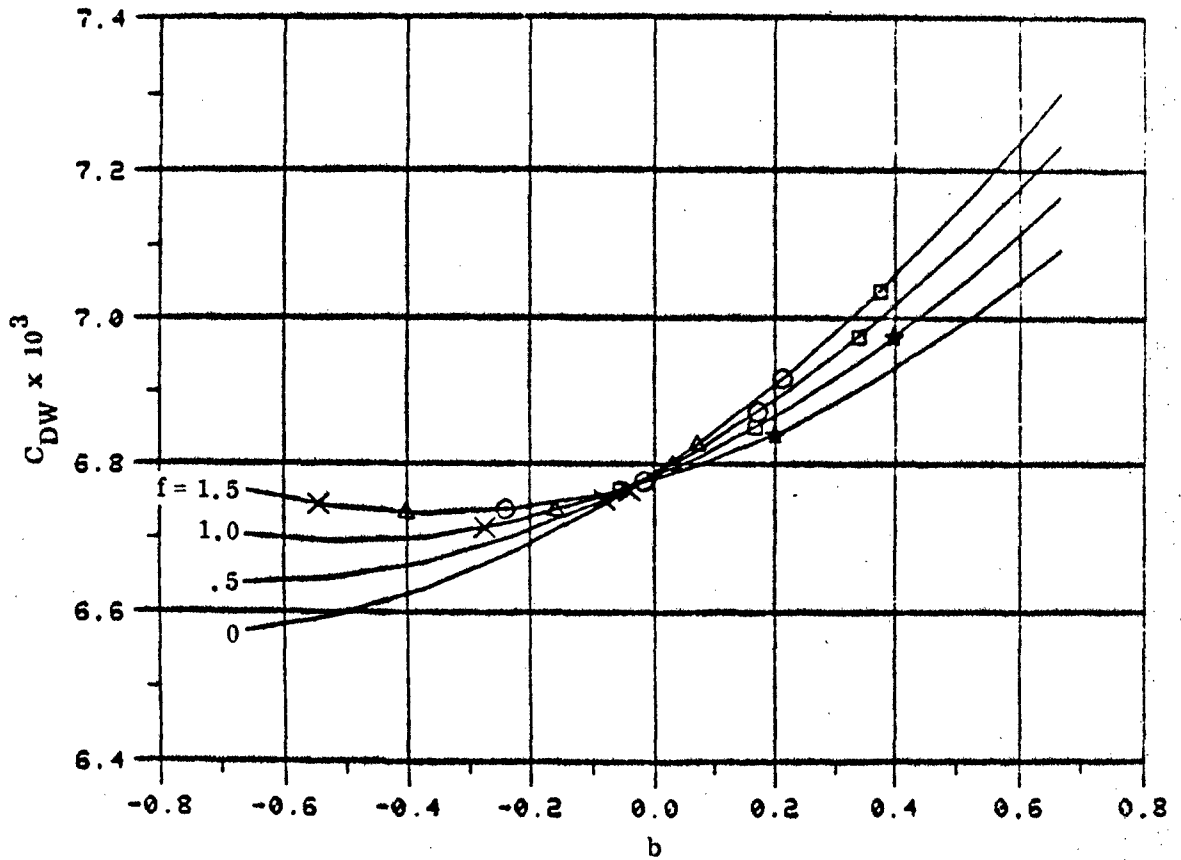


FIGURE 18b. CHARACTERISTICS OF THE WAVE DRAG EQUATION  $C_{DW}$  VS  $b$  (FOR CONSTANT  $f$ )

## 6. CONCLUDING REMARKS

The following remarks and conclusions can be made for Phase I of the wave drag reduction program.

- a. The optimization procedure using the Latin Square sampling technique and the Three-Dimensional Method of Characteristics is useful and practical. The procedure can be used for other optimization purposes besides wave drag reduction.
- b. The geometric variables and their ranges of variation should be selected carefully since the quality of the procedure and results are affected by the selection. Some guidelines on selecting the variables and ranges are given in this appendix, but experience is valuable.
- c. A new concept has been introduced to enable the optimization procedure to improve during the course of determining the optimum configuration. This concept is particularly useful when the variables and their ranges were not well chosen either because of inexperience or for the sake of compromise.
- d. Within the ranges of variation of the six chosen geometric variables, the following rule-of-thumb percentage reductions of the wave drag are obtained for the F-4 fuselage. For every inch the nose is lengthened, the wave drag is reduced by slightly over one percent. For each percent the fuselage volume is decreased, the wave drag is reduced by about 3/4 percent.

## REFERENCES

1. Redlich, O. and Watson, F. R., "On Programs for Tests Involving Several Variables," *Aeronautical Engineering Review*, Vol. 12, No. 6, June 1953, pp. 51-59.
2. Chu, C. W., "Compatibility Relations and a Generalized Finite-Difference Approximation for Three-Dimensional Steady Supersonic Flow," *AIAA Journal* Vol. 5, No. 3, March 1967, pp. 493-501.
3. Chu, C. W., "A New Algorithm for Three-Dimensional Method of Characteristics," *AIAA Journal*, Vol. 10, No. 11, November 1972, pp. 1548-1550.

APPENDIX B  
THE LATIN SQUARE METHOD

The Latin Square is a sampling method for designing an experiment.<sup>1-3</sup> An  $N^{\text{th}}$  order Latin Square is an arrangement of the  $N$  values of  $N + 1$ , or fewer, variables (where  $N$  is a prime number) in such a way that the resulting surface fitting process is efficiently performed. The method may be used for determining an approximate equation for a function of a number of variables and hence for solving extremum problems when the dependent variable is not known as an explicit function of the independent variables.

The dependent variable, in this case wave drag coefficient  $C_{DW}$ , is assumed to be a quadric function of the independent variables  $x_i$  (which are related to the geometry of the forward fuselage in this application),

$$C_{DW} = a_0 + \sum_{i=1}^6 a_i x_i + \sum_{j=1}^5 \sum_{i=2}^5 a_{ij} x_i x_j \quad (1)$$

Equation (1) is written for a 5 x 5 Latin Square with six independent variables, i. e.  $N = 5$ .

For a given set of independent variables,  $x_i$ , a new set of reduced variables, say  $z_i$ , may be determined such that the variables  $z_i$  take the values 0,  $\pm 1$ ,  $\pm 2$ ,  $\dots \pm \frac{N-1}{2}$ , according to the transformation equation

$$x_i = \frac{x_{i \max} + x_{i \min}}{2} + \frac{z_i (x_{i \max} - x_{i \min})}{N - 1} \quad (2)$$

The 5 x 5 Latin Square arrangement in terms of the levels of the reduced variables is shown in Table 1. The arrangement may appear to be at once regular

and random. It appears to be regular since all variables take orderly permuted values. It appears to be random since there seems to be no bias in representing all segments of the population. Regularity and randomness - therein lies the efficiency of the Latin Square sampling technique. It has been shown by Yates<sup>3</sup> that randomized blocks are more efficient than complete randomization and Latin Squares are more efficient than randomized blocks. He also found that on one set of experiments about 2 1/2 times as many plots were needed with the randomized blocks of 5 blocks as with the 5 x 5 Latin Squares to obtain the same accuracy (see Reference 1, pp. 202-203). Careful examination of Table 1 revealed that in all the cells having a given level of any reduced variable any one of the remaining variables takes on all possible levels once and only once. For example, if we select  $z_1 = -2$  to be the given level of the one reduced variable, then column one contains all cells having  $z_1 = -2$ . It is seen that in column one each of the five levels of any one of the remaining variables, say  $z_2$ , appears once and only once. Consequently, the number of all cells having a given level of any reduced variable is five since there are five levels for each of the other variables to take through a permutation process. Several consequences can be observed. Firstly, if we compare any two cells we find that only one of the variables has the same level in both cells, whereas all other variables have different levels. Secondly, for each reduced variable there are five groups of five cells which satisfy the condition that in each group this reduced variable takes one of the five levels. Thirdly, by a suitable rearrangement of the cells any pair of the reduced variables can take the column and row indices as their levels just as  $z_1$  and  $z_6$  do as shown in Table 1. To do this, arrange each group with the same level of one variable as a column and arrange the columns in an ascending order with respect to the levels of this variable. Within each column (or group) arrange the cells in an ascending order with respect to the

TABLE 1. A 5 x 5 LATIN SQUARE ARRANGEMENT

CELL CODE

$z_1$	$z_6$
$z_2$	$z_5$
$z_3$	$z_4$

-2	-2	-1	-2	0	-2	1	-2	2	-2
1	0	2	1	-2	2	-1	-2	0	-1
-1	2	0	-2	1	-1	2	0	-2	1
-2	-1	-1	-1	0	-1	1	-1	2	-1
2	-1	-2	0	-1	1	0	2	1	-2
1	0	2	1	-2	2	-1	-2	0	-1
-2	0	-1	0	0	0	1	0	2	0
-2	-2	-1	-1	0	0	1	1	2	2
-2	-2	-1	-1	0	0	1	1	2	2
-2	1	-1	1	0	1	1	1	2	1
-1	2	0	-2	1	-1	2	0	-2	1
0	1	1	2	2	-2	-2	-1	-1	0
-2	2	-1	2	0	2	1	2	2	2
0	1	1	2	2	-2	-2	-1	-1	0
2	-1	-2	0	-1	1	0	2	1	-2

# Best Available Copy

levels of the other variable of the pair. These properties show heuristically the efficiency of the Latin Square sampling technique which has been used for developing various optimal designs. 4-5

It may seem intricate to construct a Latin Square of this type, especially when the size exceeds  $5 \times 5$ . The following steps, however, can be followed to construct this type of Latin Square of any size as long as the number of rows (or columns) is a prime number. The steps are best explained using Table 1 as an example.

- (a) The variables  $z_1$  and  $z_6$  are assigned levels equal to the column and row indices as shown in Table 1.
- (b) For each of the diagonal cells where  $z_1 = z_6$ , the level of  $z_1$  is increased successively from  $i - 1$  to  $i - 6$  by a level equal to that of  $z_1$  in a cyclic order, in which the lowest level (i.e., -2) is considered one level higher than the highest level (i.e., 2).
- (c) The remaining levels of  $z_2$  to  $z_5$  in each row are obtained by permutation in an increasing cyclic order using the diagonal cell.

## References

1. Kempthorne, O., The Design and Analysis of Experiments, Wiley, New York, 1952.
2. Redlich, D. and Watson, R. F., "On Programs for Tests Involving Several Variables," Aeronautical Engineering Review, Vol. 12, No. 6, June 1953.
3. Yates, F., "Complex Experiments," Suppl. J. Roy. Stat. Soc., Vol. 2, 1953, pp. 181-247.
4. Powers, S. A., "Minimum Drag Bodies of Revolution by Exact Methods," NOR 63-159, Northrop Corporation, September 1963.
5. Powers, S. A., "Drag Minimization Using Exact Methods," AIAA Journal, May 1964.

## APPENDIX C

### BODY DESCRIPTION METHOD

In this Appendix, the general body description method is described in some detail and is illustrated by the body description of phase I. The technique of fitting a conic-section curve is also given.

The fuselage is described by a number of generating lines, such as the upper profile, the lower profile, the maximum half-breadth line and generating lines for the canopy. In the present body description procedure, each generating line is divided into as many segments as necessary to allow each segment to be described by a conic-section curve. At each cross section of the fuselage simple analytic curves, e.g., the ellipse or cubic, connect any two adjacent generating lines to form the contour of the cross section. The fuselage is thus described analytically by simple low order curves.

The body description procedure detailed here was developed for use in conjunction with the three-dimensional method of characteristics for calculating flow fields over smooth bodies. For a smooth body a unique normal to the surface must exist every where, and this condition of a unique normal usually requires that the curves and their slopes be continuous at the juncture between two contour curves or two segments of a generating line.

#### 1. DEFINITION OF GENERATING LINES

The fuselage is located in a right-handed coordinate system where the Y-axis is aligned with the fuselage axis, the X-axis is spanwise and the Z-axis is up. A schematic of a fuselage-canopy configuration is shown in Figure 1 and a typical cross section in Figure 2.

In general, five generating lines, each being described by two functions of Y (representing their vertical and horizontal projections  $Z_j$  and  $X_j$ , respectively, by a general curve fit of conic sections) plus an additional three lines, each being described by a single function of Y, serve to define the fuselage-canopy configuration in phase I.

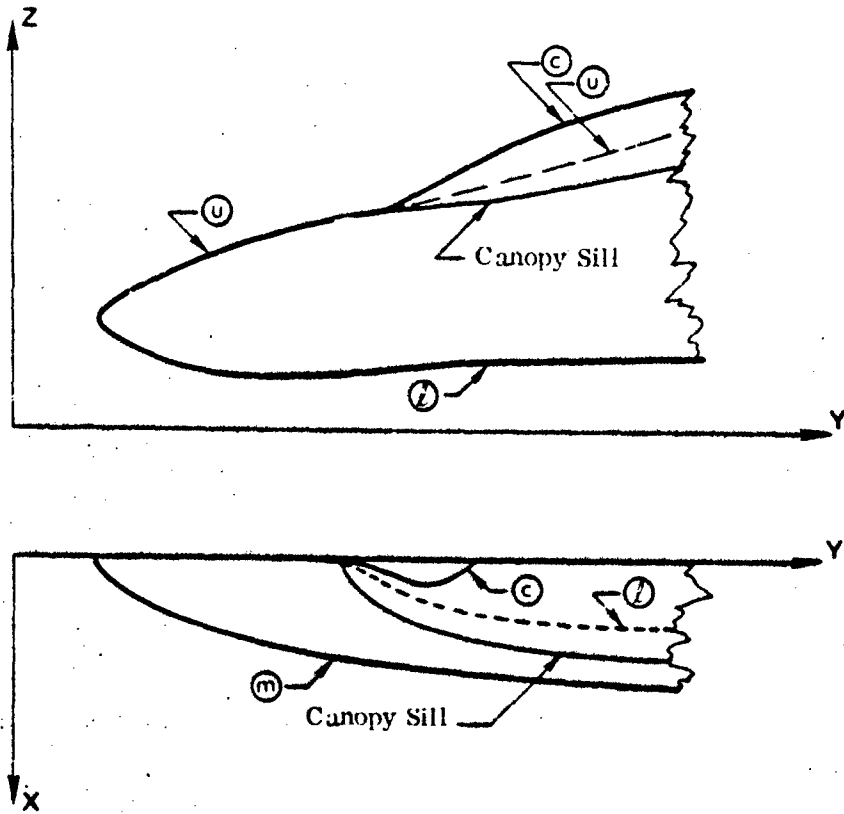


FIGURE 1. SCHEMATIC OF FUSELAGE-CANOPY CONFIGURATION

Best Available Copy

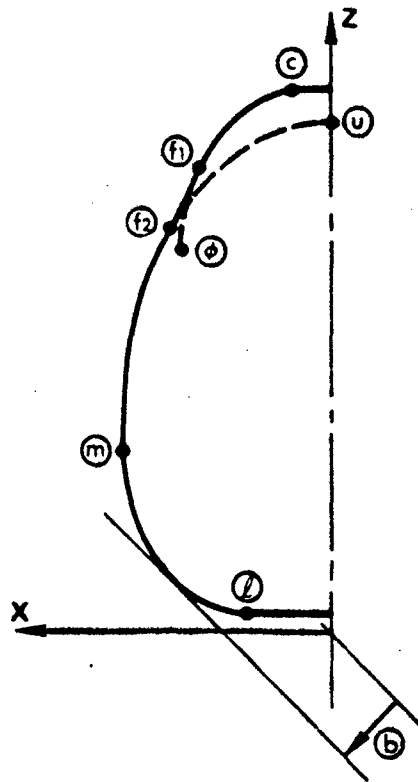


FIGURE 2. TYPICAL FUSELAGE CROSS SECTION

These are identified in Figures 1 and 2 as

- ⓪ Upper profile line
- Ⓜ Maximum half-breadth line
- Ⓛ Lower profile line
- ⓐ Canopy crown line
- Ⓟ Canopy definition line
- ⓑ Shape factor  $b$ , locating the  $45^\circ$  tangent line
- Ⓣ<sub>1</sub> Upper fairing line
- Ⓣ<sub>2</sub> Lower fairing line

where lines ⓐ, Ⓟ, Ⓣ<sub>1</sub>, Ⓣ<sub>2</sub> are required only, of course, in the region of the canopy. The conic-section curves describing the lines take the form

$$\left(\frac{z}{b}\right) = PY + Q \pm [RY^2 + SY + T]^{1/2} \quad (1)$$

Details of the determination of the coefficients  $P$ ,  $Q$ ,  $R$ ,  $S$ ,  $T$  of the general conic curves will be discussed in Section 4. Each conic-section segment must be continuous with the previous segment and, with very few exceptions, the slope must be continuous at the junctures to satisfy the requirement of a unique normal to the surface discussed above. Unlike others, line ⓑ is not a true generating line. It is actually a shape factor for the lower part of the fuselage, which expresses the distance to a tangent line as a function of  $Y$ . A full discussion of the details is presented in Section 2(c).

Lines Ⓣ<sub>1</sub> and Ⓣ<sub>2</sub> which fix, at each cross section, the extent of the fairing cubic between canopy and upper fuselage are defined by their projections in the  $YZ$ -plane, i. e.  $Z_{f_1}(Y)$  and  $Z_{f_2}(Y)$ , only. Their projections  $X_{f_1}(Y)$  and  $X_{f_2}(Y)$  are constrained to lie on the ellipses defining the canopy and upper half of the fuselage, respectively, as detailed in Section 2(d).

## 2. CONTOUR CURVES FORMING CROSS SECTIONS

As shown in Figure 2, for the most general case of a fuselage-canopy configuration with a windshield flat, the contour of the cross section begins with a straight line representing the flat from the centerline to ⓐ. The canopy contour from ⓐ to Ⓟ is circular, but can be elliptic in general. The upper fuselage is represented by an elliptic curve between Ⓜ and ⓪. The lower fuselage is represented by a general

conic-section curve from  $\textcircled{m}$  to  $\textcircled{L}$ ; the bottom flat by a straight line from  $\textcircled{L}$  to the centerline. The intersection between the canopy and the fuselage is faired by a cubic from  $\textcircled{f_1}$  to  $\textcircled{f_2}$ .

a. Canopy

The cross-sectional shape of the canopy is assumed to be circular. If there is no windshield flat,  $\textcircled{C}$  will lie on the centerline (Figure 3a) and the equation for the canopy curve is given by

$$\left(\frac{Z-Z_c}{X_c}\right)^2 + \left(\frac{X}{X_c}\right)^2 - 1 = 0 \quad (2)$$

If a windshield flat does exist,  $\textcircled{C}$  moves off the centerline as shown in Figure 3b and Equation (2), describing the canopy between  $\textcircled{\phi}$  and  $\textcircled{C}$  leads to a slope discontinuity at  $\textcircled{C}$ , the juncture between the circular arc and the windshield flat. Thus, a quarter-ellipse is used to approximate the circular arc between  $\textcircled{\phi}$  and  $\textcircled{C}$  to give a slope of  $dZ/dX = 0$  at  $\textcircled{C}$ , providing slope continuity with the flat portion of the contour. The equation for this approximating ellipse is

$$\left(\frac{Z-Z_c}{Z_c-Z_c}\right)^2 + \left(\frac{X-X_c}{X_c-X_c}\right)^2 - 1 = 0 \quad (3)$$

The details of determining the point  $\phi$ , given the locations of the canopy crown and sill lines, are presented in Section 3.

b. Upper Fuselage

The equation for the upper fuselage is

$$\left(\frac{Z-Z_m}{Z_u-Z_m}\right)^2 + \left(\frac{X}{X_m}\right)^2 - 1 = 0 \quad (4)$$

indicating that, for the body description in its present form, X is constrained to be zero for all Y.

Again it may be noted that  $\textcircled{U}$ , in the region of the canopy, is fictitious and cannot be obtained directly from three-view drawings. Details of determining  $\textcircled{U}$ , given the location of the maximum half-breadth line  $\textcircled{m}$  and the location of the canopy sill line, may be found in Section 3.

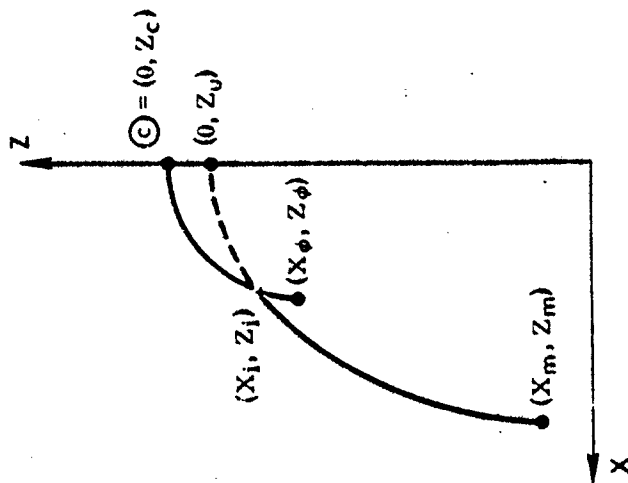
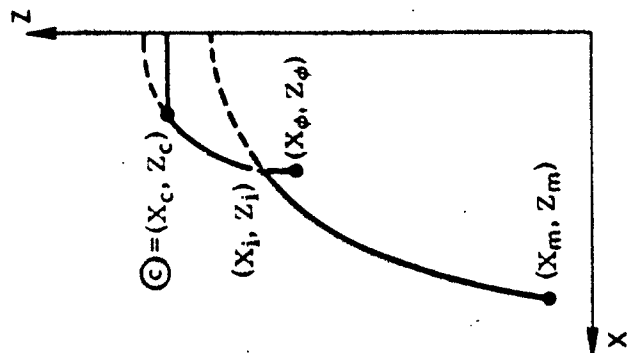


FIGURE 3. DETAILS OF CANOPY-FUSELAGE INTERSECTION

c. Lower Fuselage

Referring to Figure 2, the contour curve from (m) to (l) has a zero slope at (l) and the slope approaches infinity at (m). As in aircraft lofting practice, the shape of this contour curve is determined by specifying the distance from the origin to one of its tangent lines that makes a 45° angle with the X-axis. Hence, this distance, which is designated by b in the following derivation of the equation for the contour curve, may be regarded as a shape factor for this curve.

The equation for the 45° tangent line is

$$z = x - \sqrt{2} b$$

which, when the origin is translated to (m), becomes

$$z' = x' + H \quad (5)$$

where  $Z' = Z - Z_m$ ,  $X' = X - X_m$  and  $H = X_m - Z_m - \sqrt{2} b$ . In the new coordinate system, the general quadric equation, satisfying the conditions  $X'(Z'_l) = X'_l$ ,  $Z'(0) = 0$ ,  $(\partial X'/\partial Z')_m = 0$  and  $(\partial Z'/\partial X')_l = 0$ , reduces to

$$K(x'_l z' - z'_l x')^2 + x'(z' - z'_l) = 0 \quad (6)$$

which represents a family of curves with K as a parameter. To determine K, Eq. (5) is substituted into Eq. (6) to yield a quadratic equation of the form

$$Ax'^2 + Bx' + C = 0 \quad (7)$$

The condition for Equation (6) to be a tangent line is that Equation (7) have a double root; i. e.  $B^2 - 4AC = 0$ , which leads to

$$K = \frac{(H - z'_l)^2}{4Hx'_l z'_l (H + x'_l - z'_l)} \quad (8)$$

Equation (6) with K given by Eq. (8), then represents the contour curve from (m) to (l). The range of variation of this curve obtainable by applying this equation is illustrated in Figure 4, where a family of conic section curves is given for different values of b. By increasing the distance b, the curve is seen to vary from almost a straight line to a sharply bending curve approaching the two sides of a right triangle.

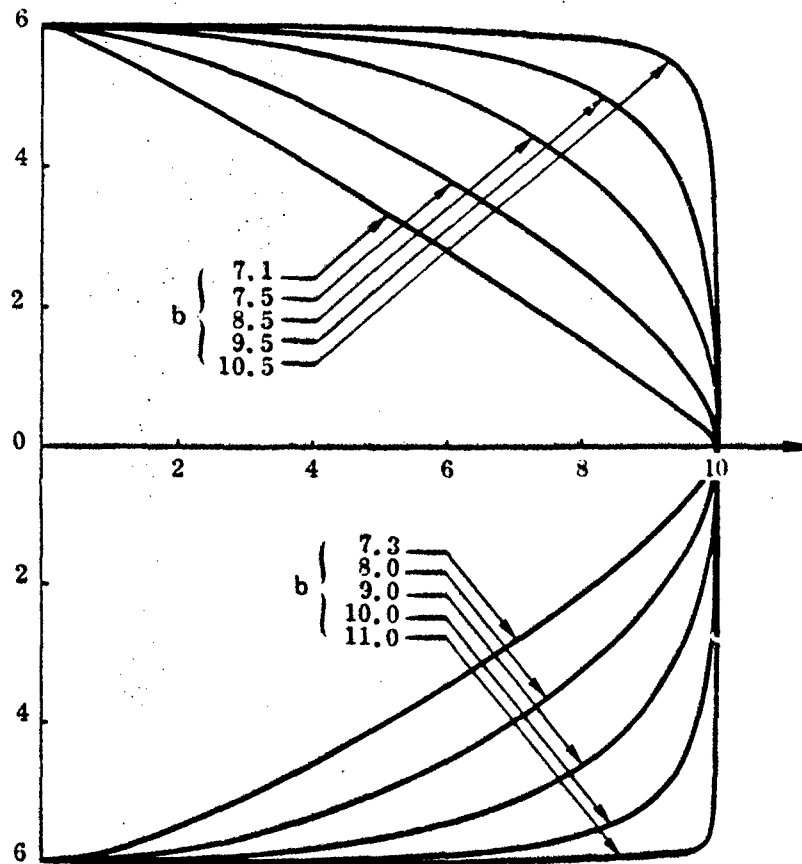


FIGURE 4, A FAMILY OF CONIC-SECTION CURVES

d. Fairing Curve

The intersection between the canopy and upper fuselage is faired by a cubic from  $(f_1)$  to  $(f_2)$ . The projections  $Z_{f_1}(Y)$  and  $Z_{f_2}(Y)$  of lines  $(f_1)$  and  $(f_2)$  on the YZ-plane are given by conic-section curves (such as Equation (1), where P, Q, R, S, T are input quantities). The projections  $X_{f_1}(Y)$  and  $X_{f_2}(Y)$  on the XY-plane are obtained by solving Eqs. (3) and (4), respectively.

$$\left. \begin{aligned} X_{f_1}(Y) &= X_c + (X_\phi - X_c) \left[ 1 - \left( \frac{Z_{f_1} - Z_\phi}{Z_c - Z_\phi} \right)^2 \right]^{1/2} \\ X_{f_2}(Y) &= X_m \left[ 1 - \left( \frac{Z_{f_2} - Z_m}{Z_u - Z_m} \right)^2 \right]^{1/2} \end{aligned} \right\} (9)$$

The fairing curve matches the slopes of the ellipses at both end points  $f_1$  and  $f_2$ . The slopes are defined by differentiation of Eqs. (3) and (4)

$$\left. \begin{aligned} \frac{\partial X_{f_1}}{\partial Z}(Y) &= - \left( \frac{Z_{f_1} - Z_\phi}{X_{f_1} - X_c} \right) \left( \frac{X_c - X_\phi}{Z_c - Z_\phi} \right)^2 \\ \frac{\partial X_{f_2}}{\partial Z}(Y) &= - \left( \frac{Z_{f_2} - Z_m}{X_{f_2}} \right) \left( \frac{X_m}{Z_u - Z_m} \right)^2 \end{aligned} \right\} (10)$$

The cubic equation that satisfies the conditions of Eqs. (9) and (10) at point  $f_1$  can be written

$$X = X_{f_1} + \frac{\partial X_{f_1}}{\partial Z} (Z - Z_{f_1}) + c \left( \frac{Z - Z_{f_1}}{Z_{f_2} - Z_{f_1}} \right)^2 + d \left( \frac{Z - Z_{f_1}}{Z_{f_2} - Z_{f_1}} \right)^3 \quad (11)$$

The coefficients  $c$  and  $d$  are obtained by applying the conditions of Eqs. (9) and (10) at point  $f_2$

$$\left. \begin{aligned} c &= 3(X_{f_2} - X_{f_1}) - \left( \frac{\partial X_{f_2}}{\partial Z} + 2 \frac{\partial X_{f_1}}{\partial Z} \right) (Z_{f_2} - Z_{f_1}) \\ d &= -2(X_{f_2} - X_{f_1}) + \left( \frac{\partial X_{f_2}}{\partial Z} + \frac{\partial X_{f_1}}{\partial Z} \right) (Z_{f_2} - Z_{f_1}) \end{aligned} \right\} (12)$$

Equation (11) with  $c$  and  $d$  given by Eq. (12) is then the cubic equation for the fairing curve from  $(f_1)$  to  $(f_2)$ . The quantities  $X_{f_1}$ ,  $X_{f_2}$ ,  $\partial X_{f_1}/\partial Z$ ,  $\partial X_{f_2}/\partial Z$  are given by Eqs. (9) and (10), while  $X_m$ ,  $X_c$ ,  $X_\phi$ ,  $Z_u$ ,  $Z_m$ ,  $Z_\phi$ ,  $Z_{f_1}$ , and  $Z_{f_2}$  are obtained from the generating lines input in the form of Equation (1).

### 3. DETERMINING GENERATING LINES AS FUNCTIONS OF Y

The generating lines defined in Section 1 are determined primarily by utilizing top and side view drawings as well as available cross-sectional views. The top and side views are used to obtain the variation of generating lines  $\textcircled{u}$  and  $\textcircled{l}$  in the  $XZ$ -plane and of line  $\textcircled{m}$  in the  $XY$ -plane. The variation of line  $\textcircled{m}$  in the  $YZ$ -plane and of line  $\textcircled{l}$  in the  $XY$ -plane are obtained primarily by utilizing cross-sectional views, as is the description of the shape parameter  $\textcircled{b}$  as a function of  $Y$ .

From Figure 2 it can be seen that line  $\textcircled{u}$ , in the region of the canopy, and line  $\textcircled{\phi}$  are, in effect fictitious lines whose description three-view drawings will not yield directly. The two lines are determined by assuming that the cross section of the canopy is a circular arc and by constraining the intersection of this circular arc and the ellipse defining the upper portion of the fuselage to lie on the canopy sill line, which in turn is well defined from available three-view drawings.

In Figure 3, let  $X_i, Z_i$  be the location of the canopy sill line for the cross section shown. Utilizing the general equation for an ellipse with center at  $X_o, Z_o$  and semi-major and minor diameters  $a$  and  $b$ , respectively,

$$\left(\frac{X-X_o}{a}\right)^2 + \left(\frac{Z-Z_o}{b}\right)^2 - 1 = 0$$

one may determine  $Z_o$  by finding  $b$  in the above equation for the ellipse through the point  $X_i, Z_i$  with known center  $X_o = 0, Z_o = Z_m$  and  $a = X_m$ , yielding

$$Z_u = Z_m + X_m \frac{(Z_i - Z_m)}{(X_m^2 - X_i^2)^{1/2}} \quad (13)$$

To determine  $Z_\phi$  and  $X_\phi$ , defining one end point of the quarter circle passing through  $Z_c, X_c$  and  $Z_i, X_i$  whose center lies on  $X_o = 0$ , it is necessary to obtain  $Z_o$  and  $r$  for the circle satisfying the following conditions

$$X_i^2 + (Z_i - Z_o)^2 = r^2 \quad (14a)$$

$$X_c^2 + (Z_c - Z_o)^2 = r^2 \quad (14b)$$

Solving for  $Z_o$  yields

$$Z_o = Z_c = \frac{X_c^2 + Z_c^2 - Z_i^2 - X_i^2}{2(Z_c - Z_i)} \quad (15)$$

and using Equation (14b) to solve for  $r$ , gives

$$x_c = r = [x_c^2 + (z_c - z_o)^2]^{1/2} \quad (16)$$

When a windshield or canopy flat exists (i. e.  $X_c \neq 0$ , as shown in Figure 3b) a slope discontinuity results at  $X_c, Z_c$ . Thus, for  $X_c \neq 0$ , the circular arc is replaced by a quarter-ellipse, passing through  $X_i, Z_i$  and one end point being  $X_c, Z_c$  with  $dX/dZ = 0$  to provide slope continuity.

This ellipse is intended to be an approximation to the circular arc determined previously. It is obtained by decreasing the canopy flat (i. e.  $X_c$ ) by an arbitrary percentage and solving for a new  $Z_\phi$  and  $X_\phi$  by an iterative procedure, utilizing  $Z_\phi$  and  $X_\phi$  of Eqs. (15) and (16) as a first approximation, while constraining the product of the two semi-axes of the ellipse to be equal to  $r^2$  of the initial circular arc.

Given a tabulation of  $X_c, Z_c, X_m, Z_m$ , and  $X_i, Z_i$ , values of  $Z_u, Z_\phi$  and  $X_\phi$  can be determined for a number of fuselage stations; their fit by a sequence of conic-section curves as a function of  $Y$  can then be accomplished in a straightforward manner by the techniques described in the following section.

#### 4. EVALUATION OF THE COEFFICIENTS FOR A CONIC SECTION

The general equation of the second degree, which represents a conic section, is

$$ay^2 + bxy + cx^2 + dy + ex + f = 0 \quad (17)$$

utilizing the coordinate system of Figure 5. The general equation appears to have six constants, but in reality has only five arbitrary constants, since Equation (17) can be divided by any of the constants, leaving an equation with five undetermined coefficients. Therefore five independent conditions are sufficient to determine a conic.

In the following sections, two ways in which these five independent conditions are supplied will be treated. Section 4(a) deals with the conic determined by five points, no three of which are collinear. Section 4(b) treats the conic determined by one point and two point slopes. By a point slope it is meant that a point is given and the slope of the curve at the point is also given.

a. Conic Determined by Five Points

Consider the problem of finding the equation of a conic through five given points, no three of which are collinear. Let the points be 1, 2, 3, 4, 5 as shown in Figure 5a.

Then,

$$\left. \begin{aligned} y - m_1x - h_1 &= 0 \\ y - m_2x - h_2 &= 0 \\ y - m_3x - h_3 &= 0 \\ y - m_4x - h_4 &= 0 \end{aligned} \right\} (18)$$

represent the equations of the lines connecting points 1-4, 1-2, 2-3, 3-4, respectively. Then the equation

$$K(y - m_1x - h_1)(y - m_3x - h_3) + (y - m_2x - h_2)(y - m_4x - h_4) = 0 \quad (19)$$

represents the family of conics through the points 1, 2, 3, 4. In this equation, K is a parameter whose value can be determined from the fifth condition, which is that the conic pass through point 5. (If point 1 is substituted into Equation (19), the result is identically equal to zero since point 1 was used to evaluate the coefficients  $m_1$ ,  $h_1$  and  $m_2$ ,  $h_2$ . The same argument holds for points 2, 3, 4.)

$$K = - \frac{(y_5 - m_2x_5 - h_2)(y_5 - m_4x_5 - h_4)}{(y_5 - m_1x_5 - h_1)(y_5 - m_3x_5 - h_3)} \quad (20)$$

After expanding Equation (19) and collecting like powers, comparison with Equation (17) shows that

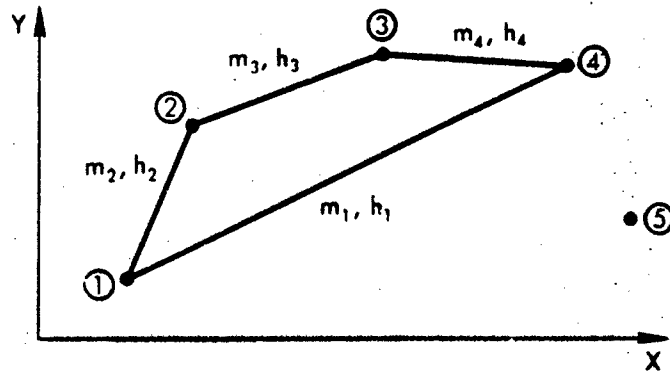
$$\left. \begin{aligned} a &= K + 1 \\ b &= -[K(m_1 + m_3) + m_2 + m_4] \\ c &= Km_1m_3 + m_2m_4 \\ d &= -[K(h_1 + h_3) + h_2 + h_4] \\ e &= K(m_1h_3 + m_3h_1) + m_2h_4 + m_4h_2 \\ f &= Kh_1h_3 + h_2h_4 \end{aligned} \right\} (21)$$

Rewriting Equation (17) in the form

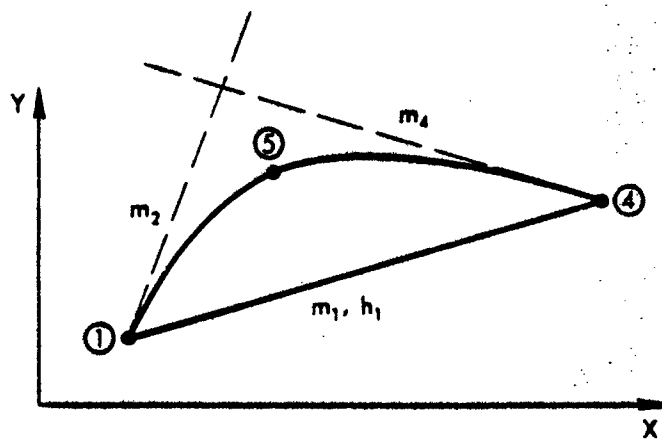
$$ay^2 + (bx + d)y + cx^2 + ex + f = 0$$

and solving, using the quadratic formula, yields

$$y = \frac{-(bx + d) \pm [(bx + d)^2 - 4a(cx + ex + f)]^{1/2}}{2a}$$



(a) Five Points



(b) Point and Two Point Slopes

FIGURE 5. DETERMINING CONDITIONS FOR CONIC

$$\begin{aligned}
&= -\frac{b}{2a}x - \frac{d}{2a} \pm \left[ \frac{b^2x^2 + 2bdx + d^2}{4a^2} - \frac{(4acx^2 + 4aex + 4af)}{4a^2} \right]^{1/2} \\
&= -\frac{b}{2a}x - \frac{d}{2a} \pm \left[ \frac{b^2x^2 + 2bdx + d^2}{4a^2} - \frac{cx^2 + ex + f}{a} \right]^{1/2} \\
y &= -\frac{b}{2a}x - \frac{d}{2a} \pm \left[ \left( \frac{b^2}{4a^2} - \frac{c}{a} \right)x^2 + \left( \frac{bd}{2a^2} - \frac{e}{a} \right)x + \left( \frac{d^2}{4a^2} - \frac{f}{a} \right) \right]^{1/2} \quad (22)
\end{aligned}$$

which can be recognized as Equation (1), with

$$\left. \begin{aligned}
P &= -b/2a \\
Q &= -d/2a \\
R &= P^2 - c/a \\
S &= -Pd/a - e/a \\
T &= Q^2 - f/a
\end{aligned} \right\} (23)$$

and the sign of the radical to be determined by evaluation.

#### b. Conic Determined by a Point and Two Point Slopes

Now consider the problem of finding the coefficients of a conic determined by one point and two point slopes. This establishes a curve that is tangent to a given line at a given point, is tangent to another line at a given point and passes through a third given point. This particular manner of determining a conic is especially suitable since it allows for specification of slope continuity at the two end points of the conic-section segment, while the great latitude afforded by the third point (control point) in fixing the shape of the curve is utilized to good advantage in obtaining a good approximation to the data to be fitted.

Compare Figures 5a and 5b. The points 1 and 2 of Figure 5a coincide in Figure 5b, and the points 3 and 4 of Figure 5a coincide in Figure 5b. The line which joins points 2, 3 and the line which joins points 4, 1 in Figure 5a therefore coincide in Figure 5b. The lines 1-2, and 3-4 of Figure 5a become tangents to the conic in Figure 5b. Thus, it can be seen that the special conditions applying to Equation (21) are  $m_1 = m_3$  and  $h_1 = h_3$ , and the constants for the conic may be written as

$$\left. \begin{aligned}
a &= K + 1 \\
b &= -[2Km_1 + m_2 + m_4] \\
c &= Km_1^2 + m_2m_4 \\
d &= -[2Kh_1 + h_2 + h_4] \\
e &= 2Km_1h_1 + m_2h_4 + m_4h_2 \\
f &= Kh_1^2 + h_2h_4
\end{aligned} \right\} (24)$$

where the value of K is now given by

$$K = - \frac{(y_5 - m_2 x_5 - h_2)(y_5 - m_4 x_5 - h_4)}{(y_5 - m_1 x_5 - h_1)^2} \quad (25)$$

The coefficients P, Q, R, S, T for the conic in form of Equation (1) may now be computed by using Eq. (25) and Eq. (24) in Eq. (23).

c. Special Forms

Two special forms of Equation (1) are worth noting due to their frequent utilization in this body description procedure.

A straight line has the coefficients

$$\begin{aligned} P &= \text{slope} \\ Q &= \text{constant} \\ R &= S = T = 0 \end{aligned}$$

A circle of radius  $r_0$ , with its center at  $x_0, y_0$ , has as its coefficients

$$\begin{aligned} P &= 0 \\ Q &= y_0 \\ R &= -1 \\ S &= 2x_0 \\ T &= r_0^2 - x_0^2 \end{aligned}$$

## APPENDIX D

### NUMERICAL SEARCH FOR MINIMUM PROCEDURE

The numerical search procedure to determine the minimum wave drag configuration involves the computation of wave drag coefficients of a large number of discrete points blanketing the entire region in the six-dimensional space bounded by the given ranges of variables. The point which has the least wave drag is taken to be the minimum wave drag configuration. The accuracy of locating the minimum is therefore dependent on the resolution of the numerical network. Accurate location of the minimum can be obtained efficiently by a search-by-steps technique where the search is first conducted using coarser grids to determine an approximate location, and then repeated in a smaller region centered around the location of the previously obtained minimum. This process can be repeated as many times as needed to obtain the desired accuracy. The major advantage of such a numerical search procedure is that the given constraints can be satisfied easily by merely rejecting points which violate the constraints during the search.

The searching procedure is summarized as follows:

1. Select the ranges of search by specifying the lower and upper limits of each of the six reduced variables:

$$(z_L)_j, (z_U)_j \quad j = 1, 6$$

2. Select the resolution for each of the variables by specifying the numbers of node points  $N_j$  ( $j = 1, 6$ ) of that variable. The resolution is given by

$$\text{resolution} = \frac{(z_U)_j - (z_L)_j}{N_j - 1}$$

# Best Available Copy

The total number of points for each search cycle is equal to the product of  $N_j$ , i.e.

$$\text{total points} = \prod_{j=1}^6 N_j$$

For example, if 10 points are specified for all variables, the total number of points is  $10^6$ .

3. Compute the six tables of variables:

$$\left. \begin{array}{l} (z_i)_j \\ (z_1)_j, (z_L)_j, (z_N)_j, (z_u)_j \end{array} \right\} \quad i = 1, N_j \quad j = 1, 6$$

4. At every possible combination of the six variables,

$$(z_i)_1, (z_i)_2, \dots, (z_i)_6$$

evaluate the given constraints (e.g., the volume). If the combination satisfies the constraint, compute the wave drag coefficient using the wave drag equation.

5. Determine the set of variables  $z'_j$  which yields the least wave drag coefficient. The configuration defined by  $z'_1, z'_2, \dots, z'_6$  is the minimum wave drag configuration unless one wishes to improve the accuracy by repeating the search.
6. If the search is to be repeated, select the new ranges of the six variables by redefining the lower and upper limits as,

$$(z_L)_j = z'_j - \Delta_j, \quad (z_u)_j = z'_j + \Delta_j$$

where  $\Delta_j$  are arbitrary increments of  $z_j$  selected to define a smaller region of search. In situations where  $(z_L)_j$  or  $(z_u)_j$  defined by the above

relations are beyond the ranges of consideration, they are then set equal to the minimum or maximum accordingly.

7. Repeat the procedure from step (2) until the desired accuracy is obtained.

## APPENDIX E

### DEMONSTRATION OF LATIN SQUARE PROCEDURE

An IR&D program has been carried out to demonstrate the Latin Square optimization procedure using the von Karman ogive as the baseline configuration. The area distribution of the slender bodies, which yield the ogive, can be expressed as

$$S(\theta) = \frac{l^2}{4} \left\{ \frac{4B}{\pi l^2} \left( \pi - \theta + \frac{\sin 2\theta}{2} \right) + \sum_{n=2}^5 a_n \left[ \frac{\sin(n+1)\theta}{n+1} - \frac{\sin(n-1)\theta}{n-1} \right] \right\}$$

where  $l$  is the length,  $B$  the base area and  $\theta = \pi$  represents the nose,  $\theta = 0$  the base; the  $a_n$ 's are the Fourier coefficients of the lineal source distribution strength. The wave drag is given by

$$\frac{D_w}{\frac{1}{2} \rho_\infty U_\infty^2} = \frac{\pi}{4} l^2 \left\{ \frac{16B^2}{\pi^2 l^4} + 2a_2^2 + 3a_3^2 + 4a_4^2 + 5a_5^2 \right\}$$

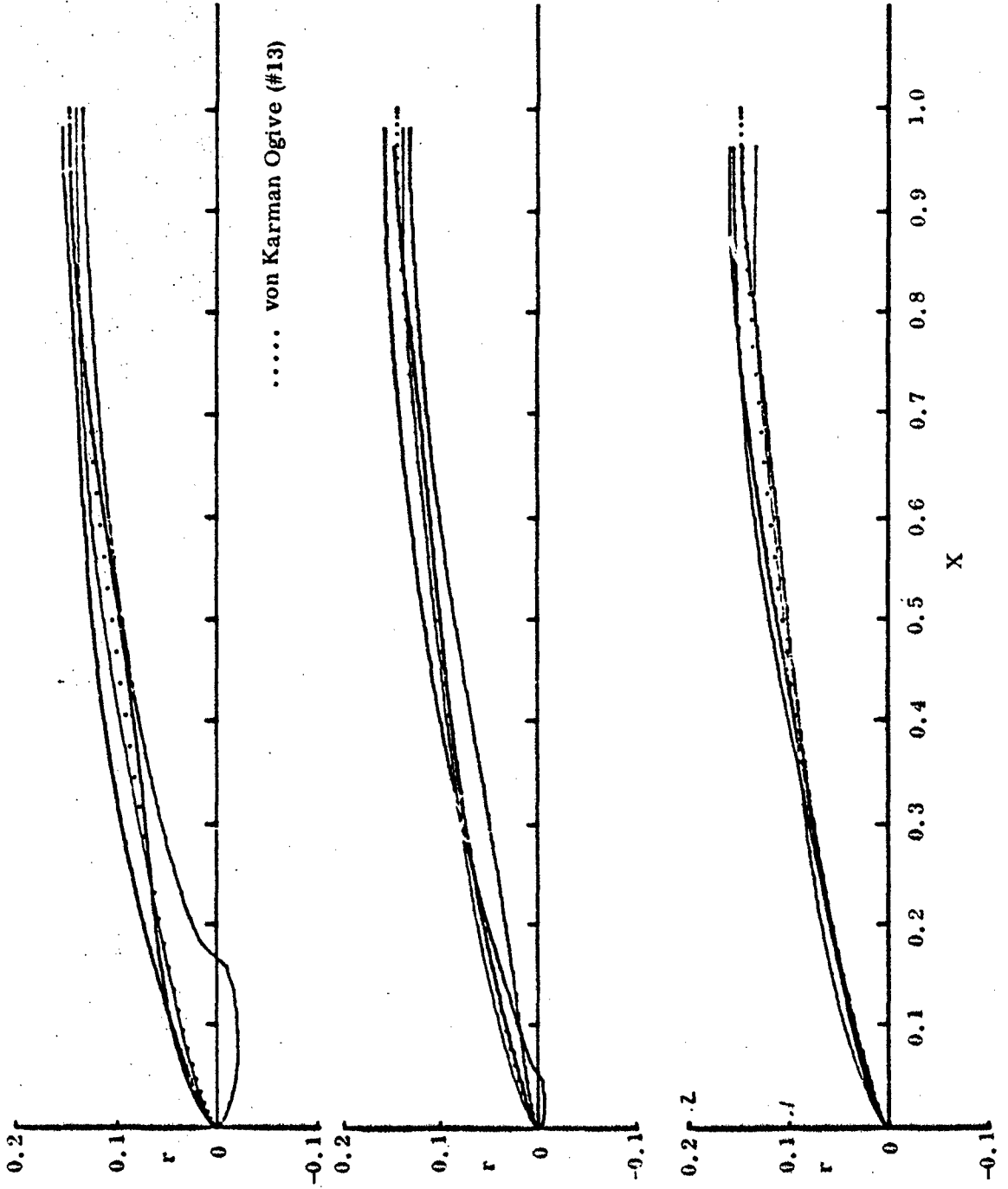
The Latin Square procedure is demonstrated in the following way: Select a set of geometric variables and their ranges of variation. This selection defines a family of configurations, over which the optimization procedure is then applied to yield the configuration with the least wave drag. If the procedure works, the minimum wave drag configuration will be a good approximation to the von Karman ogive obtained analytically.

For the 5x5 Latin Square, the six variables and their ranges are:

$x_1$	.962	$\leq$	$l$	$\leq$	1.038
$x_2$	.055	$\leq$	B	$\leq$	.079
$x_3$	-.02	$\leq$	$a_2$	$\leq$	.02
$x_4$	-.01	$\leq$	$a_5$	$\leq$	.01
$x_5$	-.02	$\leq$	$a_4$	$\leq$	.02
$x_6$	-.02	$\leq$	$a_3$	$\leq$	.02

The family of 25 configurations defined by these variables is shown in Figures 1 and 2, where the dotted lines represent the base line at  $l = 1.0$  and  $B = 0.067$ , which were selected to reflect the variables used for the F-4 during phase I study.

The demonstration of the Latin Square procedure and our finds are summarized below. A straightforward application of the original Latin Square procedure did not yield the correct minimum wave drag body. Under the constraint of given length ( $l = 1.0$ ) and base ( $B = 0.067$ ), the original procedure predicted the minimum wave drag body to correspond to  $a_2 = -.02$ ,  $a_3 = .02$ ,  $a_4 = -.002$  and  $a_5 = -.02$  while for the von Karman ogive all the a's vanish  $a_2 = a_3 = a_4 = a_5 = 0$ . Of these four variables only  $a_4$  is barely acceptable, considering the numerical accuracy. However, when the iterative type improvement, which consists of adding more nonlinear terms in the wave drag function (see Reference 1 of the main text), was applied, the optimization procedure turned out successfully. Indeed, when only one case of  $a_2 = 0$ ,  $a_3 = 0.2$ ,  $a_4 = 0$  and  $a_5 = 0$  was added to yield a square term for  $a_3$  in the wave drag function, the improved procedure predicted the minimum wave drag body to correspond to  $a_2 = -.00026$ ,  $a_3 = -.00021$ ,  $a_4 = 0.0006$ ,  $a_5 = .00031$ , which is the von Karman ogive recovered numerically.



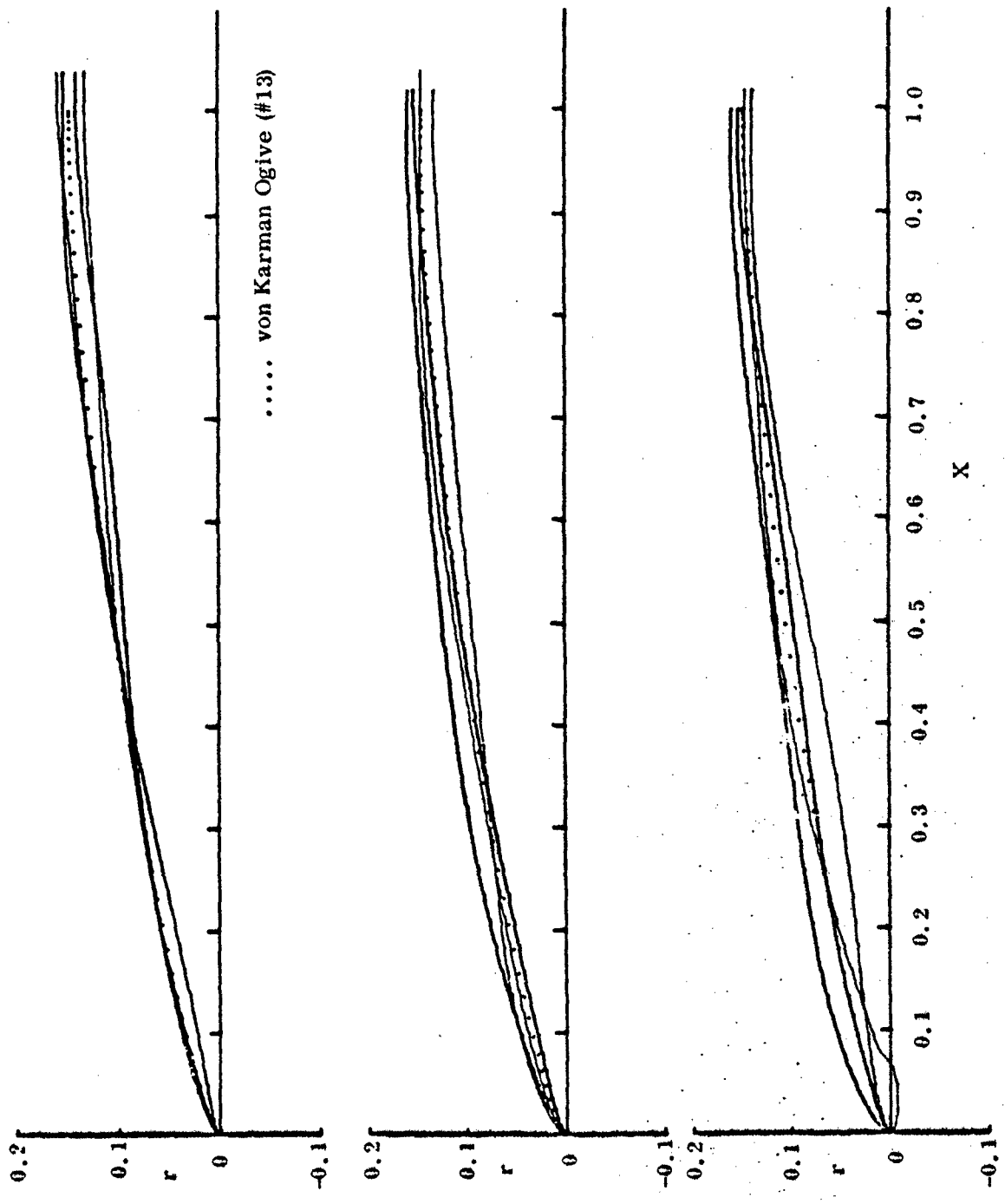


FIGURE 2. Variation Configurations (#13 to #25)

Similar results were obtained for different constraints of  $l$  and  $B$ .

In sum, the improved Latin Square optimization procedure has numerically predicted the minimum wave drag body that was obtained analytically.

**Best Available Copy**